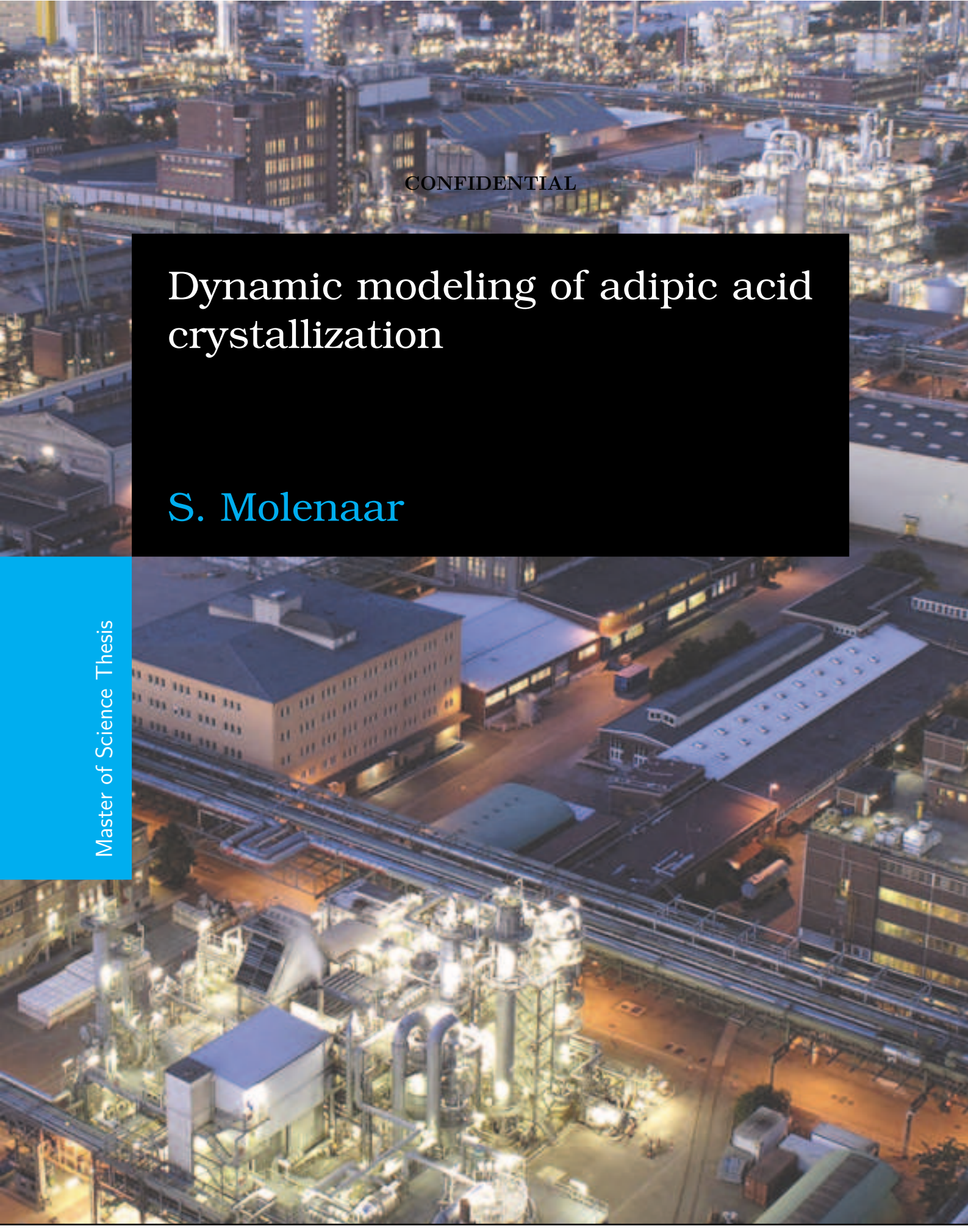

CONFIDENTIAL

Dynamic modeling of adipic acid crystallization

S. Molenaar

Master of Science Thesis

TU Delft Delft University of Technology

Reportnumber: 2464

Sustainable Processes and Energy Technologies

MSCCONFIDENTIAL

Dynamic modeling of adipic acid crystallization

Master of Science Thesis

For the degree of Master of Science in Mechanical Engineering at Delft University of Technology

S. Molenaar

August 7, 2011

Exam committee consists of:
Prof.dr.ir. Andrzej Stankiewicz
Dr.ir. Herman Kramer,
Dr.ir. Ali Mesbah
Dr. Maxim Weber (BASF)

Faculty of Mechanical, Maritime and Materials Engineering (3mE) · Delft University of Technology

The work in this thesis was supported by BASF. Their cooperation is hereby gratefully acknowledged.

Abstract

Adipic acid is a product that is produced on a large scale world wide. Its separation and purification is mostly done by crystallization. As crystallization is usually a part of a wider processing system; the quality i.e. Crystal Size Distribution (CSD) of the crystals has a large influence on the downstream processing. Therefore the CSD should be predictable and as constant as possible. In this thesis a dynamic model was developed for simulating the crystallization process of adipic acid. This model could act as a basis for a control system which predicts and controls the CSD.

A literature study was done and yielded a numerical method for solving the Population Balance Equation (PBE) and expressions for nucleation, crystal growth and agglomeration. The High Resolution Finite Volume Methods (HR-FVM) were implemented in Matlab. This implementation was tested for its accuracy and stability by solving several numerical test cases. By comparison between the numerical and the analytical solutions it was concluded that the numerical method was able to solve the PBE including different kinetics accurately.

This numerical framework was extended with a mass balance, energy balance and concentration balance to model an Mixed Suspension Mixed Product Removal (MSMPR) crystallizer. An MSMPR crystallizer is the crystallization equivalent of a stirred tank reactor. The numerical solution was in agreement with the analytical solution.

Adipic acid is known to agglomerate; therefore an agglomeration model was included in the framework. The steady state CSD of this model was compared to experimental data. The CSD is not in agreement with the experimental data. Making the agglomeration rate super saturation dependent did not yield satisfactory results. Several other size-independent agglomeration rate expressions were implemented to see if this would yield a more accurate CSD. The results were more accurate; the least square error decreased by 43.72% but the tenth and ninetieth percentile were still a bit under predicted while the fiftieth percentile was over predicted. The time required to reach steady state was three times shorter for the size-independent models (15 versus 50 hours). It can be concluded that the empirical expression of Lindenberg (Lindenberg et al., 2007) gives the most accurate CSD. In order to improve the model and also to be able to simulate the dynamics several recommendations are given at the end of this thesis.

Acknowledgements

The completion of this graduation thesis would not have been possible without the support of numerous people.

First of all I would like to thank my supervisor Dr.Ir. Herman Kramer for his guidance and advice during this graduation project. I would also like to thank my daily supervisor Dr.Ir. Ali Mesbah, not only for the support he gave me continuously throughout this graduation project but also for the many times he cleared his schedule for a meeting with me. The people within the crystallization group made it possible to express my ideas and results in regular meetings.

Another word of thanks goes out the the people at BASF. My supervisors Dr. Karsten Bartling and Dr. Maxim Weber made sure all the questions I had were answered while the students at BASF made sure my stay in Ludwigshafen was a very pleasant experience.

A word of thanks goes out to all the friends I made while studying in Delft especially the people at the P&E department. We enjoyed a lot of extra curricular activities. My fellow students and friends in room 32 have endured most of my chitchat, jokes but also some frustrations. Thanks a lot for your patience. A special word of thanks to Bert for proofreading the non confidential text of this report, making suggestions on some of the graphs and making me buy ridiculously expensive shoes.

Last but not least I want to thank my parents and my girlfriend for all the words of encouragement, motivation and above all the love I received which kept me going throughout this graduation thesis.

Delft University of Technology S. Molenaar
August 7, 2011
Delft

Table of Contents

Acknowledgements **iii**

1 Introduction **1**

1-1 Introduction . . . 1

1-2 Problem statement and approach . . . 2

1-3 Outline of this thesis . . . 3

2 Crystallization theory **5**

2-1 Introduction . . . 5

2-2 Crystallization from solution . . . 6

2-3 Nucleation . . . 8

2-3-1 Primary nucleation . . . 8

2-3-2 Secondary nucleation . . . 10

2-4 Crystal growth . . . 11

2-5 Attrition . . . 12

2-6 Agglomeration . . . 13

2-6-1 Crystal sizes . . . 14

2-6-2 Collision model . . . 16

2-6-3 Cohesion model . . . 17

2-7 Population balance equation . . . 21

2-7-1 Method of moments . . . 23

2-7-2 Finite difference methods . . . 24

2-7-3 Discretization techniques . . . 24

2-7-4 Method of weighted residuals . . . 24

2-7-5 Monte Carlo methods . . . 25

3 Modeling approach **27**
3-1 Introduction . . . 27
3-2 Process description . . . 28
3-3 Modeling purpose . . . 29
3-4 Model framework assumptions . . . 30
3-5 Dispersed solid phase . . . 31
3-5-1 Population balance equation modeling . . . 31
3-5-2 High order finite volume method with flux limiter . . . 31
3-5-3 Process model PBE . . . 33
3-6 Crystallization kinetics . . . 35
3-6-1 Nucleation modeling . . . 35
3-6-2 Crystal growth model . . . 37
3-6-3 Agglomeration model . . . 37
3-7 Continuous liquid phase . . . 41
3-8 Modeling framework . . . 43
3-8-1 Matlab implementation . . . 44

4 Experimental setup and data **47**
4-1 Experimental setup . . . 47
4-1-1 Control system . . . 47
4-1-2 CSD measuring . . . 47
4-2 Experimental data . . . 49
4-2-1 Graphical representation of the data . . . 49
4-2-2 Matching the CSD data to the process conditions data . . . 50
4-2-3 Overview of the experimental data . . . 50

5 Results and discussion **53**
5-1 Numerical test cases . . . 53
5-1-1 Pure growth . . . 54
5-1-2 Pure agglomeration . . . 55
5-1-3 Simultaneous growth and agglomeration . . . 56
5-1-4 Simultaneous growth and nucleation . . . 57
5-1-5 Simultaneous growth, nucleation and agglomeration . . . 58
5-1-6 An industrial continuous crystallizer (MSMPR) . . . 60
5-2 Process model simulations . . . 61
5-2-1 Steady state results . . . 62
5-2-2 Reasons for deviations in the modeled CSD . . . 63

6 Conclusions and recommendations **69**
6-1 Conclusions . . . 69
6-2 Recommendations . . . 70

A Population balance equation **73**

B Model equations **77**

B-1 Population balance equation 77

B-2 Mass balance 78

B-3 Concentration balance 78

B-4 Energy balance 78

C Matlab code **81**

C-1 Crystallizer main model 81

C-2 Crystallizer differential equations 88

C-3 Data matching program 91

Bibliography **97**

Glossary **103**

List of Acronyms 103

List of Symbols 103

List of Figures

1-1 Research approach 2

2-1 Solubility diagram (solid line is the saturation concentration) 7
2-2 Different stability states (Myerson, 2002) 7
2-3 Nucleation mechanisms 9
2-4 Critical free excess energy ΔG_{crit} (surface free energy ΔG_S, volume free energy ΔG_V and the total free energy $\Delta G = \Delta G_S + \Delta G_V$) 10
2-5 Two-step growth model (bulk concentration c_0, interface concentration c_1 and equilibrium concentration c^*) 11
2-6 The different kinds of adipic acid crystals 13
2-7 Collision and cohesion of two crystals forming an agglomerate 14
2-8 Brownian motion as a collision mechanism 15
2-9 The different kinds of collision mechanisms 16
2-10 Change in the number of crystals per unit volume in the crystal size range L and L+dL from Mersmann (Mersmann, 2001) 22
2-11 Advection equation; initial profile, formal and numerical solution 23

3-1 Modeling framework, the continuous liquid phase and dispersed solid phase are connected trough the kinetics 27
3-2 Process flow diagram of the Draft Tube Baffle (DTB) crystallizer at BASF Ludwigshafen (flow sensors S, temperature sensors T and pressure sensors P) 29
3-3 The different kinds of size discretization grids 33
3-4 Streamlines for particles above and below the critical Stokes number 36
3-5 The collision rate for a solid-liquid system according to Kruis and Kusters (Kruis and Kusters, 1996) (particle diameters d_{P1}/d_{P2}) 39
3-6 The agglomeration efficiency for the example case (particle diameters d_{P1}/d_{P2}) . 40
3-7 The agglomeration rate for the example case (particle diameters d_{P1}/d_{P2}) 41

3-8 The stability regions of different numerical Ordinary Differential Equation (ODE) solvers 45

4-1 Process flow diagram of the sampling loop (Ruiter, 2009) (valves HV, flow sensors HS and pumps HP) 48
4-2 A cumulative size distribution with its percentiles 50
4-3 Increase in stirrer rate from 24 to 35 to 40 rpm 51

5-1 Number density distributions after ten seconds, numerical and analytical in the case of 'pure' growth 55
5-2 Number density distributions at different elapsed times, numerical and analytical in the case of 'pure' agglomeration 56
5-3 Number density distributions at different elapsed times, numerical and analytical in the case of growth and agglomeration 57
5-4 Number density distributions at different elapsed times, numerical and analytical in the case of growth and nucleation 58
5-5 Comparison between the model results of this thesis and the model results of Qamar and Warnecke (Qamar and Warnecke, 2007) 59
5-6 The steady-state number density distribution of an MSMPR crystallizer 61
5-7 The distribution percentiles, modeling and experimental result 63
5-8 The distribution percentiles, modeling and experimental result 65
5-9 The distribution percentiles, modeling and experimental result (constant agglomeration rate) 66
5-10 The distribution percentiles, modeling and experimental result (Lindenberg et al., 2007) 68

List of Tables

3-1 Normal operating conditions for the DTB crystallizer 28
3-2 Physical properties for the adipic acid example from Kruis and Kusters (Kruis and Kusters, 1996) 39

4-1 Different sizes and characteristics crystals measured by the sensor 49
4-2 Data availability 51

5-1 Initial number density for the pure growth case 54
5-2 Initial number density for simultaneous growth and nucleation case 57
5-3 Kinetic parameters and least square error 62
5-4 Steady state percentiles experimental and modeled 62
5-5 Kinetic parameters and least square error (supersaturation dependent) 64
5-6 Steady state percentiles with and without supersaturation dependency 64
5-7 Kinetic parameters and least square error (constant agglomeration rate) 65
5-8 Steady state percentiles experimental and modeled (constant agglomeration rate) 66
5-9 Kinetic parameters and least square error ((Lindenberg et al., 2007)) 67
5-10 Steady state percentiles experimental and modeled (Lindenberg et al., 2007) . . 67
5-11 Least square errors of the different models compared to Lindenberg (Lindenberg et al., 2007) 67

Nomenclature

Roman

$3dE$	3d Equivalent diameter	m
a	Activity	$-$
$a*$	Activity in saturated state	$-$
a_1	Constant in the nucleation rate	$\#/m^4$
a_2	Lower bound for integration	m
a_3	Constant in the growth rate	m/s
a_4	Crystal growth rate exponent	$-$
a_5	Constant in agglomeration efficiency	$-$
a_6	Constant in the agglomeration rate	$-$
b	Added mass coefficient	$-$
B	Nucleation rate	$\#/m^3 \cdot s$
c	Concentration	%
C	Prefactor in root mean square velocity	$-$
$c*$	Saturated concentration	%
C_μ	Constant in the $k-\epsilon$ model	$-$
c_0	Bulk concentration	%
c_1	Interface concentration	%
c_p	Specific heat	$kJ/kg \cdot K$
d	Distance between crystals	m
$d_{stirrer}$	Stirrer diameter	m
d_1	Diameter of smallest crystal	m
d_2	Diameter of largest crystal	m
d'_p	Diameter of largest crystal	m
d_p	Diameter of smallest crystal	m
E	Elongation	$-$
F	Ferret Diameter	m
f	Relative shape function	$-$
F_{area}	Waddel disk diameter	m
F_2	Lagrangian correlation function	$-$

F_M	Mass flux solute from solution	kg/s
G	Growth rate	m/s
g	Overall growth order	$-$
G_{crit}	Critical free excess energy	J/mol
G_S	Free surface excess energy	J/mol
G_V	Free volume excess energy	J/mol
H	Heywood ratio	$-$
h_{evap}	Enthalpy of evaporation	kJ/kg
k	Turbulent kinetic energy	m^2/s^2
$K^{\pm}{}_{agg}$	Agglomeration term	m^{-1}/s
k_ψ	Parameter in efficiency factor	$-$
k_c	Constant in cementation time	$-$
k_g	Growth rate constant	$(kmol)^{1-g}m^{3g-2}s^{-1}$
k_n	Empirical nucleation rate constant	$-$
k_v	Crystal shape factor	$-$
L	Crystal length	m
L_{max}	Upper bound size domain	m
L_{min}	Lower bound size domain	m
L_i	ith percentile	m
L_m	Mean doublet diameter	m
M_T	Moment of the distribution	$-$
n	Crystal number density	$\#/m^4$
N	Impeller speed	s^{-1}
N	Total number of grid cells	$-$
$\tilde{n}$	Crystal density	$\#/m$
P_2	Sticking probability	$-$
P_3	Non-dissociation probability	$-$
r	Flux limiter	$-$
R	Universal gas constant	$8.314 J/molK$
Re_λ	Taylor microscale Reynolds number	$-$
s	Crystalline bridge length	m
S	Supersaturation ratio	$-$
S_m	Size of the smallest crystal	m
S_n	Size of the largest crystal	m
T	Temperature	K
t_c	Bridge building time	s
T_L	Lagrange time scale	s
t_r	Average interaction time	s
t_t	Small turbulent eddies lifetime	s
u'	Fluctuating average component of the local velocity	m/s
u_k	Fluctuating component of turbulent velocity in direction k	m/s
v	Crystal volume	m^3
$\dot{V}$	Volumetric flowrate	m^3/s
v_f	Root mean square fluid velocity	m/s
Vc	Crystallizer volume	m^3
w_i	One dimensional relative velocity between particles	m/s

x	Part of the crystalline bridge length	m
y	Distance between crystals	m

Greek

β	Frequency	s^{-1}
ϵ	Impeller power input	W/kg
ϵ	Liquid fraction	$-$
η_{Agglo}	Agglomeration efficiency	$-$
η_{kol}	Kolmogorov length scale	m
γ	Correction parameter	$-$
γ	Local shear rate	s^{-1}
Λ	Length scale of largest vortices	m
λ_c	Contact length	m
λ_e	Lagrangian microscale	m
λ_g	Taylor microscale	m
μ	Chemical potential	J/mol
μ	Dynamic viscosity	$Pa \cdot s$
$\mu*$	Chemical potential of the saturated solution	J/mol
μ^0	Chemical potential arbitrary reference state	J/mol
ν_f	Kinematic viscosity of the fluid	$kg/(s \cdot m)$
ρ	Density	$m3/kg$
σ	Relative supersaturation	$-$
σ_c	Crystalline bridge fracture strength	N/m^2
τ	Residence time	s
τ_{kol}	Kolmogorov time scale	s
τ_L	Lagrangian time micro scale	s
Θ	Dimensionless particle relaxation time	$-$

Subscripts

$agglo$	Agglomeration
c	Crystal
$coll$	Collision
f	Fluid
$feed$	Feed
liq	Liquid
max	Maximum
min	Minimum
out	Output
p	Particle
rec	Recycle
vap	Vapor

Chapter 1

Introduction

1-1 Introduction

Crystallization is the process of the production of a crystalline solid phase from a vapor, solution or melt (Mersmann, 2001). As a separation process it distinguishes itself from other separation processes by the ability to reach a high product purity in a single step process with low level of energy consumption and relatively mild process conditions (Virone, 2006). The aforementioned merits make it a preferable separation technique. This is also evident from the tonnage and variety of particulate crystal products produced and sold worldwide as this amounts for half the output of the modern chemical industry according to Jones (Jones, 2002).

Adipic acid is one of these particulate crystal products produced on large scale. The annual production is 2.5 billion kilograms of which 12.5% is produced by BASF (Musser, 2008). It is mainly used as a precursor for nylon production. As crystallization is usually a part of a wider processing system; the quality (or Crystal Size Distribution (CSD)) of the crystals has a large influence on the downstream processing. Therefore the CSD should be predictable and as constant as possible.

A number of kinetic phenomena occur in a crystallization process e.g. nucleation, growth, attrition and agglomeration. These phenomena are highly interrelated and their inner workings are currently not fully understood (Mersmann, 2001). This is what makes predicting the CSD of a crystallization product a non-trivial task.

Next to the difficulties with the kinetic phenomena there is another challenge when modeling a crystallization process. This challenge lies within the solution of the Population Balance Equation (PBE). The PBE is an equation which describes the development of a specific particle property during time. In control applications, only one internal coordinate system is used for describing the characteristics of a crystalline material i.e. crystal size (Braatz, 2002). Analytical solutions to the PBE are only available for some simple cases. When phenomena as agglomeration are included one must resort to numerical solution methods.

The complexities of numerically solving a PBE has sparked the interest of many scientists. A large variety of different numerical schemes was developed over the last decade, each with its own merits and drawbacks. An overview of these numerical schemes can be found in this thesis, for a detailed overview the reader is redirected to Mesbah (Mesbah, 2010).

1-2 Problem statement and approach

Previous work by de Ruiter (Ruiter, 2009) showed that agglomeration is a dominant phenomena in the crystallization process of adipic acid at BASF. If the CSD is to be described accurately by a mathematical model this phenomena should be included. This raises the following research question:

"Can the dynamics of the adipic acid crystallization process be described in terms of the product quality when nucleation, growth and agglomeration are included in a mathematical model?"

The research approach which was followed in this thesis is depicted in Figure 1-1. A literature survey was done for the different kind of kinetic phenomena which are present in a crystallization process. This survey results in correlations for the nucleation, growth and agglomeration rate. After the literature survey a mathematical framework was created for the crystallization process model. This framework includes the PBE together with the mass and energy balances and additional constitutive equations. In order to solve this system of equations a numerical method was chosen, in this case the finite volume method. This method conveniently incorporates the agglomeration rate. The created model was validated in three steps, first the numerical scheme is validated using numerical test cases which have a analytical solution. The second step is to simulate and validate a continuous Mixed Suspension Mixed Product Removal (MSMPR) which includes mass and energy balances. The third and final step is to do a parameter estimation and to replicate the results from experimental data.

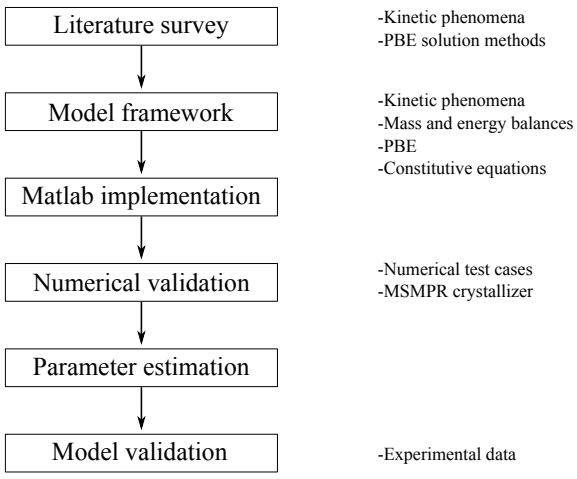

Figure 1-1: Research approach

1-3 Outline of this thesis

The remainder of this thesis has another five Chapters. Chapter 2 gives an overview of the theoretical background of crystallization as a process and also of kinetic phenomena such as: nucleation, growth and agglomeration. The subsequent Chapter 3 reviews the used modeling approach for the PBE, the crystallization kinetics and the liquid phase. At the end of Chapter 3 a model overview is given. Chapter 4 gives background information about the experimental setup and the sensors used at BASF Ludwigshafen. Also an overview of the available experimental data is given. Chapter 5 discusses the results of the thesis and Chapter 6 consists of a discussion and recommendations for further research.

Chapter 2

Crystallization theory

2-1 Introduction

Crystallization is a separation process that yields a solid product. The product can be separated either from melt, a solution or a vapor. As with most separation processes it requires non equilibrium conditions to generate a driving force. This driving force is needed for crystallization to occur. In the case of crystallization the driving force is the solutes chemical potential difference between the liquid and the solid state. Section 2-2 discusses this driving force in more detail.

Crystallization is also a process in which simultaneous heat and mass transfer occurs, it has a strong dependency on both fluid and particle mechanics. When dealing with particle mechanics a very frequently used equation is the Population Balance Equation (PBE) (Ramkrishna, 2000). This is an Partial Differential Equation (PDE) which describes the development of specific particle properties over time. Detailed information about the PBE can be found in Section 2-7.

The driving force i.e supersaturation in a crystallizer is dependent on the flows of mass and energy at one side and the crystallization kinetics on the other. Crystallization kinetics include nucleation, crystal growth, attrition and agglomeration.

In order for crystals to be created, nuclei should be formed after which they grow out to crystals. Nucleation i.e. the creation of a new crystalline phase is discussed in Section 2-3. In this Section a distinction is made between primary and secondary nucleation.

When nuclei are formed they grow out to crystals in the crystallizer, this crystal growth is discussed in Section 2-4. Attrition is the abrasion of crystals due to mechanical contact of the crystals with the hardware or other crystals which creates fragments of crystals which can act as new nuclei and grow out to be crystals. There are many mechanisms of attrition of which a selection is discussed in Section 3-6-1. From a previous study by de Ruiter (Ruiter, 2009) it is known that agglomeration is a dominant phenomena in the adipic acid crystallization process. Agglomeration is a mechanism in which crystals collide with each other and are glued

together by a crystal bridge between them. The agglomeration mechanisms are discussed in Section 2-6.

2-2 Crystallization from solution

Adipic acid is crystallized from a solution, it changes from its dissolved state to the solid state. The creation of the solid phase enables one to separate it from the liquid phase by centrifugation or by filtering. As mentioned in the introduction to this Chapter, in order for crystallization to occur there should be a driving force.

This driving force for crystallization is mathematically expressed as (Jancic and Grootscholten, 1984):

$$\Delta\mu = \mu - \mu* \tag{2-1}$$

In which μ is the chemical potential of the crystalline substance in the supersaturated state and $\mu*$ is the chemical potential of the same substance in the saturated solution. The chemical potential of a substance is related to the substance activity by:

$$\mu = \mu^0 + RT\ln(a) \tag{2-2}$$

in which μ^0 is an arbitrary reference state chemical potential and a is the substances activity.

Equation (2-2) can be used to rewrite (2-1) into:

$$\frac{\Delta\mu}{RT} = \ln\left(\frac{a}{a*}\right) = \ln(S) \tag{2-3}$$

in which the left hand side of the expression is the dimensionless driving force for crystallization and S is the supersaturation ratio.

Fundamentally the driving force for a crystallization process is the difference in chemical potential between the crystallizing substance in the crystal and in the solution phase as discussed before. Usually it is expressed as the difference between the supersaturation and saturation concentration (only valid for relatively small supersaturation values).

$$\Delta c = c - c^* \tag{2-4}$$

The saturation concentration is the concentration at which the solution is in equilibrium with the solid state. Figure 2-1 is a solubility diagram it is used to illustrate some of the terminology within this report.

In Figure 2-1 the continuous line is the curve which describes the saturation concentration at different temperatures. The slope of this curve varies with compound and partly determines if a certain crystallization technique is feasible (cooling or evaporative crystallization for example). The region below this saturation curve is called the under saturated region and the region above this line is called the supersaturated region. Another curve is plotted in Figure 2-1, the metastable limit.

Metastability can best be explained by an illustration. In Figure 2-2(a) a stable solution is depicted, it appears as a minimum. In order to change the state of this solution a large

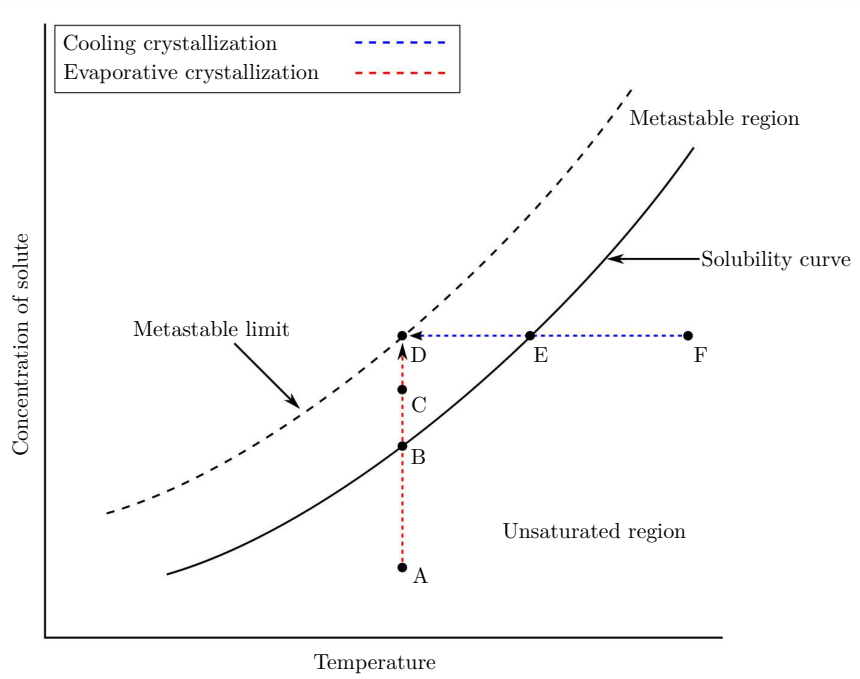

Figure 2-1: Solubility diagram (solid line is the saturation concentration)

disturbance is needed. In Figure 2-2(b) an unstable solution is depicted. An unstable is the direct opposite of a stable solution, a infinitely small disturbance can cause the state of the solution to change. A metastable solution is depicted in Figure 2-2(c). Here the solution is in a local stable state (valley) but a small disturbance can change the state towards the left side (a deeper valley). A detailed description of this metastability is given in Section 2-3.

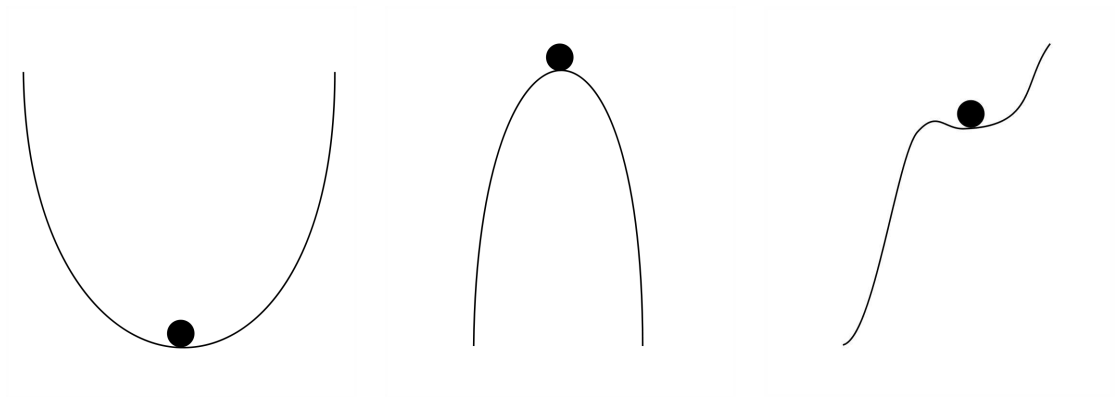

(a) Stable (b) Unstable (c) Metastable

Figure 2-2: Different stability states (Myerson, 2002)

In Figure 2-1 the line from point A to point D depicts the process of evaporative crystallization. Where supersaturation is created by evaporating the solvent at constant temperature. Point A lies in the under saturated area, in other words, the bulk concentration is lower than the saturated concentration. This means that there is no driving force or supersaturation thus

no crystallization occurs. Point B lies on the saturation curve thus the solution is saturated and there is no crystallization occurring. If one would increase the concentration to point C it would be in the metastable region. In this case there would be no spontaneous nucleation. One could increase the concentration up to a certain concentration at which spontaneous nucleation would occur this concentration is the metastable limit depicted by point D. The energy barrier which should be overcome to initiate spontaneous nucleation is described in detail in Section 2-3.

The line F-D in Figure 2-1 represents a process which is called cooling crystallization in which the supersaturation is created by cooling the solution.

2-3 Nucleation

When a solution is supersaturated the system tries to restore its equilibrium by different competing mechanisms (Mersmann, 2001). Nucleation is one of these mechanisms. While supersaturation is a prerequisite for crystallization it alone is not enough for crystallization to start. A large number of minute solid bodies, embryos, nuclei or seeds should be available to act as centers for crystallization. Nucleation is the subject of this Section, growth is explained in Section 2-4.

There are two main classes of nucleation which should be distinguished:

1. Primary nucleation, which is the formation of new nuclei in the absence of crystal matter in the solution. Consisting of heterogeneous and homogeneous primary nucleation.
2. Secondary nucleation, which is the formation of new nuclei in the vicinity of crystals present in the solution.

In the following Subsections homogeneous primary nucleation, heterogeneous primary nucleation and secondary nucleation will be discussed in more detail. All these mechanisms need to overcome a certain energy barrier before a cluster of critical size is formed. The amount of energy required i.e. the penetration into the metastable zone is different for each of the processes.

2-3-1 Primary nucleation

Primary nucleation is the formation of new nuclei from a clear liquid. Within primary nucleation there are two subclasses namely homogeneous and heterogeneous primary nucleation. Homogeneous primary nucleation only occurs when there are no foreign particles within the solution. Heterogeneous nucleation occurs when foreign particles are available.

Homogeneous primary nucleation

Homogeneous primary nucleation is the formation of nuclei from a clear liquid. Molecules in the solution associate to form a cluster. This cluster formation is a stochastic process. Different sizes of clusters can be formed spontaneously. The size of the clusters and the

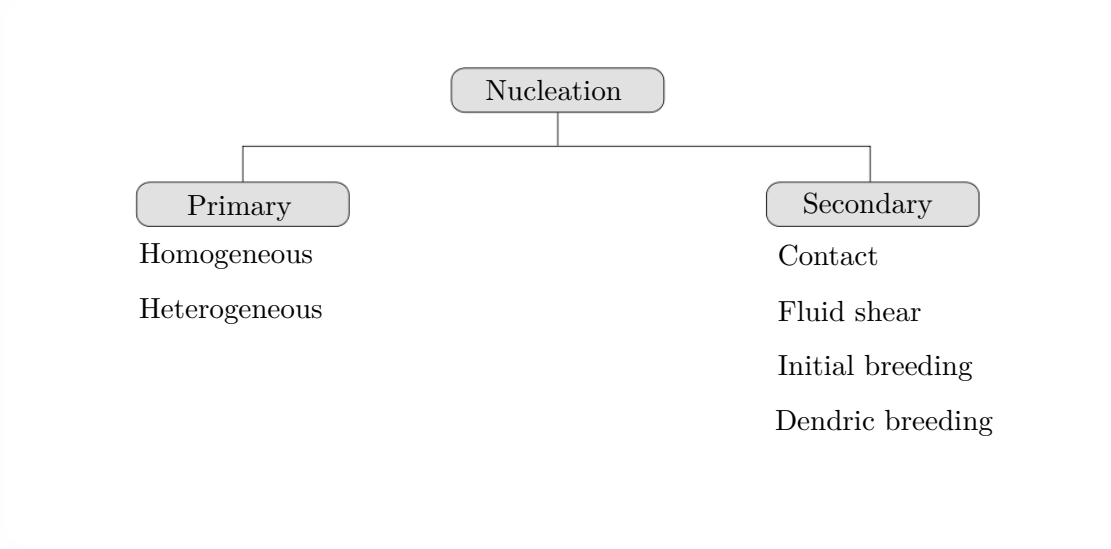

Figure 2-3: Nucleation mechanisms

rate of cluster formation is dependent on supersaturation. There exists a critical cluster size above which the cluster grows out and below which it will dissolve again. The existence of this critical size can be explained as follows: the work needed to form a cluster can be expressed by a balance between the free excess surface energy G_S and the volume excess free energy G_V.

$$\Delta G = \Delta G_S + \Delta \mathrm{G}_V \tag{2-5}$$

The two terms on the right hand side of Equation (2-5) have different signs and dependency on nucleus size ($\Delta G_V \propto L^3$ and $\Delta G_S \propto L^2$). This is the reason for the maximum in the free excess formation energy ΔG_{crit} depicted in Figure 2-4. Independent of nucleus size the system always tries to minimize the free excess energy of the nucleus so depending if the nucleus size is above or below the critical free excess energy of formation ΔG_{crit} it will grow out or dissolve.

Heterogeneous primary nucleation

In case of heterogeneous nucleation there are foreign particles in the solution. These impurities lower the overall excess free energy required for nucleation and thus at lower supersaturation heterogeneous primary nucleation is more likely to occur than homogeneous primary nucleation. This lowering of the excess free energy is mathematically expressed as:

$$\Delta G_{crit,hetero} = \phi \Delta G_{crit,homo} \tag{2-6}$$

in which ϕ is a factor which is less than unity. It is the ratio of the volume of the truncated nucleus to that of a sphere of the same volume. It is a function of the contact angle between the crystalline deposit and foreign deposit (Volmer, 1939). Expressions for ΔG can be found in Mersmann (Mersmann, 2001).

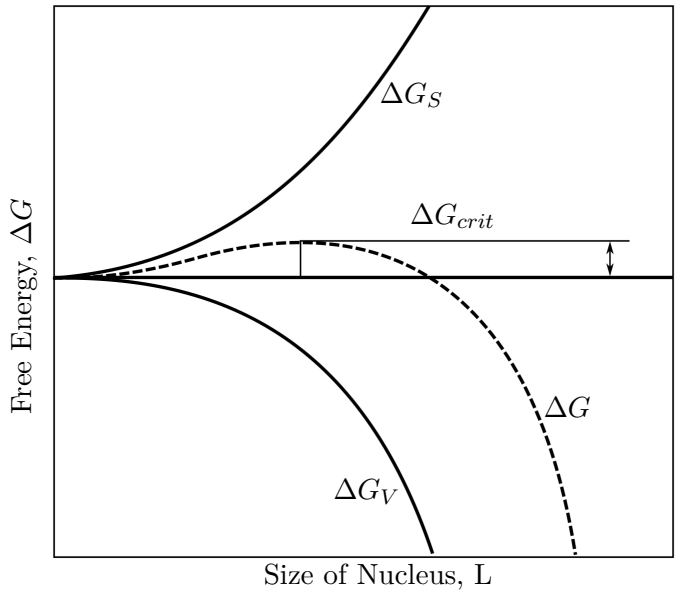

Figure 2-4: Critical free excess energy ΔG_{crit} (surface free energy ΔG_S, volume free energy ΔG_V and the total free energy $\Delta G = \Delta G_S + \Delta G_V$)

2-3-2 Secondary nucleation

When nuclei are formed in the presence of crystals the process is called secondary nucleation. The crystals have a catalytic effect on nucleation similar to foreign particles in heterogeneous primary nucleation. This is the reason why secondary nucleation occurs at much lower supersaturation levels. As depicted in Figure 2-3 there are several kinds of secondary nucleation:

Contact nucleation or attrition breeding Small pieces of crystals are removed from their parent crystals by collisions between crystals or crystals with another surface such as the crystallizer wall or impeller blades. According to Neumann (Neumann, 2001) this kind of secondary nucleation is the most dominant in industrial crystallizers.

Fluid shear breeding A process similar to attrition breeding but instead of mechanic forces, hydrodynamic forces break off small pieces of crystal.

Initial breeding or dust breeding When handling dry crystal material small fragments are created. These fragments adhere to the crystals and are washed from the surface to become suspended in the solution as new nuclei.

Dendrite or polycrystalline breeding Only with very high supersaturation needle shaped dendrites or polycrystalline aggregates are formed at the corners and edges of the parent crystal. Due to their shape they are prone to break off by mechanic or hydrodynamic forces.

2-4 Crystal growth

When stable nuclei are formed by the nucleation mechanisms described in Section 2-3 and the solution is supersaturated these nuclei start to grow. Crystal growth is a complex process and many different theories have been formulated during the last century. The cause of the complexity is mainly because the growth process consists of several steps (Mullin, 1993):

- Bulk diffusion of hydrated ions through the diffusion boundary layer
- Bulk diffusion of solvated ions through the adsorption
- Surface diffusion of solvated or unsolvated ions
- Partial or total desolvation of ions
- Integration of ions into the lattice
- Counter diffusion through the adsorption layer of the water released
- Counter diffusion of water through the boundary layer

Although the growth process has many steps, a frequently used (simplified) model is the two step model. This model is an analogy of the classical diffusion-reaction theory (Mersmann, 2001). It is depicted in Figure 2-5. The two steps which are visible are the diffusion step in which solute is transported through the solution and a surface integration step. The overall growth rate being determined by these "resistances" in series.

Although literature mentions a diversity of growth equations the following very simple equation for the overall growth rate is frequently used (Mersmann, 2001):

$$G = k_g(\Delta C)^g \tag{2-7}$$

in which g is the overall "order" of the growth process and k_g is the growth rate constant. The growth rate constant in general is a function of temperature, relative crystal/solution velocity and impurities within the system (Garside et al., 2002).

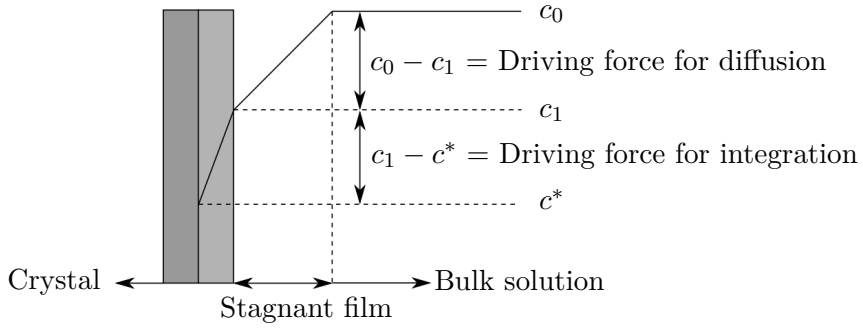

Figure 2-5: Two-step growth model (bulk concentration c_0, interface concentration c_1 and equilibrium concentration c^*)

2-5 Attrition

Attrition is a specific case of secondary nucleation. According to Neumann (Neumann, 2001) attrition is the most dominant source of secondary nuclei in a crystallizer. The breakage of small crystal fragments from their parent crystals is caused by mechanic forces such as crystal-crystal, crystal-stirrer and crystal-vessel collisions.

There have been many reports discussing this specific variant of secondary nucleation (Imran, 2007). The so-called power law is an empirical expression which expresses the secondary nucleation rate as a function of four parameters. This expression is based on the experimental work of Ottens and de Jong (Ottens and de Jong, 1973),

$$B = k_n G^a N^b M_T^c \tag{2-8}$$

in which k_n is the empirical nucleation rate constant, G is the crystal growth rate, N is the impeller speed and M_T is a moment of the distribution. Equation (2-8) can be rewritten by noting the fact that the growth rate G is directly related to the supersaturation σ as is the agitation rate to power input ϵ.

$$B = k_n \sigma^a \epsilon^b M_T^c \tag{2-9}$$

The values for a, b and c are usually deducted from experimental data. Although the power law can describe the steady-state median crystal size (PAON, 2003) it cannot capture the dynamics of a crystallizer (Ó Meadhra, 1995). Over the years some improvements were made to the power law.

The first improvement was made by Eek (Eek, 1995) he implemented the phenomena that only crystals above a certain critical size are prone to attrition. More detailed information about this phenomena can be found in Section 3-6-1. He achieved this implementation by using a so-called target efficiency. Although the model was more accurate it was not a complete solution.

The work of Ó Meadhra (Ó Meadhra, 1995) included an attrition function for the crystals. The total abraded crystal volume was distributed over the small crystal sizes. A disadvantage according to Wolf (Wolf, 2007) is that similar to the power-law this alteration has no predictive value.

A more mechanistic model is the model of Gahn and Mersmann (Gahn and Mersmann, 1997). For a detailed description the reader is referred to the original paper, here only a brief overview is given.

The model considers only crystal-impeller collisions as Gahn and Mersmann (Gahn and Mersmann, 1997) stated these were the most dominant. The model can be described in three steps:

1. Collision frequency and impact energy

   The number of collision of a crystal with the impeller (both faces and edges of the blades) are calculated. For each of these collisions the impact energy is also calculated.

2. Attrition volume and fragment distribution

   The impact energy is related to the abraded crystal volume by some material properties. These properties include hardness, shear modulus and effective fracture surface energy.

The distribution of the crystal fragments is limited in minimum size by the material properties and in maximum size by the magnitude of the impact energy.

3. Growth of attrition and parent crystals

   The growth rate of the crystals is calculated by an expression similar to the one described in Section 3-6-2. It also accounts for crystals with high internal stress dissolving.

An important assumption in model of Gahn and Mersmann (Gahn and Mersmann, 1997) is the fact that attrition occurs at the crystal corners, this is due to the higher local stresses. It is also assumed that the crystals have sufficient time to grow between two subsequent collisions, their corners will therefore redevelop.

The model of Gahn and Mersmann (Gahn and Mersmann, 1997) is mainly based on first-principles (Neumann, 2001) and thus the number of fitting parameters is greatly reduced. Unfortunately there are quite a number of physical properties of which obtaining the values can prove to be a difficult task.

2-6 Agglomeration

Adipic acid is known to agglomerate (David et al., 1991b), this agglomeration behavior can be explained by looking at Figure 2-6(a). In this picture adipic acid crystals are depicted which are created in an industrial crystallizer. The clear difference when compared with the lab scale crystal (Figure 2-6(b)) is the surfboard shape of the crystals. This surfboard shape is hydrophilic and will attract other hydrophilic surfaces. This property increases the agglomeration tendency of adipic acid. The more compact crystals in the lab scale crystallizer are therefore preferred (Ruiter, 2009).

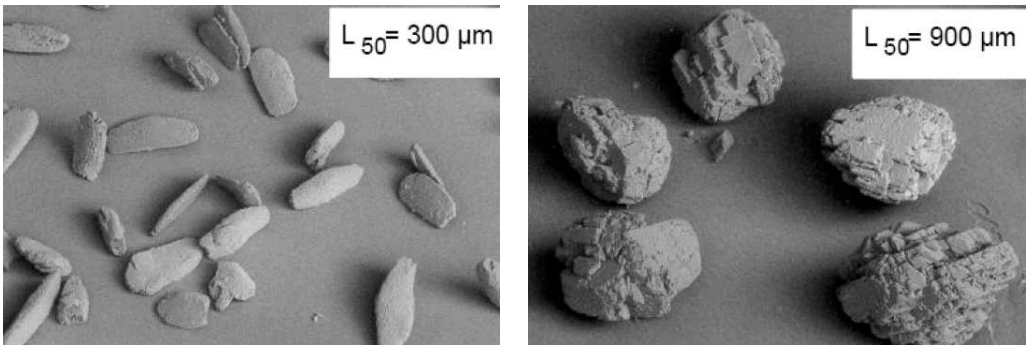

(a) Industrial scale (b) Lab scale

Figure 2-6: The different kinds of adipic acid crystals

Agglomeration kinetics are difficult to describe because of the dependence on many different conditions such as, hydrodynamic condition, the properties of the particles and interactions between particles. For clarity the agglomeration discussed in this report is as depicted in Figure 2-7.

There are two sequential steps which are necessary (Mersmann, 2001):

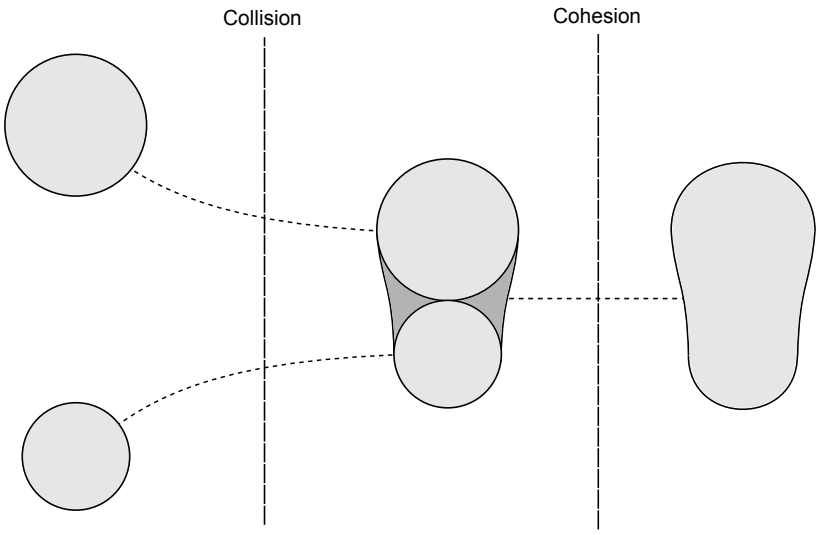

Figure 2-7: Collision and cohesion of two crystals forming an agglomerate

1. First, the particles should collide with each other, this depends on the fluid dynamics, particle size and inter particle forces.
2. Secondly, the particles should cohere, this depends on the tensile strength of the crystalline bridge and the collision and/or shear forces coming from a rotor and/or fluid dynamics.

In order to model the agglomeration of adipic acid crystals expressions describing the rate of agglomeration are needed. Most of the research done on agglomeration is based on the theory of Smoluchowski (Smoluchowski, 1917). The agglomeration rate is usually expressed as:

$$\beta_{Agglo} = \beta_{Coll} * \eta_{Agglo} \tag{2-10}$$

in which β_{Coll} is the collision rate and η_{Agglo} is the agglomeration efficiency. This efficiency can be expressed as:

$$\eta_{Agglo} = \frac{\text{Number of agglomeration events}}{\text{Number of collisions}}. \tag{2-11}$$

2-6-1 Crystal sizes

There are several models describing the collision rate of spheres in an agitated fluid phase. It is important to distinguish between different crystal sizes since different sizes of crystals have different mechanisms by which they collide and thus agglomerate. One can distinguish different types of particle size regimes when comparing the characteristic length and time scales of the particle with the ones of the turbulent motion. Before these models can be described the following parameters are introduced:

Kolmogorov length scale η_{kol} The length scale of the smallest vortices in a turbulent fluid. It is a function of kinematic viscosity ν and energy dissipation rate ϵ.

$$\eta_{kol} = \frac{\nu_f^{3/4}}{\varepsilon^{1/4}} \tag{2-12}$$

Kolmogorov time scale τ_{kol} It is an indicator of the vortex lifetime. Just as the Kolmogorov length scale it is a function of both ν and ϵ.

$$\tau_{kol} = \frac{\nu_f^{1/2}}{\varepsilon^{1/2}} \tag{2-13}$$

Length scale of largest vortices Λ Usually in the same order of magnitude as the object which provides the energy input, i.e. the stirrer.

$$\Lambda = \frac{1}{3} d_{stirrer} \tag{2-14}$$

More on the characteristic time and length scales of both the particles and the turbulence can be found in Section 3-6-3.

Very small crystals

These particles have a length scale much smaller than the length scale of the smallest turbulence or Kolmogorov scale. The particles are also much smaller than their diffusion distance. This is the path they travel due to their Brownian motion. A relative velocity between two crystals can therefore only result from the Brownian motion being in the correct orientation by coincidence this is depicted in Figure 2-8. Brownian motion is the only collision mechanism, as Brownian motion is independent of turbulence so is the collision and thus the agglomeration rate.

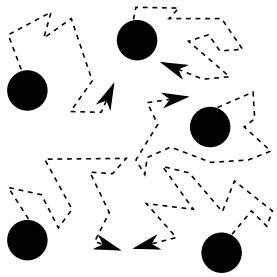

Figure 2-8: Brownian motion as a collision mechanism

Small particles

These particles have a length scale smaller than the Kolmogorov scale. The largest part of collisions in this size range is due to the viscous deformation of the smallest vortices. Due to the viscous forces there will be radial shear gradients in the vortices. Because the crystals are smaller than the length scale of these vortices they move within these profiles. Due to difference in radius of these profiles crystals can overtake each other and thus collide. This mechanism is called the shear mechanism and is depicted in Figure 2-9(a).

Another mechanism which is active in this size range is the inertia mechanism as depicted in Figure 2-9(b). With increasing size of the crystals their inertia also becomes larger. A measure for a particle's inertia is the particle relaxation time τ_p. The particle relaxation

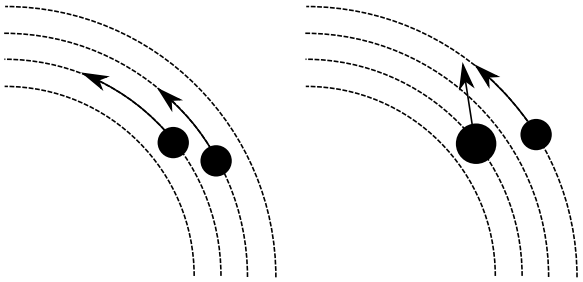

(a) Shear mechanism (b) Inertia mechanism

Figure 2-9: The different kinds of collision mechanisms

time is a measure of how fast a particle reacts to a change in its environment. Due to their inertia particles do not follow the vortices streamlines and can collide which each other. When two crystals have the same size their velocities are correlated and a collision is not possible thus only crystals with different sizes have a relative velocity and can collide by the inertia mechanism. The influence of the inertia mechanism for particles smaller than the Kolmogorov scale is usually small. The influence becomes larger with increasing crystal size and decreasing particle- and fluid velocity correlation.

Large particles

These crystals are larger than the Kolmogorov scale but still smaller than the largest vortices. These particles collide due the the aforementioned inertia mechanism. The main difference is the correlation between the particle- and fluid velocity; this decreases strongly with increasing crystal size.

2-6-2 Collision model

The different size ranges have implications on which model should be used for describing the collision rate. Different models for particle-particle collision exist in literature e.g. (Abrahamson, 1975), (Saffman and Turner, 1956) and (Yuu, 1984). These models are only valid either for crystal sizes below or above the Kolmogorov scale. The typical size range in the adipic acid crystallization at BASF is 5 to 1000 μm according to Riemann and Gerstlauer (Riemann and Gerstlauer, 2003). When the Kolmogorov scale is calculated with Equation (2-12) in becomes clear that the crystal size in the adipic crystallization process are both below and above the Kolmogorov scale. This is the reason why the collision of crystals in the process cannot accurately be described by the above models.

Another disadvantage of the aforementioned models (except Yuu (Yuu, 1984)) is the fact that their theoretical basis is laid in the classical kinetic theory of gases. One would expect some uncertainties if such a model was to be used for modeling particles in a liquid. One phenomena for which these models do not account is "added mass". In fluid mechanics this is "the inertia added to a system because an accelerating or decelerating body must move some volume of surrounding fluid as it moves through it" (Falkovich, 2011).

More recently Kruis and Kuster (Kruis and Kusters, 1996) have developed a model for particle-particle collisions in a liquid. It is also applicable for crystal sizes both below and above the Kolmogorov scale. Due to these unique features this model will be used for modeling the collision part of the agglomeration. More detailed information can be found in Section 3-6-3.

2-6-3 Cohesion model

After collision two particles should cohere to form a larger agglomerate. This cohesion step is controlled by two competing processes (David et al., 1995):

1. Growth of a crystalline bridge between the mother crystals.
2. Turbulent velocity fluctuations on the opposite sides of the agglomerate leads to a shear effect that might separate the two crystals.

The formation of a crystalline bridge requires good contact between the two crystals (David et al., 1991b). The condition can only be met if the smaller crystal is big enough to puncture the boundary layer which surrounds the larger crystal. If the smaller crystal is not large enough it will not puncture the boundary layer but it will slide over it, thus not agglomerating.

In literature there are several models described for modeling the agglomeration efficiency. The first model to be reviewed is the model of David et al. (David et al., 1991b). The authors assume that the sticking probability P_2 (agglomeration efficiency) is proportional to the non-dissociation probability of the two crystals P_3. It is also assumed inversely proportional to the time t_c needed to build up the bridge:

$$P_2 \sim \frac{P_3}{t_c}. \tag{2-15}$$

The time t_c can be estimated by the ratio between the mass of the bridge and the mass flux F_M of solute from the solution:

$$t_c = \frac{\rho_c \mathrm{v}}{F_M} \tag{2-16}$$

in which ρ_c is the crystal density. F_M depends on the growth rate G:

$$F_M = \rho_c s G. \tag{2-17}$$

Here s is the crystalline bridge surface. The volume of the crystalline bridge v can be calculated by:

$$\mathrm{v} = \frac{\pi \mathrm{S_m^2}}{4}\left(\frac{\mathrm{S_m}}{2} + \mathrm{x}\right) - \frac{\pi \mathrm{S_m^3}}{12} - \pi \mathrm{x}^2\left(\frac{\mathrm{S_n}}{2} - \frac{\mathrm{x}}{3}\right) \tag{2-18}$$

in which S_m is the size of the smallest crystal and x is a part of the crystalline bridge length (David et al., 1991b).

The surface of the crystalline bridge can be calculated by:

$$s = \pi S_m \left(\frac{S_m}{2} + x\right) \tag{2-19}$$

in which x can be calculated by:

$$x = \frac{1}{2}\left(S_n - \sqrt{S_n^2 - S_m^2}\right) \tag{2-20}$$

in which S_n is the size of the largest crystal.

The time t_c can be written as:

$$t_c = \frac{S_m}{f(\rho)G} \tag{2-21}$$

in which $f(\rho)$ is a relative shape function of both crystals.

Agglomeration can only occur if both crystals are not separated by the flow before the bridge exists. The source of this fluid shear is the velocity fluctuations. The probability of two points a distance y from each other in a turbulent flow having the same fluctuating component of velocity is expressed by the Eulerian autocorrelation function $F_1(y)$. As the crystals are convected by the average flow the probability of them staying together is the Lagrangian correlation function $F_2(y)$ (David et al., 1991b).

$$F_2(y) = 1 - \frac{y^2}{\lambda_e^2} \tag{2-22}$$

The Lagrangian micro scale λ_e is difficult to estimate and accurate measurements are lacking (David et al., 1991b). For these reasons it is assumed that the order of magnitude of the Lagrangian micro scale is similar to the order of magnitude of the Taylor micro scale λ_g. The Taylor micro scale can be approximated by (Costes and Courderc, 1988):

$$\lambda_g = u'\left(\frac{60\nu}{\varepsilon}\right)^{1/2} \tag{2-23}$$

in which ϵ is the power input. The fluctuating average component of the local velocity u' can be approximated by Laufhütte and Mersmann (Laufhütte and Mersmann, 1985):

$$u' = \sqrt{\frac{\sum_{k=1}^{3} u_k^2}{3}} = 0.3\pi N d_{stirrer}. \tag{2-24}$$

Summarizing the above the sticking probability can be approximated:

$$P_2 \sim \left[1 - \frac{(S_n + S_m)^2}{\lambda_e^2}\right] H(\lambda_e - S_n - S_m)\frac{f(\rho)G}{S_m}. \tag{2-25}$$

The authors Baldyga et al. (Baldyga et al., 2003) suggested additional models for the agglomeration efficiency.

$$\eta_{Agglo} = \exp(-t_c/t_r) \tag{2-26}$$

$$\eta_{Agglo} = (1 + k_\psi t_c/t_r)^{-1} \tag{2-27}$$

In which t_c is the cementation time required to build the crystalline bridge. T_r is the average interaction time i.e. the time between two rupture events. The parameter k_ψ is a empirical parameter. Equation (2-26) is based on theory for drop coalescence (Chester, 1991). The experiments of Baldyga and Mersmann (Baldyga et al., 2003) showed the the agglomeration rate is proportional to the growth rate. This proportionality can described better by (2-27). The cementation time and average interaction time can be approximated by different expressions which will be reviewed in this Section.

The cementation time can be approximated by considering a force balance of the particle doublet in the turbulent flow (Ilievski and Livk, 2006).

$$t_c \propto \frac{\gamma {L_m}^2}{\sigma_c \lambda_c G} \tag{2-28}$$

In which γ is the local shear rate, L_m is the mean diameter of the doublet, σ_c is the fracture strength of the crystalline bridge, λ_c is the contact length between two crystals and G is the growth rate.

Different expressions for the cementation time can be written, depending on the assumptions one makes. If λ_c and σ_c are assumed constant one obtains (Lindenberg et al., 2007):

$$t_c = k_c \frac{\gamma {L_m}^2}{G} \tag{2-29}$$

in which k_c accounts for the hydrodynamics, material properties and contact geometry. Another expression for t_c is derived by Baldyga and Mersmann (Baldyga et al., 2003):

$$t_c = \frac{1}{f(L,\lambda)} \frac{\sqrt{\rho_c (\varepsilon/\nu)^{0.5}} L_m}{G} \tag{2-30}$$

in which $f(L,\lambda)$ is a shape function defined by David et al. (David et al., 1995) and ν is the kinematic viscosity.

If one also distinguishes the type of contact between the two crystals additional expressions can be found in literature (Ilievski and Livk, 2006):

$$t_c = k_c \frac{\sqrt{\rho \nu (\varepsilon/\nu)^{0.5}} L_m}{G} \quad \text{Point contact} \tag{2-31}$$

$$t_c = k_c \frac{\rho \nu (\varepsilon/\nu)^{0.5} L_m}{G} \quad \text{Line contact} \tag{2-32}$$

in which ρ is the liquid density. For the average interaction time also multiple expressions can be derived. T_t is interpreted as the lifetime of the small turbulent eddies (Baldyga et al., 2003). This lifetime is equivalent to the Lagrangian time micro scale τ_l which can be expressed as:

$$t_t = \tau_L \approx {\mathrm{Re}_\lambda}^{0.5} (\nu/\varepsilon)^{0.5}. \tag{2-33}$$

Here, Re_λ is the Taylor micro scale Reynolds number. The authors Hounslow et al. (Hounslow et al., 2001) defined the average interaction time as:

$$t_t = \tau_{kol} = \left(\frac{\nu}{\varepsilon}\right)^{0.5} \tag{2-34}$$

in which τ_{kol} is the Kolmogorov time micro scale. According to Rielly and Marquis (Rielly and Marquis, 2001) the lifetime of a turbulent eddy is given by:

$$t_t = \frac{C_\mu^{3/4}}{\sqrt{2}} \frac{k}{\varepsilon} \tag{2-35}$$

in which $C_\mu = 0.09$ is a model constant in the $k - \epsilon$ turbulence model and k is the turbulent kinetic energy which is calculated by (Yuu, 1993):

$$k = 1.5\left(\frac{\varepsilon d_{imp}}{A''}\right)^{2/3} \tag{2-36}$$

in which A'' has a value of 6.5 (Laufhütte and Mersmann, 1985).

Another model is the model of Riemann and Gerstlauer (Riemann and Gerstlauer, 2003). The authors state that the formation of the crystalline bridge is counteracted by both mechanical and fluid dynamical effects i.e. collisions with the stirrer and fluid shear. In this model it is assumed that all the agglomeration events occur just after the crystals have passed the stirrer. In this way the crystals will have one residence time to grow a crystalline bridge without being disrupted. Thus this efficiency model only treats the disruption by fluid shear forces. The fluid shear effect is caused by a difference in the turbulent velocity fluctuations on the opposite sides of the agglomerate. The smaller the difference in the velocity fluctuations the smaller the fluid shear forces.

The similarity of the velocity fluctuations can be described by a correlation function which is a function of the distance d. The distance d is defined differently than in the work of David et al. (David et al., 1991b). In this model the following expression is used:

$$d = 2\frac{d_1 d_2}{d_1 + d_2} \tag{2-37}$$

in which d_1 and d_2 are the diameters of the crystals considered. The aforementioned correlation function can be approximated by an exponential function (Riemann and Gerstlauer, 2003). This assumption is only valid if the distance d is larger than the Kolmogorov scale.

$$\eta_{Agglo} = \exp\left(-a_5 \frac{d}{\Lambda}\right) \tag{2-38}$$

In which a_5 is a fitting factor for experimental data.

All the models considered fluid shear as the main disruptive force. The way fluid shear is modeled differs between the models but they all use a correlation function for the similarity of the fluctuating fluid velocity. All models except the model of Riemann and Gerstlauer (Riemann and Gerstlauer, 2003) are dependent on the supersaturation or growth rate. According to Mersmann (Mersmann, 2001) the agglomeration efficiency should be used as a fitting factor due to the fact that the real mechanisms are complex and difficult to describe.

The model by Riemann and Gerstlauer (Riemann and Gerstlauer, 2003) is chosen for specific reasons:

1. The efficiency model in combination with the collision kernel of Kruis and Kusters (Kruis and Kusters, 1996) has already been successfully used to model small scale lab reactors crystallizing adipic acid (Riemann and Gerstlauer, 2003).
2. Dependent on fluid shear (power input) and size-dependent (David et al., 1991b) while still able to be fitted to experimental data.
3. Due to the fact that the agglomeration efficiency is not a direct function of supersaturation the calculation of the total agglomeration rate will have a smaller computational burden which can be beneficent for control purposes. This computational burden is caused by the way that the agglomeration flux is calculated (see Section 3-5-3).

2-7 Population balance equation

The population balance equation was introduced by Hulbert and Katz (Hulburt and Katz, 1964) and was later formulated for crystallization processes by Randolph and Larson (Randolph and Larson, 1988). The PBE is a well-established mathematical framework for dynamic modeling of particle size distribution in particulate systems (Ramkrishna, 2000).

In case of a crystallization process in which the crystallizer volume is constant and the process includes crystal nucleation and growth the one-dimensional PBE can be written as (Mersmann (2001)):

$$\frac{\partial n}{\partial t} = -\frac{\partial (Gn)}{\partial L} + B(L) - D(L) + \sum_i \frac{\dot{V}_i n_i}{V_C}. \tag{2-39}$$

A full derivation of this equation can be found in Appendix A.

In Equation (2-39) the term $\partial n/\partial t$ is the change of the number density with time. The first term on the right side $\partial(Gn)/\partial L$ is the difference between the crystals growing in and out of the size range dL. The terms $B(L)$ and $D(L)$ are the birth and death term respectively. These terms account for phenomena like attrition, agglomeration, breakage and dissolution.

Let us consider the number of crystals within a small size interval between L and $L + \Delta L$ and a differential time period, see Figure 2-10. Crystals smaller than size L can enter this size interval by crystal growth but crystals with a size L to $L + \Delta L$ can grow out of this size interval.

Besides growth crystals can also enter or exit this size interval by other mechanisms. Abrasion, agglomeration, dissolution and breakage are usually incooperated in a birth and a death term.

Crystals can also enter the size domain via the feed (only if the feed contains crystals). The crystals can also exit the size domain via product removal. Within the PBE the hydrodynamic terms like the feed and the product removal are usually combined. This is the last term on the right hand side of equation (2-39).

An equation like Equation (2-39) can't be solved analytical except for very simple cases (Kumar and Ramkrishna, 1997). There are numerous numerical techniques to solve the PBE each with their own merits and drawbacks. Numerical solution of an PBE is usually accompanied with some problems like numerical diffusion and stability issues (Mesbah, 2010).

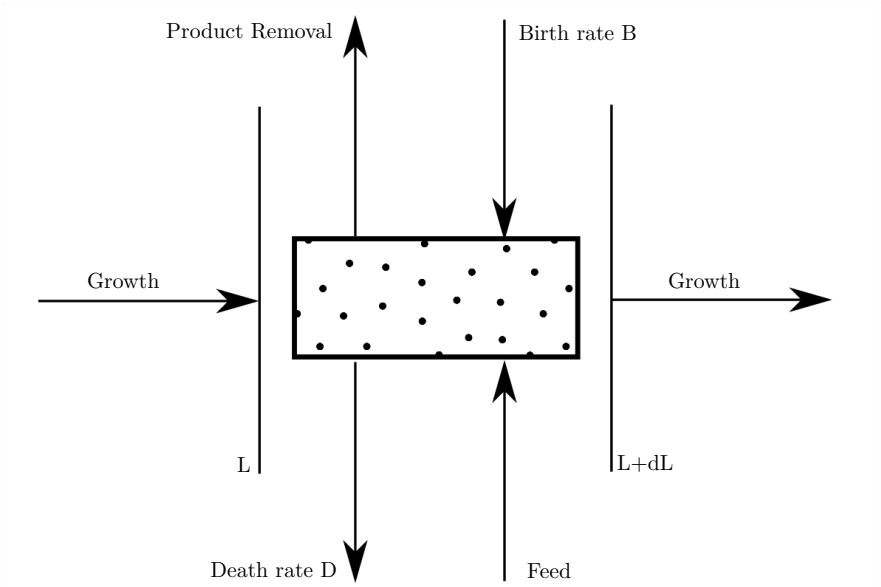

Figure 2-10: Change in the number of crystals per unit volume in the crystal size range L and L+dL from Mersmann (Mersmann, 2001)

Numerical diffusion is a phenomena which can be explained by an example based on the "advection equation" (Figure 2-11):

$$\frac{\partial C}{\partial t} + U\frac{\partial C}{\partial x} = 0. \tag{2-40}$$

This equation describes a purely advective process without any diffusion. The scalar property C is advected over distance x by the velocity U. The formal solution (blue) is that the initial profile shifts over the x-axis without changing shape (Fitzpatrick, 2011). The numerical solution (red) depicts the initial profile shifted over the x-axis by the same amount as the formal solution but the solution is smeared i.e. the peak has lowered and widened. This phenomena of smearing is called numerical diffusion, the solution behaves as if diffusion is present where it physically is not.

In this work (numerical) stability designates that any numerical errors introduced at some stage of the calculation are propagated in a mild fashion i.e. do not blow up in the subsequent steps of the method (Spijker, 1998). An example of numerical instability in solving a PBE is the calculation of negative number densities which are physically impossible.

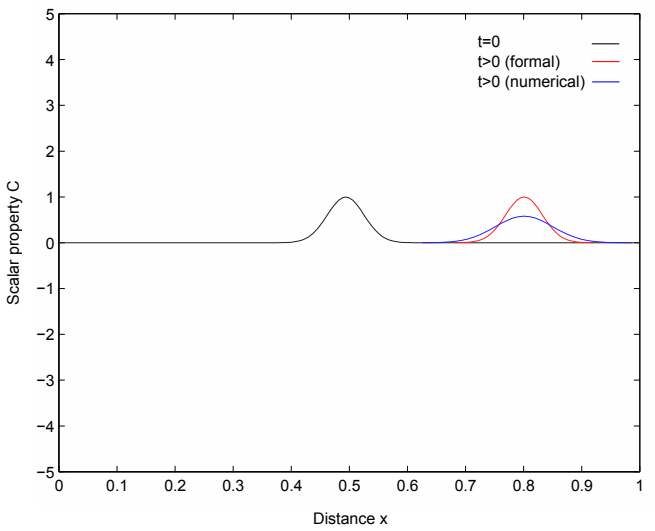

Figure 2-11: Advection equation; initial profile, formal and numerical solution

These problems are usually caused by the convective nature of the PBE. In the case of steep moving fronts and/or sharp discontinuities in the solution these problems become even more pronounced (Mesbah, 2010). These complexities have awakened the attention of many researchers to develop specialized algorithms. A short review of the different solving methods is given below. It does not act as a complete overview of all methods available, it is merely an introduction for the most commonly used schemes. For a complete review of up to date numerical schemes for the PBE the reader should consult (Mesbah, 2010), (Costa et al., 2007) or (Ramkrishna, 2000). In this report five categories of solving methods are distinguished:

- Method of moments
- Finite difference methods
- Discretization techniques
- Method of weighted residuals
- Monte Carlo simulation

2-7-1 Method of moments

The method of moments was the first numerical method for the solution of a PBE (Hulburt and Katz, 1964). This method has been widely used because of the efficiency and accuracy when coupled with CFD (Su et al., 2009). The PBE is transformed into a system of ordinary differential equations. These ordinary differential equations give the solution for the moments of the distribution. A clear disadvantage is the fact that it is not possible to retrieve the full distribution from the moments due to the fact that this problem is ill-conditioned (Randolph and Larson, 1988). According to Mesbah (Mesbah, 2010) another disadvantage is the fact that for some combinations of crystallization mechanisms (e.g. agglomeration/breakage) it is impossible to transform the PBE to closed system of moment equations. For more detailed

information the reader is referred to (Hulburt and Katz, 1964) and (Randolph and Larson, 1988).

2-7-2 Finite difference methods

According to Carnahan and Luther (Carnahan and Luther, 1990) finite difference methods are the most popular methods to solve a PDE. When a finite difference method is applied to a PBE, the partial differential terms of the PBE are approximated by finite differences. This is done by discretizing the size domain between the minimum and the maximum crystal sizes (Lee et al., 1999). According to Mesbah (Mesbah, 2010) finite difference methods may not adequately cope with the hyperbolic nature of the PBE. This could result in numerical diffusion which causes the broadening of sharp discontinuities. Another drawback of these solution methods is the fact that they conserve mass and numbers only if the number of grid cells is infinite (Patankar, 1980). A high or infinite number of grid cells translates into a high computational burden. The above drawbacks make finite difference methods less attractive for solving a PBE in a crystallization process.

2-7-3 Discretization techniques

This category comprises of both discretized population balances and finite volume methods. In the discretized population balance methods the spatial domain is divided into a finite number of grid cells. The continuous PBE is converted into a series of discrete equations by use of the mean-value theorem . This method has been used extensively in literature (David et al., 1991b), (Lister et al., 1995) and (David et al., 2003). Although this technique allows for the determination of the desired characteristics the complete construction of the entire distribution is subject to errors (Mesbah, 2010). Another drawback of this method is the fact that it often exhibits oscillatory behavior which results in negative number densities but also numerical diffusion at discontinuous fronts (Mesbah, 2010).

Recently High Resolution Finite Volume Methods (HR-FVM) used originally for gas dynamics are also used for solving the PBE. These methods are the state-of-the-art in aerodynamics, astrophysics, detonation waves and related fields where shock waves occur (LeVeque, 2004). These HR-FVM have been specifically developed to provide high accuracy while avoiding numerical diffusion and numerical dispersion (non physical oscillations) associated with other finite difference and finite volume methods (Gunawan et al., 2004). An advantage of these HR-FVM is that they are general purpose; the simulation code can be quickly modified to solve a particular problem of interest (Gunawan et al., 2004). Recently Qamar and Warnecke (Qamar and Warnecke, 2007) used HR-FVM with a flux limiter to successfully model crystallization processes including nucleation, growth and agglomeration.

2-7-4 Method of weighted residuals

The weighted residuals comprise of methods that retrieve the distribution by approximating the solution with a series of trial functions, whose coefficients are to be determined so that their sum will satisfy the PBE (Costa et al., 2007). Within the method of weighted residuals two different classes can be distinguished:

1. Weighted residual methods with global function
2. Finite element methods

The weighted residuals method with global functions is unable to capture the features of an arbitrarily shaped distribution. This is especially true if the distribution exhibits sharp changes and discontinuities (Rigopoulos and Jones, 2003). The trial functions can be tailored to accommodate a resulting distribution if knowledge about the shape of the resulting distribution is available a priori. According to Costa et al. (Costa et al., 2007) the method will in this converge and might even become computationally attractive.

The finite element methods on the other hand are capable of capturing sharp discontinuities. This is due to the fact that the solution is approximated with piecewise low-order polynomials that are locally nonzero (Rigopoulos and Jones, 2003). Thus their advantages are the accurate reconstruction of the distribution and their flexibility to cope with any formulation of the PBE. The drawbacks are the fact that it cannot cope with discontinuous distributions and steep fronts (Mesbah, 2010).

2-7-5 Monte Carlo methods

According to Gooch and Hounslow (van Peborgh Gooch and Hounslow, 1996) the Monte Carlo (MC) method is an alternative to posing and solving PBE. MC simulations were first applied to particulate processes by Spielman and Levenspiel (Spielman and Levenspiel, 1965). They studied the influence of coalescence on reactions in the dispersed phase of two-phase systems. Shah et al. (Shah et al., 1977) developed a general simulation for particulate processes.

Whenever the Crystal Size Distribution (CSD) is affected by many factors discretizing and numerically solving a PBE becomes increasingly arduous. Such complex processes lend themselves to study by MC simulations, the intrinsic simplicity of which allows the inclusion of several mechanisms and several internal coordinates in the problem (van Peborgh Gooch and Hounslow, 1996) and (Lin et al., 2002).

MC uses probabilistic tools to sample a finite subset of a system in order to infer its properties. Thus instead of discretizing the PBE and then numerically integrating it, a MC simulation simulates the evolution of the system as a series of particulate events (Shah et al., 1977). Each event may influence one or more particles, thereby altering the property distribution and the system behavior as a whole. Instead of expressions coupled to the PBE the particulate phenomena (kinetics) are described in terms of their transition probabilities usually referred to as frequencies.

Other advantages are the possibility to study finite-size effects, spatial correlations and local fluctuations. This is something that cannot be done by continuum mean field treatment (Smith and Matsoukas, 1998). A drawback of MC is that the method is typically computationally expensive.

Chapter 3

Modeling approach

3-1 Introduction

The modeling framework used in this thesis is depicted in Figure 3-1. When modeling a crystallization process there are two distinct phases one should model; the continuous liquid phase and the dispersed solid phase. The continuous phase is usually modeled using mass and energy balances. The dispersed solid phase is modeled using a Population Balance Equation (PBE). These two phases are connected by the crystallization kinetics i.e. nucleation, growth and agglomeration.

This Chapter starts with a Section explaining the process which is modeled. The subsequent Section discusses the modeling purpose. Based on the modeling purpose several assumptions are done which are reviewed in Section 3-4. Section 3-5 discusses the modeling of the dispersed solid phase. The crystallization kinetics are reviewed in Section 3-6. The modeling of the continuous liquid phase is discussed in Section 3-7. Section 3-8 gives an overview of the modeling framework.

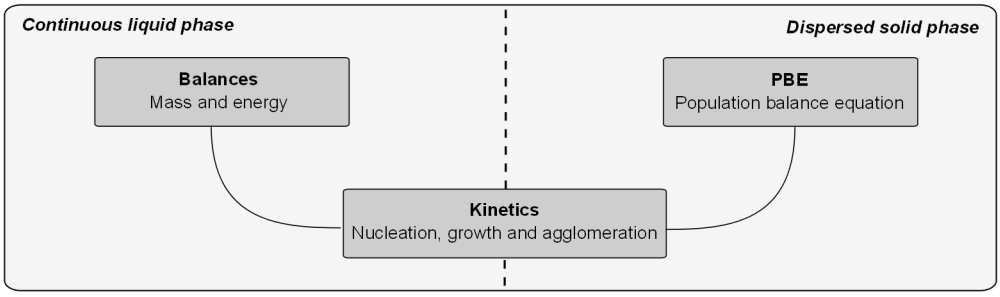

Figure 3-1: Modeling framework, the continuous liquid phase and dispersed solid phase are connected trough the kinetics

3-2 Process description

The final step in the production process of adipic acid is the crystallization from solution. At BASF Ludwigshafen this is done in a so-called Draft Tube Baffle (DTB) crystallizer. This type of crystallizer allows for larger crystals to grow and small crystals to be dissolved in the recirculation loop. In the crystallizer there is a slow moving impeller which thrusts the solution upwards. Small crystals move upwards to the solution surface where there is the highest supersaturation and they grow out. At a certain crystal size the gravitational force on the crystal is larger than the impellers thrust and thus this crystal will settle in the bottom where it is removed as product.

The feed (S02) stream in Figure 3-2 enters the crystallizer and contains a solution of adipic acid and water, it does not contain any crystals.

The DTB crystallizer is operated at adiabatic evaporative cooling i.e. the solvent is evaporated by the use of vacuum, this creates the supersaturation. This vacuum is created using a steam ejector. A steam ejector makes use of the venturi effect to create an under pressure. For high vacuum multiple ejectors are needed. This evaporation of the solvent creates a vapor flow (S04) which is removed from the crystallizer.

The product stream (S05) is split into two separate streams. One of these streams is heated by the heat exchanger and is recirculated into the crystallizer (S06). The other stream is the final product stream (S07) which is redirected to subsequent process steps such as centrifugation and drying.

The process flow diagram of the crystallizer in use at BASF is depicted in Figure 3-2. An overview of the normal operating conditions is given in Table 3-1.

Table 3-1: Normal operating conditions for the DTB crystallizer

Operating condition	Sensor	Value	Units
Feed flow rate	F1229	18	m^3/hr
Recirculation flow rate	F1501	60	m^3/hr
Product flow rate	F1331	16	m^3/hr
Crystallizer temperature	T1502	60	$C°$
Product temperature	T1503	60	$C°$
Recirculation temperature	T1501	65	$C°$
Crystallizer pressure	P1500	0.2	bar
Crystallizer level	L1501	74	%
		34	m^3

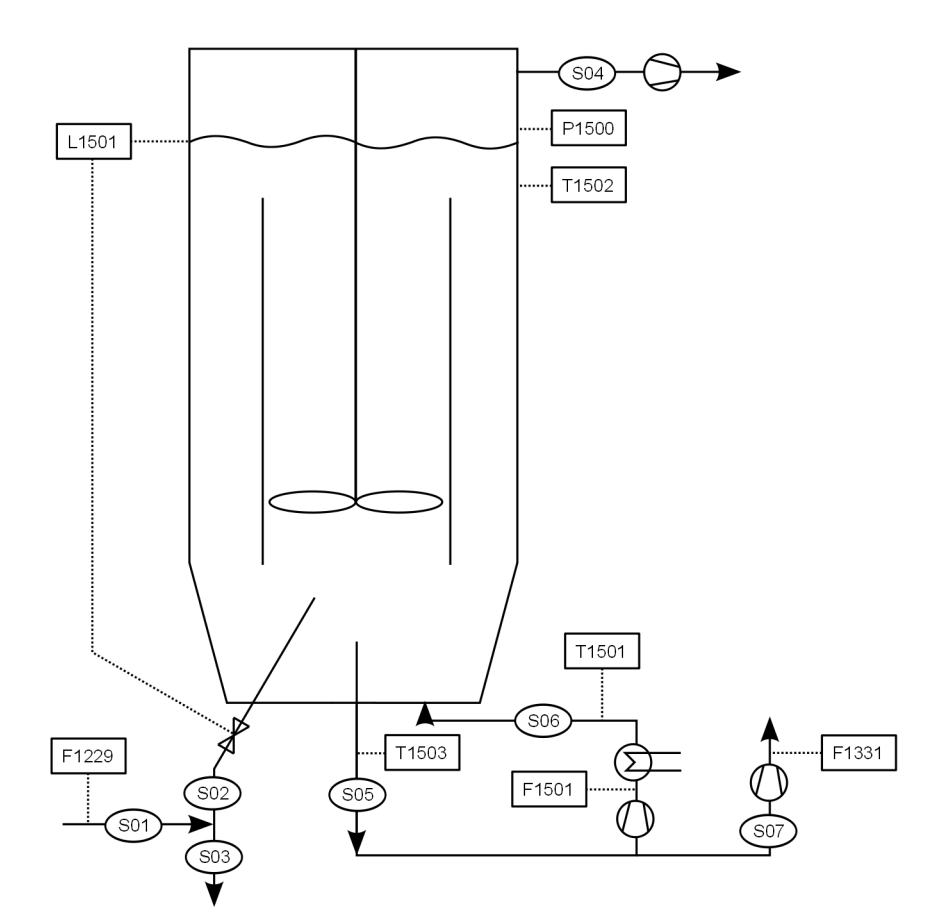

Figure 3-2: Process flow diagram of the DTB crystallizer at BASF Ludwigshafen (flow sensors S, temperature sensors T and pressure sensors P)

3-3 Modeling purpose

The intended use of the model dictates the assumptions one makes and the equations one uses. The intended use of the model developed in this thesis is model-based control. From a control point of view, the main criteria which should be controlled are the properties of the produced crystals i.e. size distribution and mean size (Moldovanyi and Lakatos, 2005). As mentioned earlier these properties greatly influence the downstream processing of the crystal product.

In model-based control applications, empirical power-law functions are the most commonly used kinetic relationships to model the total nucleation rate and the size-independent growth rate (Braatz and Hasebe, 2002). In this thesis empirical functions are used for both the growth and the secondary nucleation rate. More information can be found in Sections 3-6-1 and 3-6-2 respectively.

3-4 Model framework assumptions

In order to restrict the complexity of the model the following simplifying assumptions are made:

- crystallizer can be modeled by a well-mixed single compartment
- constant temperatures of feed, output, recirculation and product stream;
- a crystal-free feed stream;
- constant crystallization volume;
- equal liquid fractions of the output, recirculation and product stream;
- equal number densities of the output, recirculation and product stream;
- negligible power input by the impeller;
- negligible heat of crystallization;
- negligible heat losses to the environment;
- temperature of the output stream is equal to the crystallizer temperature;
- the solid phase is pure and single-component;
- solute and crystal-free vapor stream;
- constant material properties during the isothermal operation;
- negligible primary nucleation and breakage;
- formation of nuclei of infinitesimal size;
- size-independent growth of crystals;
- the attrition caused by the recirculation pump is negligible;

3-5 Dispersed solid phase

3-5-1 Population balance equation modeling

As discussed in Section 2-7 there are different methods for solving a PBE. Each method has its advantages and drawbacks. The method chosen for this model is a high order finite volume method with flux limiter. This method is capable of describing sharp discontinuities and steep moving fronts (Qamar and Warnecke, 2007). Model-based control strategies require that the numerical solutions should be obtainable in a time-scale commensurate with the process time scale (Kumar and Ramkrishna, 1997). The computational burden is relatively low compared to the other types of solution methods (Mesbah, 2010). The aforementioned characteristics makes the high order finite volume method with flux limiter best suited for the solution of the PBE in on line control applications (Mesbah, 2010). In the next Section the underlying notion of the high order finite volume method is reviewed.

3-5-2 High order finite volume method with flux limiter

The finite volume methods involve discretization of the spatial variable domain and the use of piecewise functions to approximate derivatives with respect to the spatial variable (Mesbah, 2010). The procedure results in a Ordinary Differential Equation (ODE) for each grid point. This system of ODE's can be solved by any standard ODE solver (Qamar, 2008).

This procedure is explained below for a relatively simple case. The following equation is a PBE which only accounts for crystal growth (Qamar, 2008):

$$\frac{\partial n}{\partial t} = -\frac{\partial \left[Gn\right]}{\partial L}. \tag{3-1}$$

The spatial variable L is divided into a number of subintervals Ω_i with $i = 1, ..., N$ and Ω_i is bounded by the cell boundaries $(L_{i-1/2}, L_{i+1/2})$ this is depicted in Figure 3-3(a).

The cell centered finite-volume discretization of Equation (3-1) results in:

$$\int_{\Omega_i} \frac{\partial n_i}{\partial t} = -\left[(Gn)_{i+1/2} - (Gn)_{i+1/2}\right]. \tag{3-2}$$

The average value of the number density in each cell Ω_i is defined as:

$$n_i = \frac{1}{\Delta L}\int_{\Omega_i} n dL. \tag{3-3}$$

Equation (3-2) can then be written as:

$$\frac{\partial n_i}{\partial t} = -\frac{\left[(Gn)_{i+1/2} - (Gn)_{i+1/2}\right]}{\Delta L}. \tag{3-4}$$

Equation (3-4) shows that both the values for growth and the number density are required at the cell-face. For growth these values can be directly obtained from the kinetics. The estimation of the number density at the cell-face poses a difficulty as only the values at

the cell centers are known. According to Qamar (Qamar, 2008) the way the cell-face fluxes $(\mathrm{Gn})_{i\pm1/2}$ are approximated mainly determines the accuracy of a finite volume method.

The cell-face fluxes can be approximated by a first order upwind scheme:

$$(\mathrm{Gn})_{i+1/2} = (Gn)_i, \quad (\mathrm{Gn})_{i-1/2} = (Gn)_{i-1}. \tag{3-5}$$

According to Mesbah (Mesbah, 2010) this scheme does not exhibit instability but it does suffer from numerical diffusion unless a fine grid mesh is used thus increasing the computational burden. There are numerical schemes that exhibit less numerical diffusion; the higher order linear or quadratic interpolation schemes are such schemes. Qamar (Qamar, 2008) uses a piecewise polynomial interpolation formula:

$$(\mathrm{Gn})_{i+1/2} = (Gn)_i + \frac{1+k}{4}((Gn)_{i+1} - (Gn)_1) + \frac{1-k}{4}((Gn)_i - (Gn)_{i-1}),$$

$$(\mathrm{Gn})_{i-1/2} = (Gn)_{i-1} + \frac{1+k}{4}((Gn)_i - (Gn)_{i-1}) + \frac{1-k}{4}((Gn)_{i-1} - (Gn)_{i-2}). \tag{3-6}$$

In Equation (3-6) $k \in [-1, 1]$ and for different values of k it will result in a weighted blend between the central and the fully one-sided scheme. Unfortunately this high order scheme suffers from under- and overshoot and lack of positivity in regions of truly strong variations (Qamar, 2008). This drawback can be relieved by implementing a flux limiter.

A flux limiter provides a way to achieve positivity of the solution. This limiting function defines a high order accurate scheme in smooth regions of the solution where no wiggles will arise. When there is a sharp gradient in the solution the limiter prevents wiggles and enforces positivity. The limiter function is a switch between a high order and a first order scheme (Qamar, 2008).

With the flux limiter implemented, Equation (3-6) can be written as:

$$(\mathrm{Gn})_{i+1/2} = (Gn)_i + \frac{1}{2}\left(\frac{1-k}{2} + \frac{1+k}{2} r_{i+1/2}\right)\left((Gn)_i - (Gn)_{i-1}\right). \tag{3-7}$$

In which $r_{i+1/2}$ is the flux limiter which will be discussed in the next section.

This section showed the steps to discretize the PBE for a simple test case and reviewed the underlying notion of the high order finite volume method with flux limiter. In the next Section the derivation of the actual discretized process PBE is given.

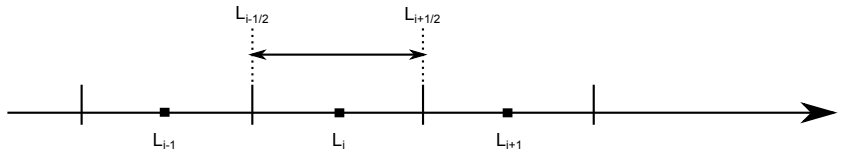

(a) Regular cell centered finite volume grid (Qamar, 2008)

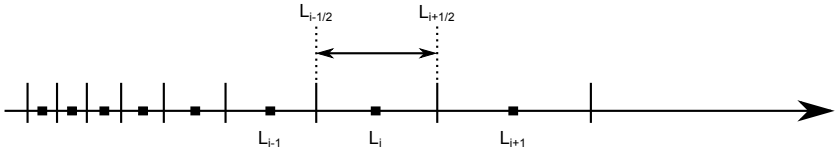

(b) Geometrical cell centered finite volume grid

Figure 3-3: The different kinds of size discretization grids

3-5-3 Process model PBE

Size domain discretization

As mentioned in the previous chapter when numerically solving the PBE the first step is to discretize the size-domain. For this discretization two types of grids are possible.

Regular grid (Figure 3-3(a)) If N is the total number of grid cells, a grid of $[L_{min}, L_{max}]$ is denoted by $(L_{i-1/2})_{i\in\{1,...,\mathrm{N+1}\}}$. In which L_{min} is the lower bound and L_{max} is the upper bound value of size domain. The grid center and boundary values are given by:

$$\begin{aligned} L_i &= \left(\frac{L_{i-1/2} + L_{i+1/2}}{2},\right) \\ L_{1/2} &= L_{min}, \quad L_{N+1/2} = L_{max}, \\ L_{i+1/2} &= L_{min} + i\Delta L_i, \quad \text{for i=1,2,...N-1} \\ \Delta L_i &= L_{i+1/2} - L_{i-1/2}. \end{aligned} \tag{3-8}$$

Geometrical grid (Figure 3-3(b)) In some cases it is useful to use a geometric grid, this type of grid can capture initial profiles properly. The reason for this is that the initial step sizes are much smaller then the final step size. A typical geometric grid is given by:

$$L_{i+1/2} = L_{min} + 2^{(i-N)/q}(L_{max} - L_{min}). \tag{3-9}$$

Discretizing the PBE

The most important equation in the model is the PBE given by equation (2-39). Based on the assumptions stated in Section 3-4 the PBE can be written as:

$$\frac{\partial n(t,L)}{\partial t} + \frac{\partial [G(t,L)n(t,L)]}{\partial L} = \frac{\dot{V}_{rec} n(t,L)}{V} - \frac{\dot{V}_{out} n(t,L)}{V} + {K^{\pm}}_{agg}(t,L) \tag{3-10}$$

In which $n(t,L)$ is the length based number density, $G(t,L)$ is the crystal growth and $K^{\pm}_{agg}(t,L)$ is the agglomeration term. The agglomeration term is defined as:

$$K^{\pm}{}_{agg}(t,L) = \frac{1}{2}\int_0^x \beta(t,x-x',x')f(t,x-x')f(t,x')dx' - \int_0^\infty \beta(t,x,x')f(t,x)f(t,x')dx' \tag{3-11}$$

in which x is the crystal volume, the first term of Equation (3-11) accounts for the formation of particles with a volume x resulting from the merging of two particles with a volume x' and $x-x'$ respectively. The second term is a death term describing the loss of particles of volumes x by agglomeration with other particles of any size. The agglomeration coefficient β_{agg} describes the rate at which crystals of volume x and x' produce a particle of volume $x+x'$. This is a non-negative and symmetrical function.

In order to apply the finite volume scheme, Equation (3-10) should be discretized. Instead of discretizing the original PBE the PBE is first multiplied by the crystal volume $k_v L^3$. This multiplication results in a conservative finite volume formulation. The authors Filbet and Laurencot (Filbet and Laurencot, 2004) have rewritten the PBE for aggregation problems in a form which can be readily solved by a finite volume scheme. This rewritten PBE is also a conservative finite volume discretization. This scheme was thoroughly validated from a theoretical and numerical point of view (Qamar, 2008). Thus by discretizing the PBE multiplied by the crystal volume the agglomeration flux can conveniently and accurately be implemented.

$$\begin{aligned} k_v L^3\frac{\partial n(t,L)}{\partial t} + k_v L^3\frac{\partial[G(t,L)n(t,L)]}{\partial L} &= k_v L^3\frac{\dot{V}_{rec}n(t,L)}{V} - k_v L^3\frac{\dot{V}_{out}n(t,L)}{V} + ... \\ & \quad k_v L^3 Q_{agg}(t,L). \end{aligned} \tag{3-12}$$

The second term on the left hand side can be rewritten by using the product rule for derivatives. For $\tilde{n}(t,L) = k_v L^3 n(t,L)$ equation (3-12) can be rewritten as:

$$\begin{aligned} \frac{\partial\tilde{n}(t,L)}{\partial t} &= -\frac{\partial[G(t,L)\tilde{n}(t,L)]}{\partial L} + 3\frac{G(t,L)\tilde{n}(t,L)}{L} + \frac{\dot{V}_{rec}\tilde{n}(t,L)}{V} - ... \\ & \quad \frac{\dot{V}_{prod}\tilde{n}(t,L)}{V} - \frac{\partial\tilde{F}'_{agg}(t,L)}{\partial L}. \end{aligned} \tag{3-13}$$

Equation (3-13) is integrated over the control volume $\Omega_i = [L_{i-1/2}, L_{i+1/2}]$.

$$\begin{aligned} \int_{\Omega_i}\frac{\partial\tilde{n}(t,L)}{\partial t} &= -\int_{\Omega_i}\frac{\partial[G(t,L)\tilde{n}(t,L)]}{\partial L} + 3\int_{\Omega_i}\frac{G(t,L)\tilde{n}(t,L)}{L} + \int_{\Omega_i}\frac{\dot{V}_{rec}\tilde{n}(t,L)}{V} - ... \\ & \quad \int_{\Omega_i}\frac{\dot{V}_{prod}\tilde{n}(t,L)}{V} - \int_{\Omega_i}\frac{\partial\tilde{F}'_{agg}(t,L)}{\partial L}. \end{aligned} \tag{3-14}$$

If $\tilde{n}_i = \tilde{n}_i(t)$ equation (3-14) becomes:

$$\frac{\partial\tilde{n}_i}{\partial t} = -\frac{1}{\Delta L}[(G\tilde{n}_i)_{i+1/2} - (G\tilde{n}_i)_{i-1/2}] - \frac{1}{\Delta L}[F_{i+1/2} - F_{i-1/2}] + 3\frac{G_{i+1/2}\tilde{n}_i}{L_i} + \frac{\dot{V}_{rec}\tilde{n}_i}{V} - \frac{\dot{V}_{prod}\tilde{n}_i}{V} \tag{3-15}$$

in which the fluxes for growth and agglomeration (from Filbet and Laurencot (Filbet and Laurencot, 2004)) can be calculated by:

$$(G\tilde{n})_{i+1/2} = G_{i+1/2}\left(\tilde{n}_i + \frac{\Delta L_i}{2\Delta L_{i-1/2}}\phi(r_i^+)(\tilde{n}_{i+1} - \tilde{n}_i)\right), \tag{3-16}$$

$$(F)_{i+1/2} = 3k_v L^2\left(\sum_{k=0}^{i}\Delta x_k \tilde{n}_k\left\{\sum_{j=\alpha_{i,k}}^{N}\int_{\Omega_j}\frac{\beta(x',x_k)}{x'}dx'\tilde{n}_j + \int_{x_{i+1/2}-x_k}^{x_{\alpha_{i,k}-1/2}}\frac{\beta(x',x_k)}{x'}dx'\tilde{n}_{\alpha_{i,k}-1}\right\}\right). \tag{3-17}$$

In which $\phi(r_i^+)$ is the flux limiter, it is defined as:

$$\phi(r_i^+) = \frac{|r_i{}^+| + r_i{}^+}{1 + |r_i{}^+|}, \tag{3-18}$$

$$r_i{}^+ = \frac{\tilde{n}_i - \tilde{n}_{i-1} + \varepsilon}{\tilde{n}_{i+1} - \tilde{n}_i + \varepsilon}. \tag{3-19}$$

In the above equation $r_i{}^+$ is called the upwind-ratio of two consecutive solution gradients and is always evaluated with a small value for $\epsilon = 1e^{-10}$ to avoid a division by zero.

3-6 Crystallization kinetics

3-6-1 Nucleation modeling

Secondary nucleation model

Secondary nucleation is the process where nuclei are formed in the presence of crystals. In reality crystals are born over a distribution of sizes and exhibit a size dependent growth rate and growth rate dispersion (Ó Meadhra, 1995). In modeling it is usually assumed that all crystals are born at a near-zero size and all grow with the same growth rate. The reason for this assumption is that the required information about the phenomena present are not available.

A great deal of work has been dedicated to empirical modeling of contact nucleation in a variety of crystallization systems (Mesbah, 2010). Most of these correlations were related to properties of the crystallizing solution, the mechanical agitation in the crystallizer and a property representing the Crystal Size Distribution (CSD). Due to the fact that these correlations are empirical they cannot be used for a predictive model but they can be used for a descriptive model as in this thesis.

As mentioned in Section 2-3-2 secondary nucleation can occur by several mechanisms. According to Mersmann et al. (Mersmann et al., 1988) contact nucleation, i.e. attrition dominates in industrial solution crystallization. Attrition is a two-step process (Mesbah, 2010):

1. Generation of attrition fragments
2. Growth of the attrition fragments

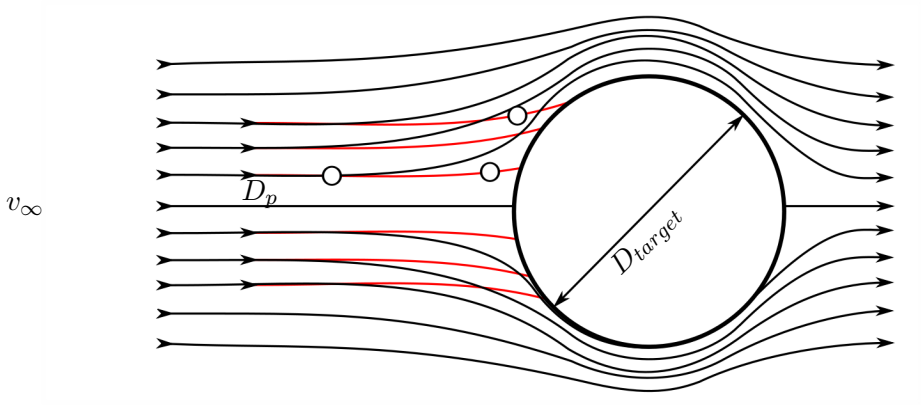

Figure 3-4: Streamlines for particles above and below the critical Stokes number

The generation of attrition fragments is mainly by crystal-crystal and crystal-hardware collisions. According to Gahn and Mersmann (Gahn and Mersmann, 1997) the crystal hardware collisions are the most dominant collisions due to the fact that their occurrence and their kinetic impact energy are quite high.

In this thesis the following expression for contact nucleation is used (Ruiter, 2009):

$$B_0 = a_1 \sum_{a_2}^{N} n_i L_i^3 \Delta L_i. \tag{3-20}$$

In which a_1 is the nucleation parameter which is usually deduced from experimental data, and a_2 is the lower boundary for integration.

This lower boundary for integration is a result of the fact that particles with small inertia e.g. small mass and/or velocity will not contribute to crystal impeller collisions (Wolf, 2007). The physical reason behind this is inertial deposition. This is the phenomenon that particles with low inertia tend to follow the stream over an object (e.g. stirrer blade) and thus will not collide. Particles with higher inertia will follow the stream but can imping on the object because of their inertia. This process is depicted in Figure 3-4.

3-6-2 Crystal growth model

As mentioned in Section 2-4 crystal growth is the outgrowth of nuclei by the addition of solute molecules from the supersaturated solution. It is a difficult process to comprehend; that is why in modeling usually simplified models are used. In this work a simplified relation is used to express the growth rate.

$$G = a_3\left(\frac{c - c_{sat}}{c_{sat}}\right)^{a_4} = a_3\sigma^{a_4} \tag{3-21}$$

It is a function of driving force i.e. supersaturation (relative) σ and two fitting factors a_1 and a_2. The factor a_1 is the growth rate constant and a_2 is the growth order. The growth rate order a_2 has a value of one for diffusion limited growth and a value larger than 1 for surface limited growth. This expression was taken from Ó Meadhra (Ó Meadhra, 1995).

3-6-3 Agglomeration model

As discussed earlier in section 2-6 the agglomeration model consists of two parts, the collision kernel and the agglomeration efficiency. For this model the collision kernel of Kruis and Kusters (Kruis and Kusters, 1996) is chosen.

Collision kernel

The advantages of the Kruis and Kusters (Kruis and Kusters, 1996) collision kernel are:

- Capable of predicting collision rates for particles both below and above the Kolmogorov scale
- Applicable to liquid systems (e.g. inclusion of virtual mass)

For a complete derivation of the model the reader is referred to the original paper of Kruis and Kusters (Kruis and Kusters, 1996). What follows below is the derivation specific for the adipic acid crystallization case. The collision rate of particles with sizes d_P and d'_P can be described by:

$$\beta_{Coll}(d_P, d'_P) = \left(\frac{8\pi}{3}\right)^{1/2}\left(\frac{d_P + d'_P}{2}\right)^2\sqrt{3w_i^2} \tag{3-22}$$

in which w_i is the one dimensional relative velocity between particles. This relative velocity can be expressed by:

$$\begin{aligned} w_i^2 \;=\; & \left(v_f^2(1-b)^2\frac{\gamma}{\gamma-1}\right) * \ldots \\ & \left(\frac{(\Theta_{P1}+\Theta_{P2})^2 - 4\Theta_{P1}\Theta_{P2}[(1+\Theta_{P1}+\Theta_{P2})/((1+\Theta_{P1})(1+\Theta_{P2}))]^{1/2}}{\Theta_{P1}+\Theta_{P2}}\right) * \ldots \\ & \left(\frac{1}{(1+\Theta_{P1})(1+\Theta_{P1})} - \frac{1}{(1+\gamma\Theta_{P1})(1+\gamma\Theta_{P1})}\right) \end{aligned} \tag{3-23}$$

in which v_f is the root mean square fluid velocity, b is the added mass coefficient, γ is a correction constant for the small particle velocity correlation and Θ is dimensionless particle relaxation time.

The root mean square velocity v_f can in the case of homogeneous turbulence set equal to the isotropic fluctuation velocity u_f.

$$v_f^2 = u_{f,iso}^2 = C * (\varepsilon\Lambda)^{2/3} \tag{3-24}$$

in which C is a prefactor which has the value $C = 2$ according to Riemann and Gerstlauer (Riemann and Gerstlauer, 2003) and Λ is the integral length scale which is in the same order of magnitude as the object responsible for the energy input i.e. the stirrer (Riemann and Gerstlauer, 2003).

$$\Lambda = \frac{1}{3} d_{stirrer} \tag{3-25}$$

The added mass coefficient b can be calculated by:

$$b = \frac{3\rho_f}{2\rho_P + \rho_f} \tag{3-26}$$

in which ρ_f and ρ_p are the density of the fluid and the particle respectively.

The correction factor γ can be evaluated by:

$$\gamma = 2\left(\frac{T_L}{\tau_L}\right). \tag{3-27}$$

In this equation T_L is the Lagrange time scale and τ_L is the Lagrange micro time scale. They can be calculated

$$T_L = 0.4\frac{\Lambda}{\sqrt{v_f^2}}, \tag{3-28}$$

$$\tau_L = \left(2\frac{v_f^2}{\varepsilon^{3/2}}\nu_f^{1/2}\right)^{1/2}. \tag{3-29}$$

The dimensionless particle relaxation time Θ_P is defined as:

$$\Theta_{Pi} = \frac{\tau_P}{T_L}. \tag{3-30}$$

The particle relaxation time can be calculated by:

$$\tau_P = \frac{\rho_P d_P^2}{18\mu}. \tag{3-31}$$

With Equations (3-22) to (3-31) it is possible to calculate the collision rate of crystals within the size range under investigation. For an example from literature (Kruis and Kusters, 1996) the collision rate is depicted in Figure 3-5. The physical properties for this example are given in Table 3-2.

From Figure 3-5 it can be seen that for small particles the collision rate decreases tremendously. This is due to the fact that small particles like this can only collide by their random

Property	Symbol	Value	Units
Particle density	ρ_p	2000	kg/m^3
Particle density	ρ_f	1000	kg/m^3
Fluid dynamic viscosity	μ_f	$1e^{-3}$	Ns/m^2
Specific mean power input	ϵ	5	W/kg
Root mean square velocity	ν_f^2	270	$-$
Correction factor	γ	0.1	m/s

Table 3-2: Physical properties for the adipic acid example from Kruis and Kusters (Kruis and Kusters, 1996)

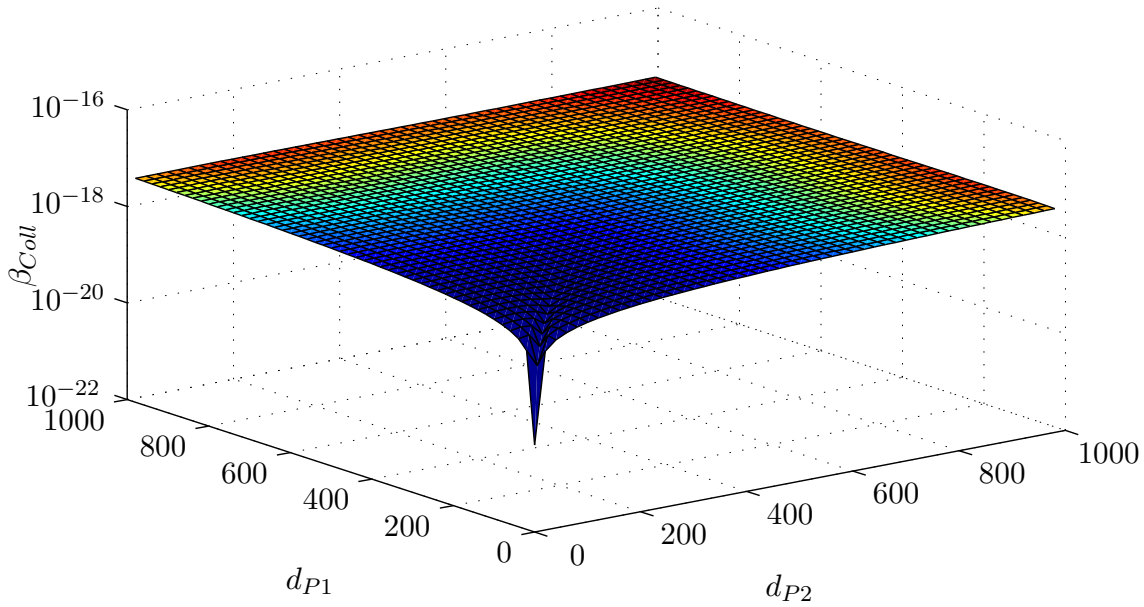

Figure 3-5: The collision rate for a solid-liquid system according to Kruis and Kusters (Kruis and Kusters, 1996) (particle diameters d_{P1}/d_{P2})

Brownian motion. When the particle size increases the particles can collide by both the shear and inertia mechanism as stated in Section 2-6. The collisions by these mechanisms occur much more frequently (Riemann and Gerstlauer, 2003). On the diagonal a small indent is seen. This small decrease in collision frequency has to do with the fact that particles with the same size (within the Kolmogorov range +/- 20μm) have correlated velocities. This means that the crystals will follow the same fluid stream lines and will collide less frequent. For similar sized particles with a larger diameter this correlation deteriorates and so does the decreases in the collision rate.

In order to calculate the number of agglomeration events, the agglomeration efficiency should be calculated.

Agglomeration efficiency

As mentioned before the agglomeration efficiency can be defined by:

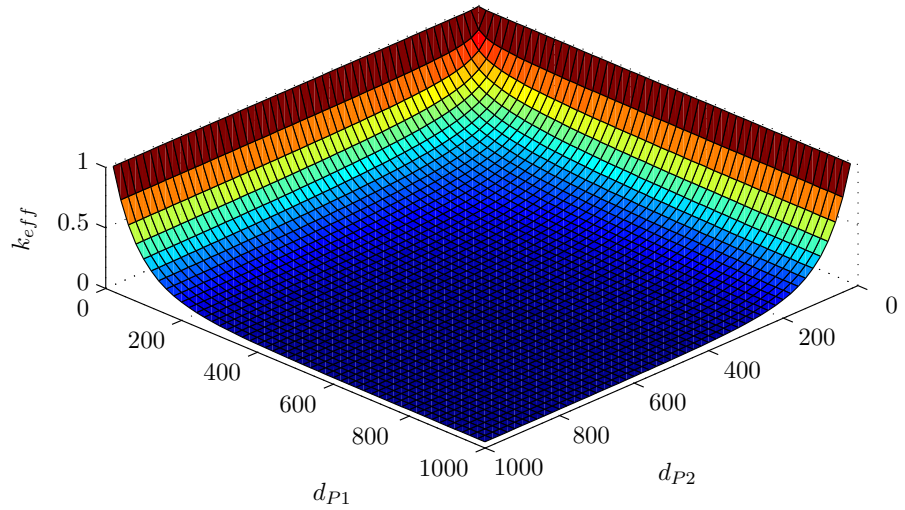

Figure 3-6: The agglomeration efficiency for the example case (particle diameters d_{P1}/d_{P2})

$$\eta_{Agglo} = \frac{\text{Number of agglomeration events}}{\text{Number of collisions}}. \tag{3-32}$$

In this report the expression for agglomeration efficiency of Riemann and Gerstlauer (Riemann and Gerstlauer, 2003) is used:

$$\eta_{Agglo}(d) = \exp\left(-a_5 \frac{d}{\Lambda}\right) \tag{3-33}$$

in which a_5 is a parameter which is extracted from experimental data. The distance d can be calculated by:

$$d = 2\frac{d_P d'_P}{d_P + d'_P} \tag{3-34}$$

where d_P and d'_P are the aforementioned particle diameters.

Agglomeration rate

As mentioned before, agglomeration is a two step process. When the collision rate is multiplied with the agglomeration efficiency the result is the total agglomeration rate. For modeling purposes a parameter a_6 is added to fit the model data to experimental data. This results in:

$$\beta_{Agglo} = a_6 \beta_{Coll} \eta_{Agglo}. \tag{3-35}$$

In Figure 3-7 the total agglomeration rate of the example case is depicted. It is clear that the agglomeration rate of crystals with the same size is small. Small crystals agglomerate with large crystals much easier, this is also a result of the experiments of David et al. (David et al., 1991a).

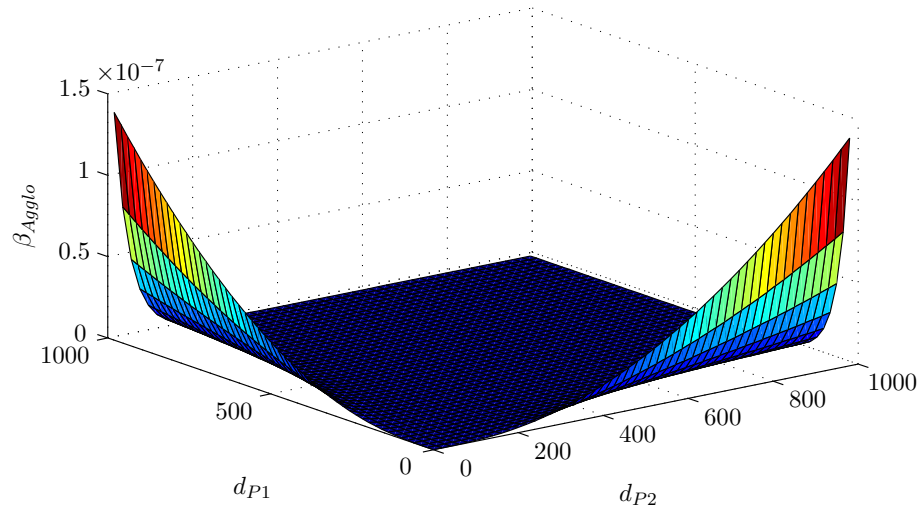

Figure 3-7: The agglomeration rate for the example case (particle diameters d_{P1}/d_{P2})

3-7 Continuous liquid phase

The continuous liquid phase in a crystallizer consists of both solvent and solute. In this thesis the continuous liquid phase is modeled on the basis of conservation laws i.e. mass and energy balances. There are four volumetric flow rates in the crystallizer model:

1. The feed flow rate $[m^3/s]$
2. The product flow rate $[m^3/s]$
3. The recirculation flow rate $[m^3/s]$
4. The vapor flow rate $[m^3/s]$

Of these four flow rates the product and recirculation flow rate are known while the feed and vapor flow rate are unknown. Making use of the total mass balance and the energy balance a system of algebraic equations can be derived which can be solved for the unknown flow rates.

As will be shown, both the total mass balance, the energy balance and the concentration balance contain a term $d\varepsilon/dt$. This term describes the evolution of the liquid fraction with time. Based on the PBE an expression for this term can be derived:

$$\frac{d\varepsilon}{dt} = -3k_v \int_0^\infty GnL^2 dL + \frac{\dot{V}_{out}}{V_C}(1-\varepsilon) - \frac{\dot{V}_{rec}}{V_C}(1-\varepsilon) - k_v \int_0^\infty L^3 K_{agg} dL \tag{3-36}$$

With the assumptions stated in Section 3-4 the total mass balance can be written as:

$$\begin{aligned} \frac{d\varepsilon}{dt}\left[\rho_{liq} - \rho_{crys}\right] V &= \dot{V}_{feed}\rho_{liq} - \dot{V}_{out}\left[\varepsilon\rho_{liq} + (1-\varepsilon)\rho_{crys}\right] + \ldots \\ &\quad \dot{V}_{rec}\left[\varepsilon\rho_{liq} + (1-\varepsilon)\rho_{crys}\right] - \dot{V}_{vap}\rho_{vap}. \end{aligned} \tag{3-37}$$

The energy balance can be rewritten as:

$$\begin{aligned}\frac{d\varepsilon}{dt}\left[V_C\rho_{liq}c_{p,liq}T - V_C\rho_{crys}c_{p,crys}T\right] &= \dot{V}_{feed}\rho_{liq}c_{p,liq}T_{feed} + ... \\ &\quad \dot{V}_{rec}[\varepsilon\rho_{liq}c_{p,liq}T_{rec} + (1-\varepsilon)\rho_{crys}c_{p,crys}T_{rec}] - ... \\ &\quad \dot{V}_{out}[\varepsilon\rho_{liq}c_{p,liq}T + (1-\varepsilon)\rho_{crys}c_{p,crys}T] - ... \\ &\quad \dot{V}_{vap}\rho_{vap}h_{evap}. \end{aligned} \tag{3-38}$$

Equations (3-36), (3-37) and (3-38) can be combined to form a system of algebraic equations with an equal number of equations and unknowns, thus it is solvable. This results in the calculation of both the feed and the vapor flow rate.

As discussed before, the driving force of crystallization i.e. supersaturation is usually expressed as equation (2-4):

$$\Delta c = c - c^*$$

in which c^* is the supersaturation concentration, which in this model is only a function of the known crystallizer temperature. The actual solute concentration c should be calculated and evolves with time. An ODE is required describing the change of concentration with time. The basis of this ODE is the concentration balance. Simplified with the above assumptions it can be rewritten as:

$$\begin{aligned}\frac{dc}{dt} &= \frac{1}{V\varepsilon\rho_{liq}}\Big[\dot{V}_{feed}\rho_{liq}c_{feed} - \dot{V}_{out}\left[\varepsilon\rho_{liq}c + (1-\varepsilon)\rho_{crys}\right] + \dot{V}_{rec}\left[\varepsilon\rho_{liq}c + (1-\varepsilon)\rho_{crys}\right] - \\ &\quad \frac{d\varepsilon}{dt}\left[\rho_{liq}c - \rho_{crys}\right]V\Big]. \end{aligned} \tag{3-39}$$

Equations (3-36) to (3-39) comprise a system of equations which can be solved resulting in the feed flow rate, the vapor flow rate and the concentration (at time t). Thus defining the complete continuous liquid phase. For the complete derivations of equations (3-37) to (3-39) the reader is directed to Appendix B.

3-8 Modeling framework

According to Mesbah (Mesbah, 2010) the crystallization kinetics relate the dynamic evolution of crystal population (PBE) to the state variables of the continuous phase.

In this model framework the solute concentration is calculated using both mass and energy balances. The solute concentration determines the supersaturation which is the driving force for crystallization kinetics. The crystallization kinetics are the cause of CSD evolution and therefore link the dispersed solid phase PBE to the continuous liquid phase.

For easy reproduction of the model described in this thesis an overview of the complete model framework is given in this Section.

Dispersed solid phase

N times an ODE describing the PBE in every grid cell (3-15):

$$\frac{\partial \tilde{n}_i}{\partial t} = -\frac{1}{\Delta L}[(G\tilde{n}_i)_{i+1/2} - (G\tilde{n}_i)_{i-1/2}] - \frac{1}{\Delta L}[F_{i+1/2} - F_{i-1/2}] + 3\frac{G_{i+1/2}\tilde{n}_i}{L_i} + \frac{\dot{V}_{rec}\tilde{n}_i}{V} - \frac{\dot{V}_{prod}\tilde{n}_i}{V}.$$

Crystallization kinetics

Algebraic equation describing the secondary nucleation rate (3-20):

$$B_0 = a_1 \sum_{a_2}^{N} n_i L_i^3 \Delta L_i.$$

Algebraic equation describing the growth rate (3-21):

$$G = a_3 \left(\frac{C - C_{sat}}{C_{sat}} \right)^{a_4} = a_3 \sigma^{a_4}.$$

Algebraic equation describing the agglomeration rate (3-35):

$$\beta_{Agglo} = a_6 \beta_{Coll} \eta_{Agglo}.$$

Continuous liquid phase

An algebraic system of equations by combining equation (3-37), (3-38) and (3-39). The solution to this algebraic system of equations will yield both the feed and the vapor flow rate.

$$\begin{aligned} \frac{d\varepsilon}{dt}\left[\rho_{liq} - \rho_{crys}\right] V &= \dot{V}_{feed}\rho_{liq} - \dot{V}_{out}\left[\varepsilon\rho_{liq} + (1-\varepsilon)\rho_{crys}\right] + ... \\ &\quad \dot{V}_{rec}\left[\varepsilon\rho_{liq} + (1-\varepsilon)\rho_{crys}\right] - \dot{V}_{vap}\rho_{vap} \end{aligned}$$

$$\begin{aligned}\frac{d\varepsilon}{dt}\left[V_C\rho_{liq}c_{p,liq}T - V_C\rho_{crys}c_{p,crys}T\right] &= \dot{V}_{feed}\rho_{liq}c_{p,liq}T_{feed} + ... \\ &\quad \dot{V}_{rec}[\varepsilon\rho_{liq}c_{p,liq}T_{rec} + (1-\varepsilon)\rho_{crys}c_{p,crys}T_{rec}] - ... \\ &\quad \dot{V}_{out}[\varepsilon\rho_{liq}c_{p,liq}T + (1-\varepsilon)\rho_{crys}c_{p,crys}T] - ... \\ &\quad \dot{V}_{vap}\rho_{vap}h_{evap}\end{aligned}$$

$$\frac{d\varepsilon}{dt} = -3k_v\int_0^\infty GnL^2dL + \frac{\dot{V}_{out}}{V_C}(1-\varepsilon) - \frac{\dot{V}_{rec}}{V_C}(1-\varepsilon) - k_v\int_0^\infty L^3K_{agg}dL$$

ODE describing the solute concentration at time t (3-39):

$$\begin{aligned}\frac{dc}{dt} &= \frac{1}{V\varepsilon\rho_{liq}}\Big[\dot{V}_{feed}\rho_{liq}c_{feed} - \dot{V}_{out}\left[\varepsilon\rho_{liq}c + (1-\varepsilon)\rho_{crys}\right] + \dot{V}_{rec}\left[\varepsilon\rho_{liq}c + (1-\varepsilon)\rho_{crys}\right] - \\ &\quad \frac{d\varepsilon}{dt}\left[\rho_{liq}c - \rho_{crys}\right]V\Big].\end{aligned}$$

3-8-1 Matlab implementation

The complete model framework is implemented in Matlab. The set of ODE's is solved using a built-in ODE solver. The system of discretized PBE's is a stiff system of differential equations. Although there is no formal definition of "stiffness" in literature it can be defined as a problem which contains widely varying timescales i.e. some components of the solution decay much more rapidly than others.

The problem with "stiff" systems lays within the stability of the numerical method. In literature the stability of a numerical method is assessed using the stability region (Shampine, 2003). This is a plot of the area in which the product of the time step with the eigenvalue of the equation result in a stable numerical integration. Explicit numerical integration schemes like Matlab's ODE45 solver (Runge-Kutta) have a finite stability region, depicted as the interior of the curves in Figure 3-8(a). Explicit numerical integration schemes such as Matlab's ODE23s are so called "A-stable" (Shampine, 2003) i.e. the stability region encompasses the whole left plane of the coordinate system (first and second order backwards differentiation). This is depicted in Figure 3-8(c), in this figure the stability regions are the exteriors of the curves.

With this difference in stability regions it can be explained why it is not computationally efficient to use an ordinary ODE45 solver for a stiff system of differential equations. A solver like ODE45 is a so-called variable time step solver. This means that during the integration process the solver continuously adjusts the time step to ensure both accuracy and stability Shampine (2003).

The reason why this can be very computationally inefficient can be illustrated by the following situation. The ODE45 solver is used to solve a relatively simple system of differential equations. This means that in order to ensure a good accuracy the time step can be quite large. The solver will increase the time step up to a certain point where the integration will become

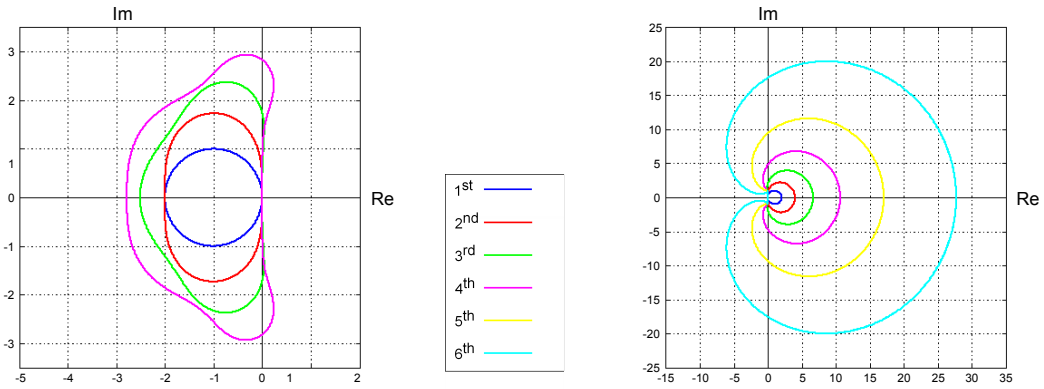

(a) Runge Kutta orders 1-4

(c) Backwards Differentiation orders 1-6

Figure 3-8: The stability regions of different numerical ODE solvers

unstable i.e. errors will start to grow out instead of diminish. At this point the calculation is called a failure and the time step is decreased to make the integration stable again. This process is an iterative process and will continue until the system of differential equations is solved. The occurrence of a lot of failures will result in a high computational burden.

A stiff solver such as the ODE23 solver has no stability criteria due to the fact that it is "A-stable". Thus a conflict between the accuracy and the stability will never occur. The size of the time step is therefore only determined by the required accuracy of the solution. This will result in much less failures and thus a smaller computational burden. An illustrative example can be found in Shampine (Shampine, 2003). For the aforementioned reason a stiff solver is chosen in favor of a normal solver.

The other part of the model framework consists of a system of algebraic equations. This system is solved using Matlab's backslash operator and results in the vapor and feed volumetric flows. The complete Matlab code can be found in Appendix C.

Chapter 4

Experimental setup and data

In order to validate the model developed in this thesis experimental data is required. The methodology and the equipment which was used to acquire the data is discussed in the first Section (4-1). Section (4-2) discusses the actual process data and its post-processing.

Due to the fact that the crystallizer itself is already discussed in Section 3-2 it is omitted in this Chapter to avoid repetition.

4-1 Experimental setup

4-1-1 Control system

In order to achieve the desired product quality a control system is in place. The crystallizer temperature (T1502) is compared with a set point temperature. If this temperature is different from the set point temperature, the set point for the pressure is adjusted. The adjustment in pressure causes a change in the amount of solvent which is evaporated and thus controls the crystallizer temperature. The magma level in the crystallizer is also monitored (L1501). The level in the crystallizer is controlled by the feed flow, this flow is adjusted by a valve. The temperature of the outgoing stream (T1503) is monitored and should be the same as the crystallizer temperature (T1502). If this is not the case this usually is an indication of a blockage in the crystallizer causing a shortcut from the feed to the outflow. The product flow is also measured (F1331), the amount of flow is controlled by the product pump.

4-1-2 CSD measuring

In order to measure the Crystal Size Distribution (CSD) a sensor is required. At BASF a new on line image analysis sensor was developed by the research group of Dr. Michael Schäfer. This sensor is called a Hüllstrom sensor and was developed to overcome the technical limitations of the existing CSD measuring sensors. In this thesis a brief description of the sensor and

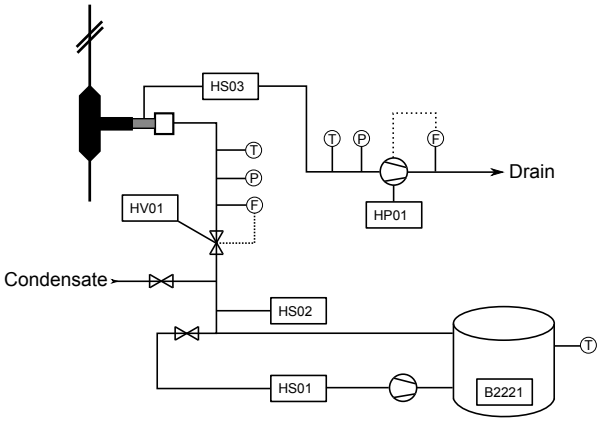

Figure 4-1: Process flow diagram of the sampling loop (Ruiter, 2009) (valves HV, flow sensors HS and pumps HP)

the software is given. For a complete description the reader is directed to de Ruiter (Ruiter, 2009).

The CSD sensor is placed in the product stream (S05) via a t-connector . The t-connector has a larger diameter to keep the overall flow velocity constant around the sensor. The sensor takes a sample of the product stream which is diluted before the measurement. The dilution is done with two sheathed streams, in this way the sample stream is squeezed between these streams and all the particles are orientated in the same manner. In this way all the particles can be measured individually.

The solution used for the sheathed streams is prepared in a separate tank (B2221). The solution is recirculated throughout the plant by stream (HS01). A small portion of stream (HS01) is used for the sheathed streams (HS02). The temperature, pressure and flow rate of this stream are measured. The flow rate can be altered using valve (HV01). After measurement the diluted product stream (HS03) exits the sensor where the temperature and the pressure are measured once more. Pump (HP01) determines the flow rate which is taken from the sensor head to the drain.

Two possible problems with this method are the mixing of the streams and possible formation of "schlieren". In order to avoid the mixing of streams all flow characteristics are chosen such that the streams are laminar. The formation of "schlieren" is due to the existence of a chemical potential difference between the sheathed and the product stream. Light will refract at the boundary between the two streams causing a difficulty to measure the particles correctly. In order to avoid this problem the sheathed streams should mimic the product stream (same concentration and temperature).

Due to the squeezing of the product stream all the particles are orientated in the same manner and can be photographed by the sensor. These images are processed by image software. This software uses anti-shading correction for all the pictures. This means that dirt on the lens and also particles which can stick on the lens are removed resulting in a clearer picture and a more accurate measurement.

Using the image software makes it possible to measure partly transparent crystals as well. The software recognizes the borders of the crystals and converts it into a solid particle. Overlapping

or touching crystals are counted as one crystal. In order to alleviate this problem the particle density within the image should not be too high. This can be accomplished by altering the outlet stream (HS03) by changing the pump (HP01) settings. After post-processing the software translates the images to several crystal sizes and characteristics which are tabulated in Table 4-1.

Table 4-1: Different sizes and characteristics crystals measured by the sensor

Size or characteristics	Equation	Explanation
Maximum Ferret diameter	F_{max}	The maximum diameter of a crystal
Minimum Ferret diameter	$F_{min} = A_{crystal}/F_{max}$	The minimum diameter of a crystal
Waddel disk diameter	$F_{area} = 2\sqrt{\frac{A_{crystal}}{\pi}}$	The diameter of a circle with the same area as the crystal
Elongation	$E = F_{max}/F_{min}$	The ratio between the maximum and minimum diameter
Heywood	$H = \frac{P}{2\sqrt{\pi A_{crystal}}}$	The ratio of the perimeter of the crystal and the perimeter of a sphere with the same area as the crystal
Volume	$V = 0.55 F_{max} F_{min}^2$	The volume of a rectangular cuboid of the maximum and the minimum diameter times a shape factor
3D Equivalent diameter	$3dE = \sqrt[3]{\frac{6V}{\pi}}$	The diameter of a perfect sphere with the same calculated volume as the crystal

4-2 Experimental data

A variety of data was gathered in earlier research by de Ruiter (Ruiter, 2009) and BASF. Besides the CSD data, operational data is also required to validate the model. This operational data such as pressures, temperatures and flows are all continuously monitored at the production site at BASF. This section will start by explaining the way in which the CSD data is displayed in the report. The section ends with an overview of the available experimental data.

4-2-1 Graphical representation of the data

The crystal size distributions measured by the sensor are written to data files as a cumulative distribution (Figure 4-2(a)). The change of the cumulative distribution with time can be plotted on a surface graph but reading data from these graphs is rather inaccurate. A better alternative is to look at the change with time of different percentiles of the cumulative

distribution (Figure 4-2(b)). In this thesis L_{10}, L_{50} and L_{90} are chosen as the representative percentiles. The tenth percentile (L_{10}) means that 90% of the particles are larger than this value. By plotting the L_{10}, L_{50} and L_{90} an indication of the mean crystal size and the width of the distribution is given.

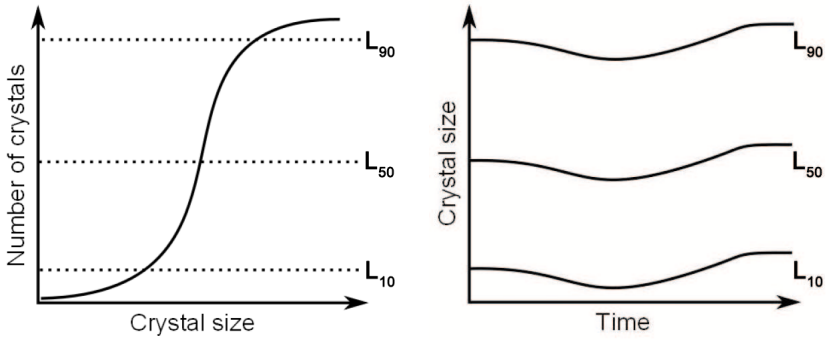

(a) Cumulative distribution (b) The 10th, 50th and 90th percentiles

Figure 4-2: A cumulative size distribution with its percentiles

4-2-2 Matching the CSD data to the process conditions data

Next to the CSD data the process conditions are required to validate the model. These are continuously monitored and saved by a variety of computer programs. The CSD data is not monitored continuously, this causes a time mismatch. The CSD data should be shifted in order to be orientated at the correct time. Due to the amount of data this is a quite cumbersome process. A Matlab script was written to automate this process. The Matlab script can be found in Appendix C-3. This Matlab script uses Microsoft Excel files as an input, the data is saved by the monitoring system as a RAW text file. This means the text files should be converted to Excel files.

4-2-3 Overview of the experimental data

The data can be sorted into two categories: steady-state and dynamic data. The steady-state data describes the operation of the crystallizer at steady-state conditions. The dynamic data includes data sets where one of the process variable i.e. temperature, flow rate or stirrer speed is perturbed. An overview of the dynamic data available is given in Table 4-2.

A part of the model validation is a parameter estimation to estimate the values of the experimental parameters a_1 to a_6 in the model framework. As mentioned earlier de Ruiter (Ruiter, 2009) described agglomeration as being a dominant phenomenon in adipic acid crystallization. The best suited dynamic data set is the one with the change in impeller speed because impeller speed is proportional to power input one of the most dominant parameters in agglomeration.

The increase in stirrer rate results in an increase in all the percentiles as depicted in Figure 4-3. This increase is more pronounced in the 50^{th} and 90^{th}. percentile. The reason for this increase is that with in increasing stirrer rate, the power input is increased. This increase

Table 4-2: Data availability

Process variable changed	Units	Change	Date
Recirculation rate	m^3/hr	60 -> 30 -> 60	08.04.2009
Recirculation rate	m^3/hr	60 -> 30 -> 60	14.04.2009
Recirculation rate	m^3/hr	60 -> 70 70 -> 60 60 -> 30	20.07.2009
Recirculation rate	m^3/hr	30 -> 60	21.07.2009
Crystallizer temperature	$°C$	60 -> 65	07.07.2009
Crystallizer temperature	$°C$	65 -> 65	07.07.2009
Stirrer rate	rpm	24 -> 35 -> 40	06.08.2009
Outlet flow	m^3/hr	Short disturbances	26.07.2009
Outlet flow	m^3/hr	Upward/downward step	27.07.2009

in power input results in a higher collision rate and thus a higher agglomeration rate. At a certain stirrer rate the attrition and fluid shear forces become larger i.e. the agglomeration efficiency becomes smaller and the agglomeration rate decreases again. The comparison with model results can be found in Section 5-2.

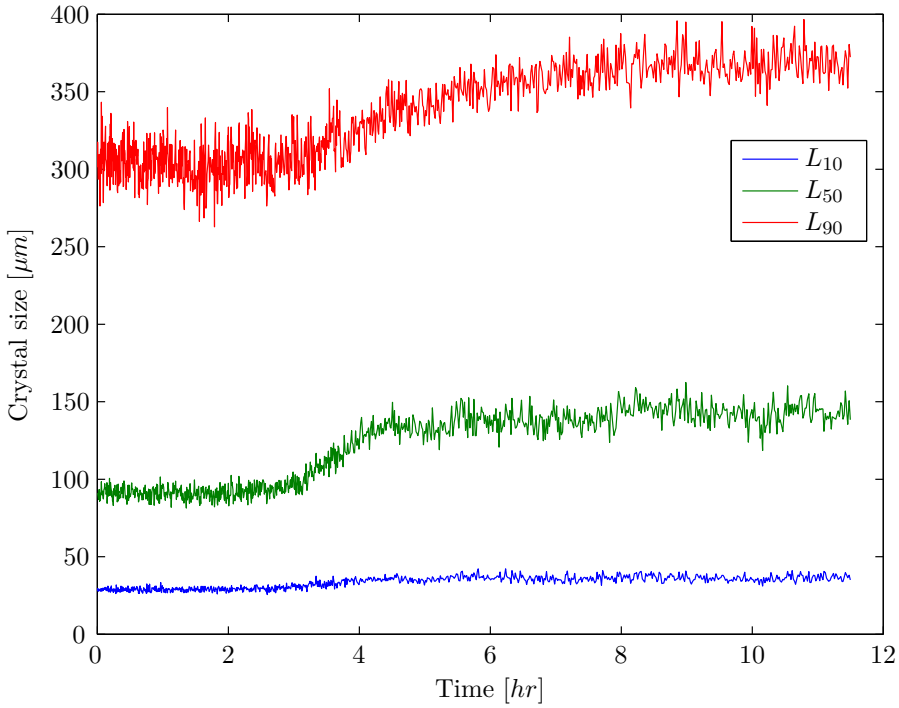

Figure 4-3: Increase in stirrer rate from 24 to 35 to 40 rpm

Chapter 5

Results and discussion

In this chapter the results are discussed, it is conveniently divided into two parts:

1. Results of the numerical test cases
2. Results of the process model simulations

5-1 Numerical test cases

In order to see if the numerical method can accurately describe the different kinetics in crystallization several numerical test cases are modeled. These test cases have an analytical solution. In this way the numerical results can be compared to the analytical results. The following test cases are modeled:

- Pure growth
- Pure agglomeration
- Simultaneous growth and agglomeration
- Simultaneous nucleation and growth
- Simultaneous growth, nucleation and agglomeration
- An industrial continuous crystallizer (MSMPR)

As one can see the list does not contain nucleation only. There is no need to model nucleation alone as the Population Balance Equation (PBE) would be rewritten into an Ordinary Differential Equation (ODE) which could be solved with any standard ODE solver. This case would have no connection with the numerical scheme. As far as the case for simultaneous growth, nucleation and agglomeration is concerned, there is no analytical solution available for this case thus it is not possible to compare the numerical and analytical results. However the numerical results can be compared to the results from Qamar (Qamar, 2008).

5-1-1 Pure growth

The first test case is pure growth, the volume size range $x = 0 : 20\mu m$ is divided into 100 grid cells with equal size (regular grid). Growth rate has the value $G(x) = 0.1$. The initial number distribution is given in table 5-1. This is a slightly altered example from Leonard and Niknafs (Leonard and Niknafs, 1991).

It is a initial distribution with very sharp peeks (large gradients) this was chosen to test the performance concerning numerical diffusion. According to Qamar (Qamar, 2008) normal initial particle distributions are of the Gaussian-type but sharp peeks can occur due to process operation (e.g. injection of seeds into a initially super-saturated solution, this will result in a burst of near zero-sized particles due to secondary nucleation).

Table 5-1: Initial number density for the pure growth case

x	$f(0,x)$
$2 < \mathrm{x} \leq 4$	$\frac{1}{\sqrt{0.32\pi}} \exp(-500(0.1x - 0.3)^2)$
$6 < \mathrm{x} \leq 8$	1
$10 < \mathrm{x} \leq 12$	$1 - \lvert x - 11 \rvert$
$14 < \mathrm{x} \leq 16$	$\sqrt{1 - 100(0.1x - 1.5)^2}$
elsewhere	0

The analytical solution to this problem is relatively easy, the initial distribution just shifts in time due to the constant (size-independent) growth, thus:

$$f(t,x) = f_0(x - Gt). \tag{5-1}$$

The result of the model is depicted in figure 5-1. It can be seen that the numerical results are in good agreement with the analytical results but there is a small amount of numerical diffusion visible. This is due to the solution of the hyperbolic growth term in the PBE.

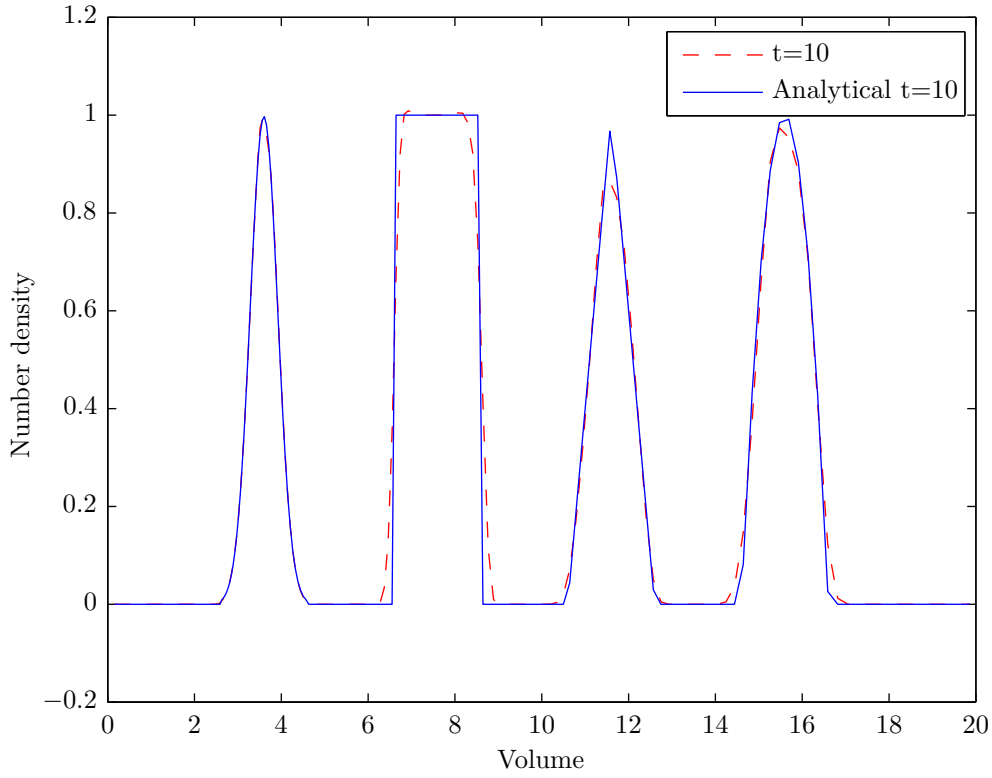

Figure 5-1: Number density distributions after ten seconds, numerical and analytical in the case of 'pure' growth

5-1-2 Pure agglomeration

The case for pure agglomeration is an example from Scott (Scott, 1968). The initial density distribution is given by equation (5-2). The agglomeration kernel β is taken constant $\beta = \beta_0$. The values of β, N_0 and x_0 are all taken as 1.

$$f(0,x) = \frac{N_0}{x_0} \exp(-x/x_0) \tag{5-2}$$

The analytical solution is given by:

$$f(t,x) = \frac{4N_0}{x_0(\tau+2)^2} \exp\left(\frac{-2x'}{\tau+2}\right) \tag{5-3}$$

in which $\tau = N_0\beta_0 t$ and $x' = x/x_0$.

It can be seen from figure 5-2 that the results are similar to the analytical solution. However it is clear that at the right face of the distribution there is an offset in the values. This offset does not seem to be increasing with time. According to Qamar (Qamar, 2008), this smearing of the solution was also observed in other numerical schemes. A clear explanation of this smearing is not yet available.

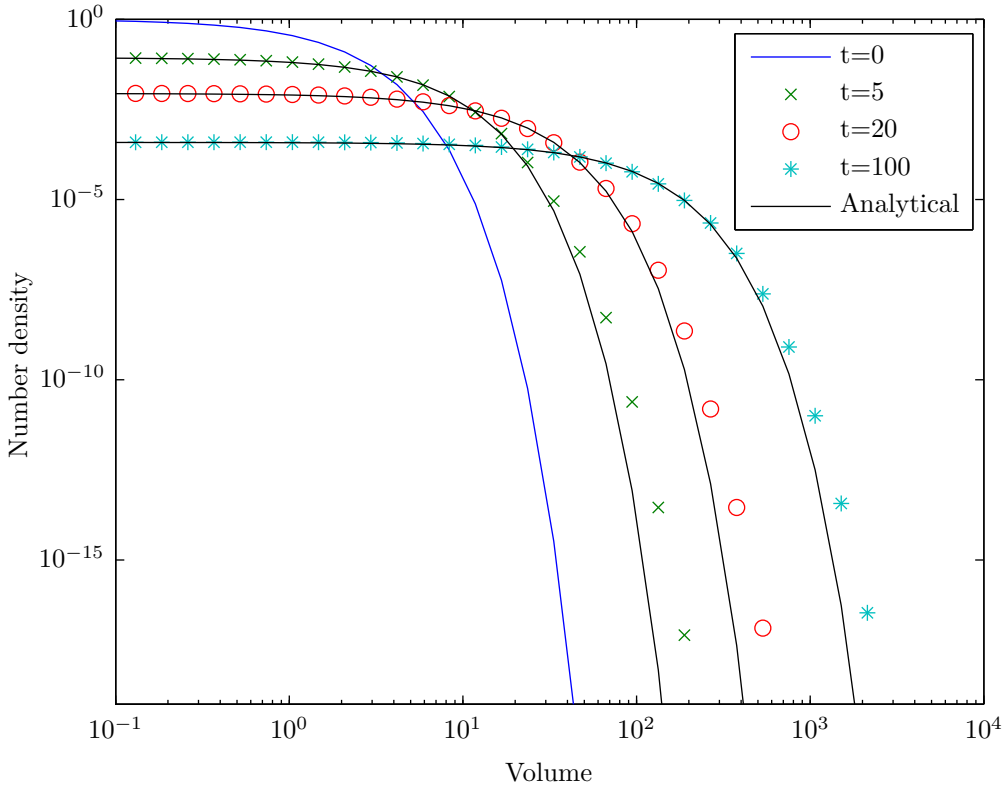

Figure 5-2: Number density distributions at different elapsed times, numerical and analytical in the case of 'pure' agglomeration

5-1-3 Simultaneous growth and agglomeration

The case with simultaneous growth and agglomeration is from Kumar and Ramkrishna (Kumar and Ramkrishna, 1997) and treats a case with constant agglomeration kernel and size-dependent growth. The initial distribution has the form of equation (5-2). Growth has a value of $G = G_0 x$ with $G_0 = 1$, the agglomeration kernel is $\beta = 10$. The analytical solution is given by:

$$f(x,t) = \left(\frac{{M_0}^2}{M_1}\right) exp\left(\frac{-M_0}{M_1}x\right) \tag{5-4}$$

with $M_0 = 2N_0/(2 + BN_0t)$ and $M_1 = N_0x_0exp(G_0t)$.

The results can be seen in figure 5-3. The simulation results are in good agreement with the analytical results. Again there is some smearing of the result which was also observed in sub-section 5-1-2.

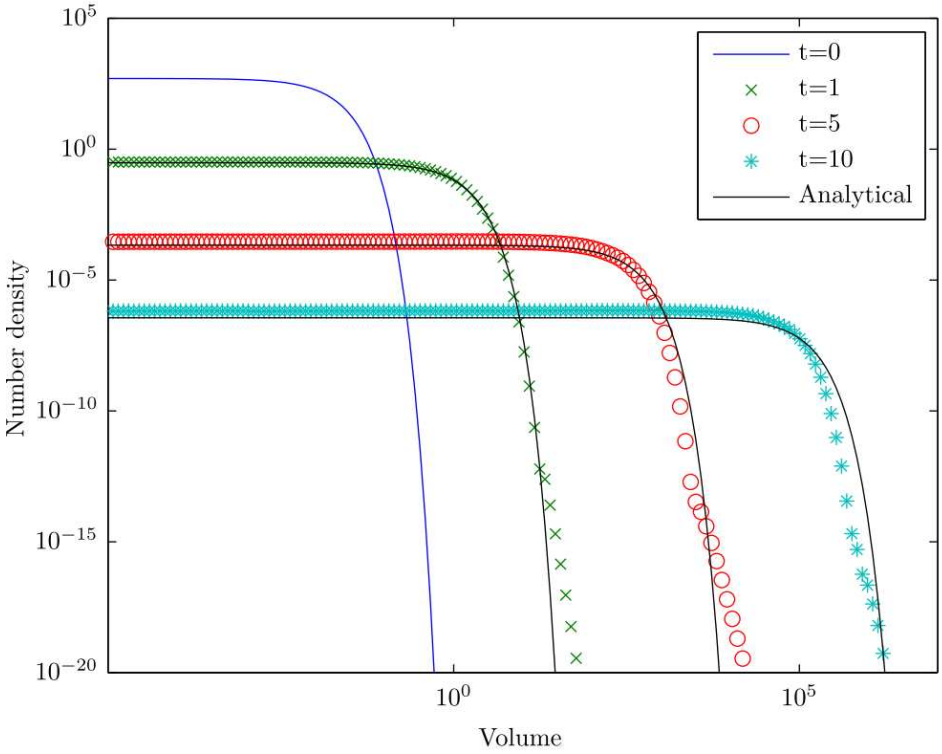

Figure 5-3: Number density distributions at different elapsed times, numerical and analytical in the case of growth and agglomeration

5-1-4 Simultaneous growth and nucleation

This case is from Lim et al. (Lim et al., 2002) and is a case with simultaneous growth and stiff nucleation. The reason why a case with stiff nucleation is chosen is because this is similar to what will be used to model nucleation in the adipic acid crystallization case. The initial number density is given in table 5-2 and is a square step.

Table 5-2: Initial number density for simultaneous growth and nucleation case

x	$f(0,x)$
$0.4 < x \leq 0.6$	100
elsewhere	0.01

The stiff nucleation takes place at the minimum crystal volume:

$$f(0,t) = 100 + 10^6 exp(-10^4(t-0.215)^2). \tag{5-5}$$

The growth rate is given by $G = 1$, the volume ranges from 0 to 2.0 and the time range is given by $0 \leq 0.5$. As seen in figure 5-4 the numerical model approximates the analytical solution reasonable but numerical diffusion is clearly visible.

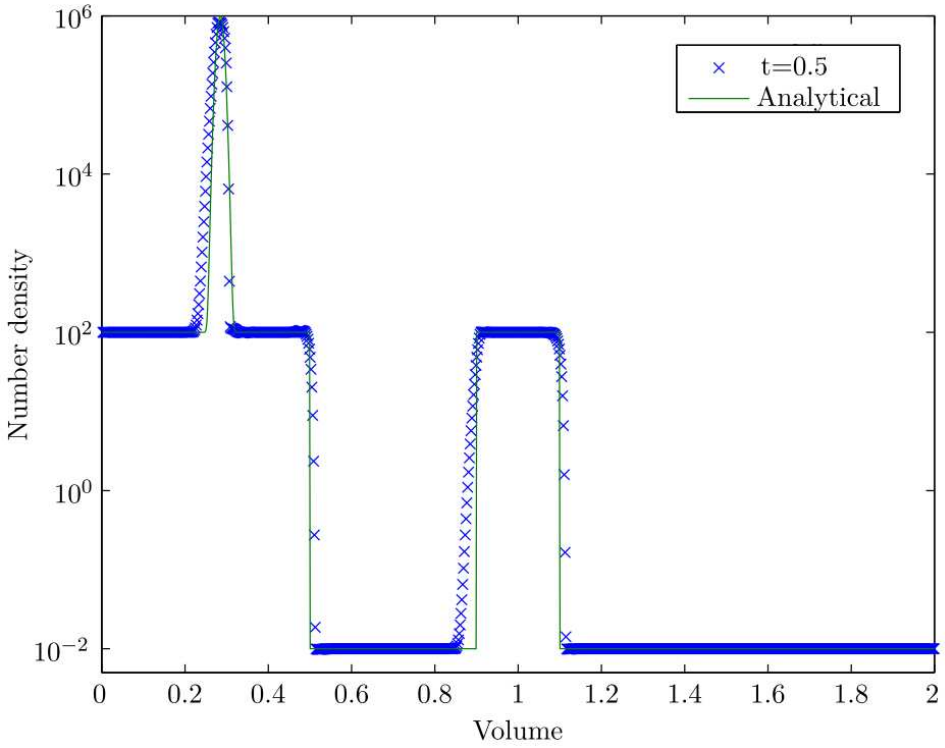

Figure 5-4: Number density distributions at different elapsed times, numerical and analytical in the case of growth and nucleation

5-1-5 Simultaneous growth, nucleation and agglomeration

This case has been discussed in Qamar and Warnecke (Qamar and Warnecke, 2007) and as mentioned before it does not have an analytical solution. The initial number distribution is the same as (5-2). The nucleation is exponential and is given by equation (5-6) and the agglomeration is constant with $\beta(x, x') = \beta_0$.

$$S(x) = B_0/x_{0,n} exp(-x/x_{0,n}) \tag{5-6}$$

When the results of this thesis are compared with the results from Qamar and Warnecke (Qamar and Warnecke, 2007) it can be seen that both the trends of the curves as well as the order of magnitude are similar.

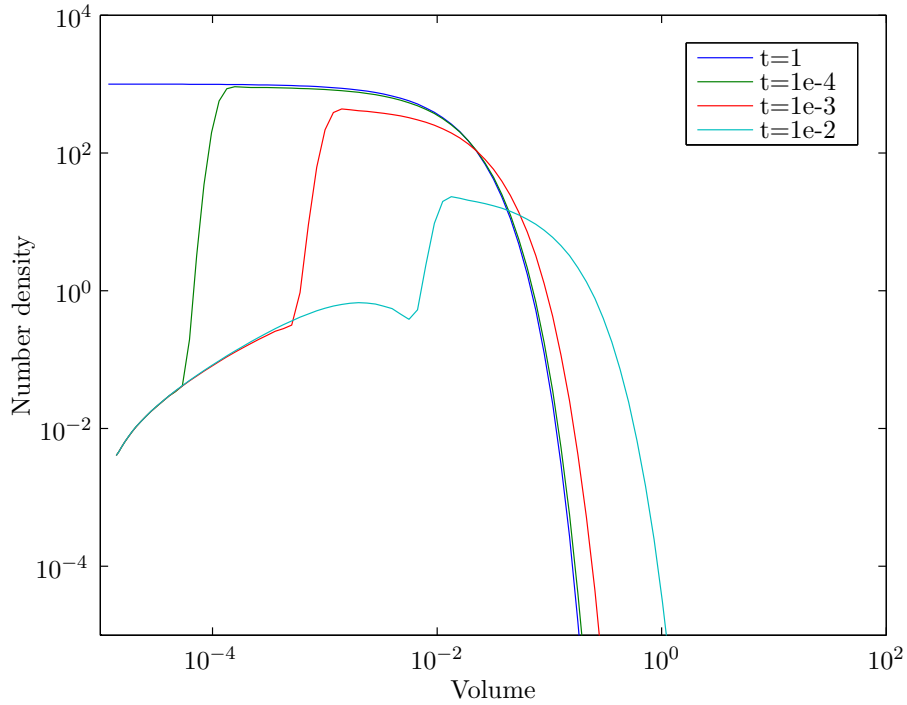

(a) Number density distributions at different elapsed times in the case of growth, nucleation and agglomeration (this thesis)

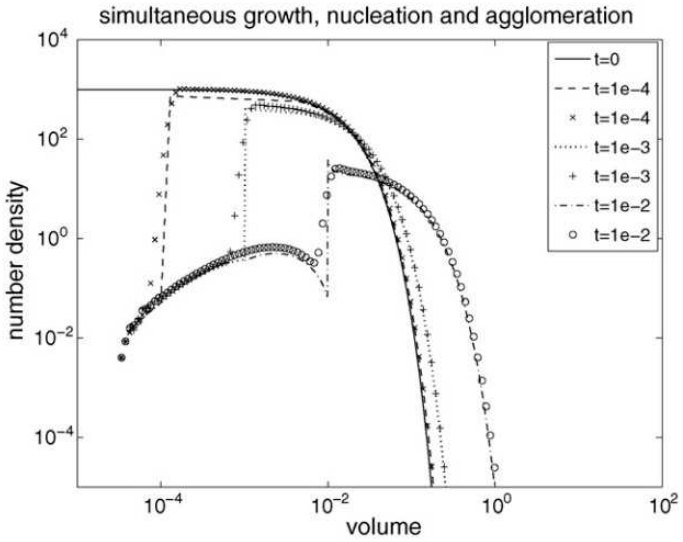

(b) Number density distributions at different elapsed times in the case of growth, nucleation and agglomeration ((Qamar and Warnecke, 2007))

Figure 5-5: Comparison between the model results of this thesis and the model results of Qamar and Warnecke (Qamar and Warnecke, 2007)

5-1-6 An industrial continuous crystallizer (MSMPR)

This test case is a simulation of an industrial continuous crystallizer. The crystallizer considered is a so-called Mixed Suspension Mixed Product Removal (MSMPR) crystallizer. This type of crystallizer is the crystallization equivalent of a Continuous Stirred Tank Reactor (CSTR) in reactor engineering, an ideal case model. It can be interpreted as follows (Mesbah, 2010):

- Constant nucleation rate at all points in the magma
- Constant growth rate and independent of crystal size and location
- All volume elements of mother liquor contain a mixture of particles ranging in size from nuclei to large particles
- Particle size distribution is independent of location in the crystallizer and is identical to the size distribution in the product

The MSMPR crystallizer has the same dimensions and properties as the adipic acid crystallizer at BASF Ludwigshafen. For modeling this MSMPR crystallizer a model similar to the one discussed in section 3-8 is used (excluding agglomeration).

According to Randolph and Larson (Randolph and Larson, 1988) the MSMPR has an analytical solution. The steady state number density distribution can be described by:

$$n(L) = n(0) \exp\left(-\frac{L}{G\tau}\right) \tag{5-7}$$

in which τ is the residence time, which can be calculated by:

$$\tau = \frac{V_c}{\dot{V}_{prod}}. \tag{5-8}$$

It is clear from figure 5-6 that the model accurately describes the steady-state number density of the MSMPR crystallizer. This is a clear indication that the model framework developed in section 5-6 can accurately describe an industrial crystallizer. In Section 5-2 the agglomeration phenomenon is also taken into account and the results are compared to experimental data.

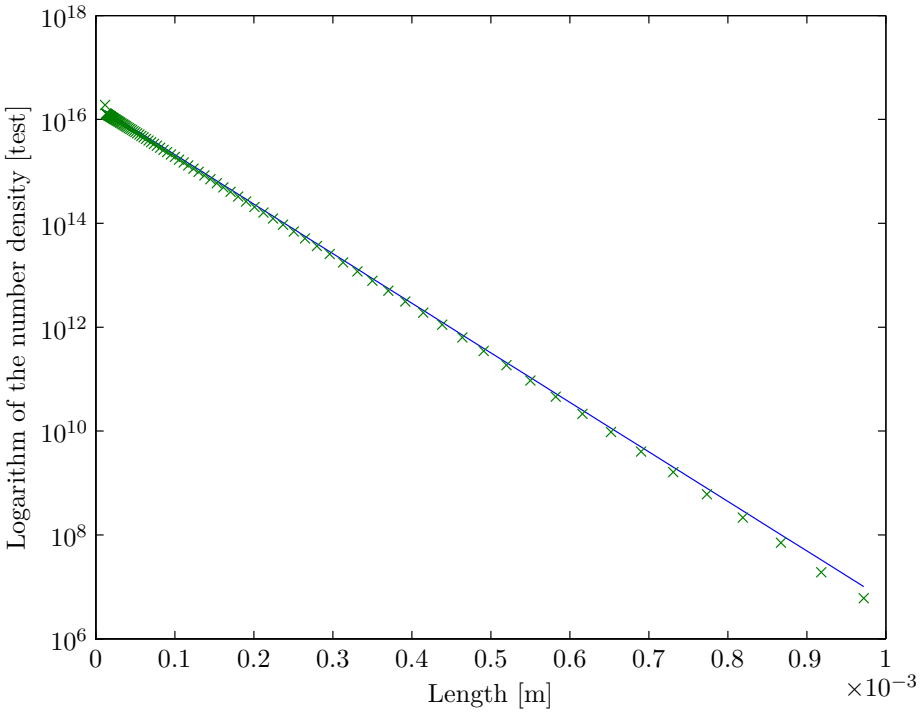

Figure 5-6: The steady-state number density distribution of an MSMPR crystallizer

5-2 Process model simulations

In Section 5-1-1 to 5-1-5 it was shown that a PBE including nucleation, growth and agglomeration can accurately be solved. In Section 5-1-6 an MSMPR crystallizer was modeled which also included a concentration, total mass and energy balance. The results were similar to the analytical case. In this Section the model is extended to include agglomeration and its results are compared to experimental Crystal Size Distribution (CSD) data.

The model was run for an amount of time in which it reached its steady state. Mass flows, mean crystal size and the distribution percentiles were monitored to ensure that it arrived at steady state. The model equations contain a number of parameters which should be fitted to the experimental data.

This data fitting or parameter estimation is done by using Matlab's build in FMINCON optimization routine. According to MathWorks:

"FMINCON attempts to find a constrained minimum of a scalar function of several variables starting at an initial estimate. This is generally referred to as constrained nonlinear optimization or nonlinear programming."

The scalar function mentioned above is the objective function. This objective function has the form of a non-weighted least square method and is described as:

$$f_{objective} = \sum_{i} (L_{i,model} - L_{i,experimental})^2 \qquad i = 10, 50, 90 \qquad (5\text{-}9)$$

Thus by minimizing the objective function the error between the model and the experimental data is minimized.

5-2-1 Steady state results

In this Section the steady state results of the model are reviewed. The nucleation rate is given by Equation (3-20) and the crystal growth rate is described by Equation (3-21). The agglomeration rate is modeled by a product of the collision kernel and the agglomeration efficiency Lindenberg et al. (2007):

- The collision kernel of Kruis and Kusters (1996) discussed in Section 3-6-3
- The agglomeration efficiency by Riemann and Gerstlauer (2003) as discussed in Section 3-6-3

In Table 5-3 the different values for the kinetic parameters are given as well as the value for the means square error.

Table 5-3: Kinetic parameters and least square error

Parameter	Description	Value
a_1	Nucleation parameter	$4e^{13}$
a_2	Nucleation order	$3.7e^{-5}$
a_3	Growth parameter	$1e^{-7}$
a_4	Growth order	0.7
a_5	Agglomeration parameter	$9e^{4}$
a_6	Agglomeration efficiency factor	5.0
$f_{Objective}$	Least square error	3199.3

The percentiles of this model run can be seen in Figure 5-7. It is clear from this figure that the model reaches steady state conditions in approximately 50 hours. This time is longer than the mentioned startup time in Ruiter (2009). The steady state percentile values are given in Table 5-4.

Table 5-4: Steady state percentiles experimental and modeled

Percentile	Experimental [μm]	Modeled [μm]	Deviation [%]
L_{10}	30.00	70.96	136.53
L_{50}	90.00	128.26	42.51
L_{90}	300.00	307.58	2.46

It is clear that both the L_{10} and the L_{50} are over estimated while the L_{90} is predicted with a 2.46% deviation. In the next Section possible reasons for this deviation will be discussed.

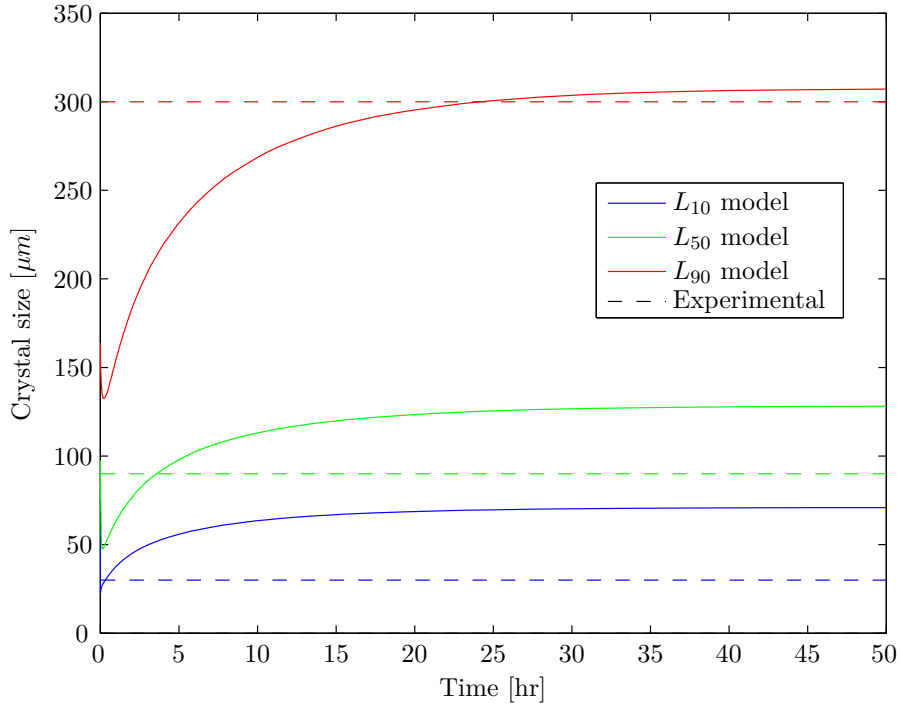

Figure 5-7: The distribution percentiles, modeling and experimental result

5-2-2 Reasons for deviations in the modeled CSD

As seen in the previous Section the modeled CSD was deviating from the experimental CSD this became clear by comparing the percentiles of both the distributions. For this deviation two possible causes can be thought of:

1. Numerical errors in solving the PBE
2. Incorrect expression for the agglomeration kinetics

As mentioned by several authors Mesbah (2010) and Su et al. (2009) obtaining a numerical solution of the PBE has multiple pitfalls e.g. numerical diffusion and instability (explained in Section 2-7). In Section 5-1 several examples are given for numerical test cases. All crystallization kinetics were modeled alone and in combinations. (nucleation, growth and agglomeration). The numerical results of the MSMPR crystallizer case were also in good agreement to the analytical solution. Thus it can be concluded that the numerical scheme is accurately implemented and that the results are correct.

The main difference between the final model case and the numerical test cases is the inclusion of a size dependent agglomeration rate. Thus in investigating possible causes for the deviation from experimental data the expression for agglomeration should also be investigated.

As discussed in Section 3-6-3 the expression for the agglomeration rate is not a function of supersaturation. Several authors have claimed that agglomeration rate indeed is a function

of supersaturation Lindenberg et al. (2007) and David et al. (1991b). Thus to make the agglomeration rate supersaturation dependent the following expression is used:

$$\beta_{Agglo} = a_6 \beta_{Coll} \eta_{Agglo} \sigma^{a_7}. \tag{5-10}$$

in which a_7 is the order of the supersaturation dependency. The kinetics for nucleation and growth remain unchanged. The parameter values of the kinetics can be found in Table 5-5.

Table 5-5: Kinetic parameters and least square error (supersaturation dependent)

Parameter	Description	Value
a_1	Nucleation parameter	$4e^{13}$
a_2	Nucleation order	$3.7e^{-5}$
a_3	Growth parameter	$1e^{-7}$
a_4	Growth order	0.7
a_5	Agglomeration parameter	$9e^{4}$
a_6	Agglomeration efficiency factor	$1e^{9}$
a_7	Agglomeration order of supersaturation dependence	1
$f_{Objective}$	Least square error	3011.4

From Figure 5-8 it can be seen that with the supersaturation dependency the time required for reaching steady state is approximately the same as without the supersaturation dependency (50 hours). The L_{10} and L_{50} are again overestimated while the L_{90} is correctly modeled. A comparison between the model with and without the super saturation dependency can be found in Table 5-6. The least square error decreases 5.87% by including supersaturation in the agglomeration expression.

Table 5-6: Steady state percentiles with and without supersaturation dependency

Percentile	Supersaturation independent [μm]	Supersaturation dependent [μm]	Absolute deviation [%]
L_{10}	70.96	70.3276	0.89
L_{50}	128.26	126.8803	1.09
L_{90}	307.58	304.9951	0.84

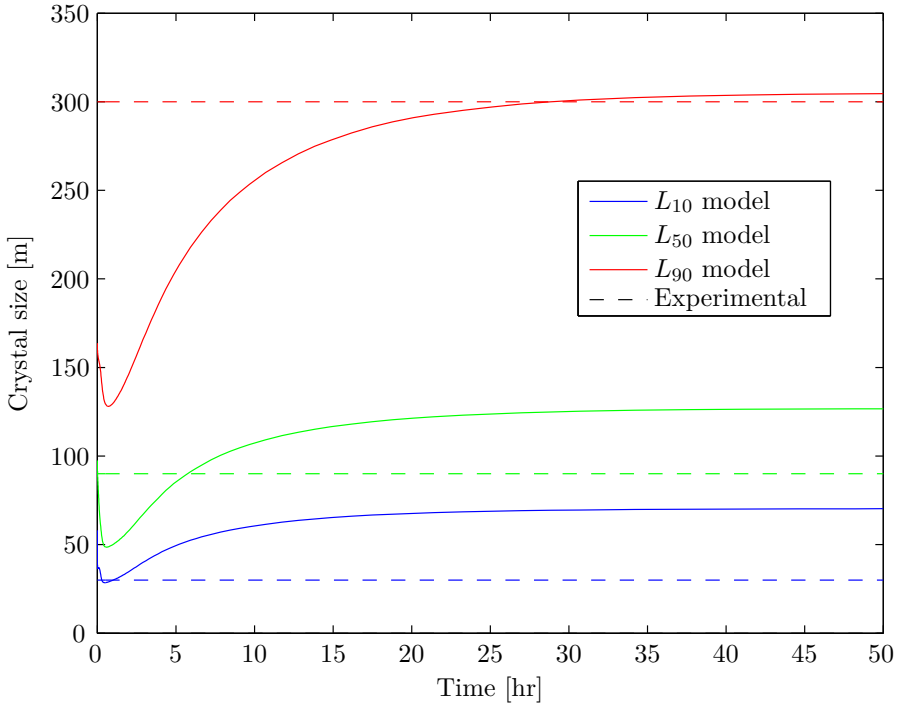

Figure 5-8: The distribution percentiles, modeling and experimental result

Instead of using a size-dependent agglomeration rate one could also use a constant size-independent agglomeration rate as used in the numerical test cases (Section 5-1). Again nucleation and crystal growth are described by the expressions given earlier. The values of the kinetic parameters can be found in Table 5-7.

Table 5-7: Kinetic parameters and least square error (constant agglomeration rate)

Parameter	Description	Value
a_1	Nucleation parameter	$1.8e^{12}$
a_2	Nucleation order	$3.70e^{-7}$
a_3	Growth parameter	$1e^{-7}$
a_4	Growth order	0.7
a_5	Constant agglomeration kernel	$1e^{-15}$
$f_{Objective}$	Least square error	2866.6

Depicted in Figure 5-9 are the CSD percentiles of the distribution with a constant agglomeration rate. The time needed to reach steady state conditions is approximately 15 hours which is a 70% decrease compared to the mechanistic model. In this model run both the L_{10} and L_{90} are modeled correctly while only the L_{50} is over estimated. A comparison of the steady state percentile values can be found in Table 5-8. Compared to the mechanistic model independent of supersaturation the least square error decreased 10.40%. Compared to the supersaturation dependent mechanistic model the decrease is 4.81%.

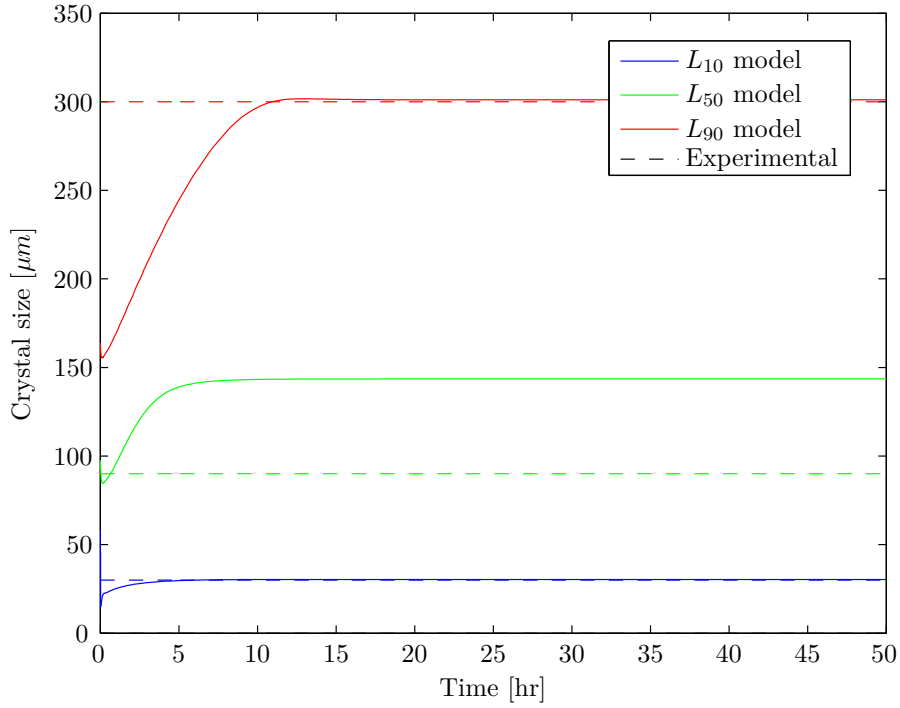

Figure 5-9: The distribution percentiles, modeling and experimental result (constant agglomeration rate)

Table 5-8: Steady state percentiles experimental and modeled (constant agglomeration rate)

Percentile	Experimental [μm]	Modeled [μm]	Absolute deviation [%]
L_{10}	30.00	30.35	1.17
L_{50}	90.00	142.528	58.36
L_{90}	300.00	301.1274	0.38

Another approach could be to model the agglomeration flux with an empirical correlation which has a dependency on both the supersaturation and the power input by the stirrer. This expression combines the size independence of the constant agglomeration rate with the dependency on supersaturation (growth) and impeller input from the mechanistic model. An expression from Lindenberg et al. (2007) is used:

$$\beta_{Agglo} = a_8 * G^{a_9} * \varepsilon^{a_{10}} \tag{5-11}$$

The values for the kinetic parameters can be found in Table 5-9.

The least square error is 1800.7 as can be seen in Table 5-9. This translates in a CSD where the L_{10} and L_{90} are slightly underestimated while the L_{50} is overestimated. This is the most accurate CSD. The time to reach steady state is again 15 hours. A comparison with an absolute deviation is given in Table 5-10.

Table 5-9: Kinetic parameters and least square error ((Lindenberg et al., 2007))

Parameter	Description	Value
a_1	Nucleation parameter	$8e^{12}$
a_2	Nucleation order	$3.7e^{-5}$
a_3	Growth parameter	$1e^{-7}$
a_4	Growth order	0.7
a_5	Agglomeration parameter	$6e^{-9}$
a_6	Agglomeration order of growth dependence	0.7
a_7	Agglomeration order of power dependence	0.7
$f_{Objective}$	Least square error	1800.7

Table 5-10: Steady state percentiles experimental and modeled (Lindenberg et al., 2007)

Percentile	Experimental [μm]	Modeled [μm]	Absolute deviation [%]
L_{10}	30.00	24.18	19.40
L_{50}	90.00	130.46	44.96
L_{90}	300.00	288.66	3.78

It is clear that different expressions for the agglomeration rate result in different CSD's. The supersaturation dependence of the mechanistic model did not change the resulting CSD significantly. According to the model results the models which are size-dependent require a longer time to reach the steady state. The least square errors for the models which are size-independent are smaller compared with the size-dependent models. The errors are compared in Table 5-11.

Table 5-11: Least square errors of the different models compared to Lindenberg (Lindenberg et al., 2007)

Agglomeration rate expression	Least square error [μm]	Absolute deviation compared to Lindenberg (Lindenberg et al., 2007) [%]
(Lindenberg et al., 2007)	1800.7	–
Constant	2866.6	37.18
Supersaturation dependent	3011.4	40.20
Supersaturation independent	3199.26	43.72

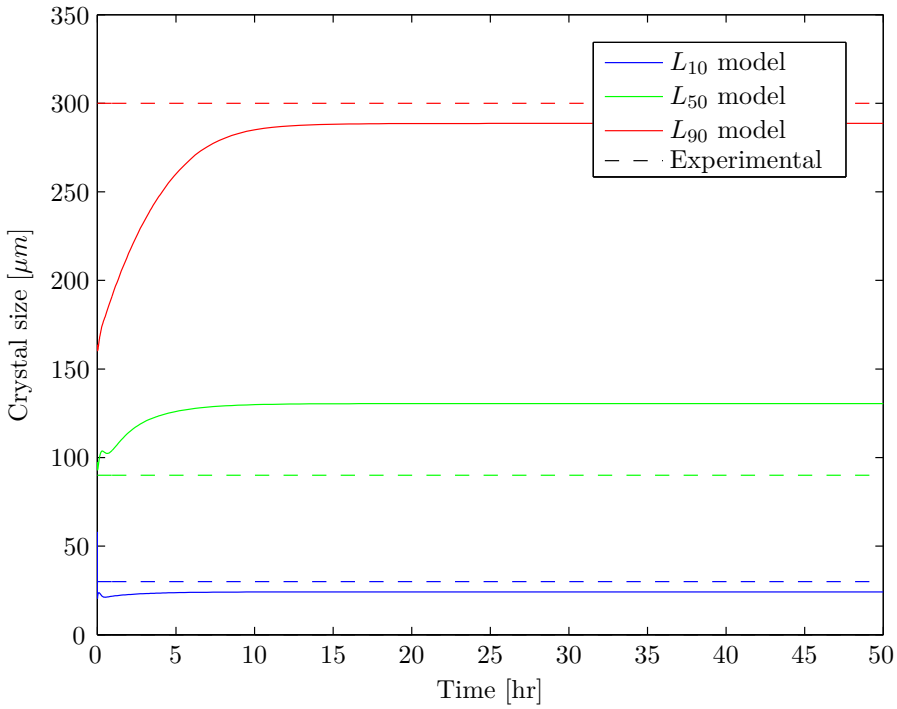

Figure 5-10: The distribution percentiles, modeling and experimental result (Lindenberg et al., 2007)

Chapter 6

Conclusions and recommendations

6-1 Conclusions

In this thesis a dynamic model for adipic acid crystallization was developed in order to answer the following research question:

"Can the dynamics of the adipic acid crystallization process be described in terms of the product quality when nucleation, growth and agglomeration are included in a mathematical model?"

The development of the process model was done in several step. The first step consisted of a small literature study for numerical methods to solve a Population Balance Equation (PBE). It was concluded that the High Resolution Finite Volume Methods (HR-FVM) with flux limiter was the best suited for this particular problem. The HR-FVM method is capable of describing sharp discontinuities and steep moving fronts found in crystallization processes with a limited amount of numerical diffusion (Qamar, 2008). Besides its accuracy the computational burden of the HR-FVM is relatively low compared to other types of solution methods (Mesbah, 2010). The aforementioned properties ensure that the numerical solution is accurate and obtained in a time-scale commensurate with the process time scale (Kumar and Ramkrishna, 1997).

The Matlab implementation of this numerical method was tested using several numerical test cases from literature. These test cases included nucleation, growth and agglomeration with different initial distributions. Based on the numerical test cases it can be concluded that the HR-FVM can indeed solve the PBE with reasonable accuracy and a small computational burden.

The numerical method was extended with mass, energy and a concentration balance to model the actual crystallization process. Without agglomeration this model is equal to an Mixed Suspension Mixed Product Removal (MSMPR). The simulation results of the MSMPR where compared with the analytical solution. It was concluded that the model extended with the mass, energy and concentration balance can accurately describe the steady-state Crystal Size Distribution (CSD) of such an MSMPR.

Another literature study was done on the subject of agglomeration as this was described to be a dominant phenomena in adipic acid crystallization by de Ruiter (Ruiter, 2009). The size scale of the crystals have a large influence on the way the crystals collide with each other. Due to the process conditions the size scale of the crystals in the BASF adipic acid crystallization process extends from below to above the Kolmogorov length scale. As a result there are several mechanisms by which the crystals collide. It was concluded that the only model capable of describing such a system is the collision model of Kruis and Kusters (Kruis and Kusters, 1996). The agglomeration efficiency is described by an expression from Riemann and Gerstlauer as this expression has already been used in literature to model an adipic acid crystallization process, it can be fitted to experimental data while keeping its dependency on fluid shear and it has low computational burden.

The model was extended once more to include the agglomeration rate. The experimental parameters were determined using a minimization of the least square error between the model and experimental steady state percentiles. The modeled CSD deviated from the experimental data. The L_{90} was predicted correctly while the L_{10} and L_{50} were over predicted. Making the agglomeration rate dependent on supersaturation made no significant improvements. Several other agglomeration rate expressions were implemented. The results improved especially for the empirical expression which is dependent on growth and power input (Lindenberg et al., 2007). The least square error decreased 43.72%. The L_{10} and L_{90} are slightly under predicted while the L_{50} is over predicted. Thus it can be concluded that the steady-state CSD can best be described by the empirical expression of Lindenberg (Lindenberg et al., 2007).

Summarizing the above and answering the research question; with the current model framework it is proven not possible to describe the dynamics of the crystallization process as the steady state can not be accurately predicted. Several recommendations are given in the next Section.

6-2 Recommendations

There are several possibilities that should be investigated to see if the predicted steady state CSD can be improved to match the experimental data. In the current model an empirical expression is used for attrition (secondary nucleation). It should be investigated if a more mechanistic model could produce a more accurate steady-state CSD.

The primary source for attrition is the impeller within the crystallizer. Another possible source for attrition fragments could be the pump in the recirculation stream. This pump could also be a source for crystal breakage.

Besides the pump there is also a heat exchanger implemented in the recirculation stream. Although the temperature increase is currently implemented in the energy balance the dissolution of small crystals is not. This dissolution should be further investigated.

One of the assumptions is that there is no difference in the number density between the output, product and recirculation stream. It should be investigated if this is the case and if not it should be investigated if compartmental modeling could improve the results of the model.

It is recommended to gather more experimental data. Currently no usable startup data is available. The number of usable data sets with a change in process conditions is also quite

limited. These data sets are required when the experimental parameters are to be determined for reproducing the dynamics of the system.

As the collision rate and the agglomeration efficiency are both strongly dependent on the hydrodynamic conditions within the crystallizer it is recommended to do produce a computational fluid dynamic model of the crystallizer. Such a model can result in useful insights concerning the hydrodynamic conditions and can be used to verify some of the assumptions in both the collision rate and agglomeration efficiency.

Appendix A

Population balance equation

For the complete derivation the reader is directed to (Mersmann, 2001).

The number density is the limiting value of the number of particles per unit volume in the crystal size interval ΔL.

$$n = \lim_{\Delta L \to 0} \frac{\Delta N}{\Delta L} = \frac{dN}{dL} \tag{A-1}$$

In order to derive an expression for the number density balance in differential form the particle numbers in a differential crystal size interval should be examined. This interval dL can be entered by crystals that are in the feed and can exit trough product removal (in case of a continuous crystallization process). Crystals can grow into and out of the size interval. In real crystallizers the processes of crystal breakage, abrasion, agglomeration and dissolution occur. These processes are usually captured by a birth and death rate.

The number of particles that exists in a differential interval and in an infinitely small volume dV at time t is expressed as:

$$dN = ndV. \tag{A-2}$$

The total number of particles (within volume V) is:

$$N_T(V) = \int_V ndV. \tag{A-3}$$

If a balance is made for a specific volume it can be expressed as:

$$\text{Particle density} = \text{Particle inflow} - \text{Particle outflow} + \text{Netto number of births.}$$

In mathematical form this results in:

$$\frac{d}{dt}\int_V n dV = \int_V [B(L) - D(L)]dV. \tag{A-4}$$

According to (Mersmann, 2001) the left hand side can be rewritten resulting in:

$$\int_V \left(\frac{\partial n}{\partial t} + \nabla(v \cdot n)\right) dV = \int_V [B(L) - D(L)]dV. \tag{A-5}$$

Equation (A-5) can be rewritten as:

$$\int_V \left(\frac{\partial n}{\partial t} + \nabla v_e \cdot n + \nabla v_i \cdot n + D(L) - B(L)\right) dV. \tag{A-6}$$

As is visible from equation (A-6) the vector v from equation (A-5) consists of two parts, the internal and the external part. The vector v_e is given by the external coordinate system (e.g. the crystallizer) and can be determined using a force balance on the specific particle. The internal part v_e orientates itself along an internal coordinate system. The linear growth rate $G = dL/dt$ yields the most important factor for internal velocity (in supersaturated solutions).

The terms n, $B(L)$ and $D(L)$ are only functions of time and not of position because ideally mixing is assumed. Ideally mixing results in roughly the same particle distributions in the entire volume. The external part of the velocity vector can be rewritten as a surface integral (Gauss theorem).

$$\int_V \nabla v_e \cdot n dV = \int_S v_n \cdot n dS \tag{A-7}$$

In equation (A-7) the vector v_n is the mean particle velocity perpendicular to the surface. The parameter S is the sum of all moving surfaces of the system:

- The inflow and outflow of a total of k particle flows $\dot{V}_i$

$$\int_{S_m} v_n \cdot n dS = \sum_k \dot{v}_i n_i \tag{A-8}$$

- The change in the solid-free systems volume

$$\int_{S_s} v_n \cdot n dS = n\frac{dV_s}{dt} \tag{A-9}$$

- The change in aperture volume due to suspended particles

$$\int_{S_e} v_n \cdot n dS = -n\frac{dV_e}{dt} \tag{A-10}$$

In equations (A-8) to (A-10) S_S represents the free surface of the liquid, V_S is the solid-free volume of the liquid, S_e is the total solid-liquid phase boundary and V_e is the total particle volume. Equations (A-9) and (A-10) can be combined:

$$\int_{S_s} v_n \cdot n dS + \int_{S_s} v_n \cdot n dS = n \frac{dV}{dt}. \tag{A-11}$$

Which can be rewritten into:

$$\int_{V} \nabla v_e \cdot n dV = \sum_k \dot{V}_i n_i + n \frac{dV}{dt}. \tag{A-12}$$

When equations (A-7) and (A-12) are combined, integrated and divided by volume V it results in:

$$\frac{\partial n}{\partial t} + \nabla v_i \cdot n + n \frac{\partial V}{V \partial t} + D(L) - B(L) + \sum_k \dot{V}_i n_i = 0. \tag{A-13}$$

If only the linear growth rate G contributes to the internal velocity then equation (A-13) can be rewritten to:

$$\frac{\partial n}{\partial t} + \frac{\partial (Gn)}{\partial L} + n \frac{\partial V}{V \partial t} + D(L) - B(L) + \sum_k \dot{V}_i n_i = 0. \tag{A-14}$$

When it is assumed that the total volume does not change with time, equation (A-14) can be rewritten to result in:

$$\frac{\partial n}{\partial t} + \frac{\partial (Gn)}{\partial L} + D(L) - B(L) + \sum_k \dot{V}_i n_i = 0. \tag{A-15}$$

Appendix B

Model equations

In order to derive the model equations the assumption given in Section 3-4 are taken as valid.

B-1 Population balance equation

$$\frac{\partial n}{\partial t} + \frac{\partial Gn}{\partial L} = \frac{\dot{V}_{feed} n_{feed}}{V_C} - \frac{\dot{V}_{out} n_{out}}{V_C} + \frac{\dot{V}_{rec} n_{rec}}{V_C} + K_{agg} \tag{B-1}$$

The feed is crystal free, see assumptions.

$$\frac{\partial n}{\partial t} + \frac{\partial Gn}{\partial L} = -\frac{\dot{V}_{out} n_{out}}{V_C} + \frac{\dot{V}_{rec} n_{rec}}{V_C} + K_{agg} \tag{B-2}$$

Multiplying with $k_v L^3$ and integrating over the complete size domain:

$$\int_0^\infty k_v L^3 \frac{\partial n}{\partial t} dL + \int_0^\infty k_v L^3 \frac{\partial Gn}{\partial L} dL = -\int_0^\infty k_v L^3 \frac{\dot{V}_{out} n_{out}}{V_C} dL + \int_0^\infty k_v L^3 \frac{\dot{V}_{rec} n_{rec}}{V_C} dL + \int_0^\infty k_v L^3 K_{agg} dL. \tag{B-3}$$

The second term on the left hand side can be rewritten by using integration by parts.

$$\int_0^\infty k_v L^3 \frac{\partial n}{\partial t} dL = k_v \int_0^\infty 3GnL^2 dL - \int_0^\infty k_v L^3 \frac{\dot{V}_{out} n_{out}}{V_C} dL + \int_0^\infty k_v L^3 \frac{\dot{V}_{rec} n_{rec}}{V_C} dL + \int_0^\infty k_v L^3 K_{agg} dL. \tag{B-4}$$

Substituting $k_v m_3 = 1 - \varepsilon$ wherever possible:

$$\frac{\partial \varepsilon}{\partial t} = -3k_v \int_0^\infty GnL^2 dL + \frac{\dot{V}_{out}}{V_C}(1-\varepsilon) - \frac{\dot{V}_{rec}}{V_C}(1-\varepsilon) - k_v \int_0^\infty L^3 K_{agg} dL. \tag{B-5}$$

B-2 Mass balance

$$\begin{aligned}\frac{d}{dt}\left[V(\varepsilon\rho_{liq}+(1-\varepsilon)\rho_{crys})\right] &= \dot{V}_{feed}\left[\varepsilon_{feed}\rho_{liq}+(1-\varepsilon_{feed})\rho_{crys}\right]-\dot{V}_{out}\left[\varepsilon_{out}\rho_{liq}+(1-\varepsilon_{out})\rho_{crys}\right]+...\\ &\quad \dot{V}_{rec}\left[\varepsilon_{rec}\rho_{liq}+(1-\varepsilon_{rec})\rho_{crys}\right]-\dot{V}_{vap}\rho_{vap} \qquad \text{(B-6)}\end{aligned}$$

With the assumptions as stated before equation (B-6) can be rewritten to:

$$\begin{aligned}\frac{d}{dt}\left[V(\varepsilon\rho_{liq}+(1-\varepsilon)\rho_{crys})\right] &= \dot{V}_{feed}\rho_{liq}-\dot{V}_{out}\left[\varepsilon\rho_{liq}+(1-\varepsilon)\rho_{crys}\right]+...\\ &\quad \dot{V}_{rec}\left[\varepsilon\rho_{liq}+(1-\varepsilon)\rho_{crys}\right]-\dot{V}_{vap}\rho_{vap}. \qquad \text{(B-7)}\end{aligned}$$

The left hand side can be rewritten by using integration by parts:

$$\begin{aligned}\frac{d\varepsilon}{dt}\left[\rho_{liq}-\rho_{crys}\right]V &= \dot{V}_{feed}\rho_{liq}-\dot{V}_{out}\left[\varepsilon\rho_{liq}+(1-\varepsilon)\rho_{crys}\right]+...\\ &\quad \dot{V}_{rec}\left[\varepsilon\rho_{liq}+(1-\varepsilon)\rho_{crys}\right]-\dot{V}_{vap}\rho_{vap}. \qquad \text{(B-8)}\end{aligned}$$

B-3 Concentration balance

$$\frac{d}{dt}V\left[\varepsilon\rho_{liq}c+(1-\varepsilon)\rho_{crys}\right]=\dot{V}_{feed}\rho_{liq}c_{feed}-\dot{V}_{out}\left[\varepsilon\rho_{liq}c+(1-\varepsilon)\rho_{crys}\right]+\dot{V}_{rec}\left[\varepsilon\rho_{liq}c+(1-\varepsilon)\rho_{crys}\right] \qquad \text{(B-9)}$$

The left hand side can be rewritten by using integration by parts:

$$\frac{d\varepsilon}{dt}\left[\rho_{liq}c-\rho_{crys}\right]V+\frac{dc}{dt}V\varepsilon\rho_{liq}=\dot{V}_{feed}\rho_{liq}c_{feed}-\dot{V}_{out}\left[\varepsilon\rho_{liq}c+(1-\varepsilon)\rho_{crys}\right]+\dot{V}_{rec}\left[\varepsilon\rho_{liq}c+(1-\varepsilon)\rho_{crys}\right]. \qquad \text{(B-10)}$$

Rewriting equation (B-10) to concentration gives:

$$\frac{dc}{dt}=\frac{1}{V\varepsilon\rho_{liq}}\left[\dot{V}_{feed}\rho_{liq}c_{feed}-\dot{V}_{out}\left[\varepsilon\rho_{liq}c+(1-\varepsilon)\rho_{crys}\right]+\dot{V}_{rec}\left[\varepsilon\rho_{liq}c+(1-\varepsilon)\rho_{crys}\right]-\frac{d\varepsilon}{dt}\left[\rho_{liq}c-\rho_{crys}\right]V\right]. \qquad \text{(B-11)}$$

B-4 Energy balance

$$\begin{aligned}\frac{d}{dt}\left[\varepsilon V_C\rho_{liq}c_{p,liq}T+(1-\varepsilon)V_C\rho_{crys}c_{p,crys}T\right] &= \dot{V}_{feed}[\varepsilon_{feed}\rho_{liq}c_{p,liq}T_{feed}+(1-\varepsilon_{feed})\rho_{crys}c_{p,crys}T_{feed}]+...\\ &\quad \dot{V}_{rec}[\varepsilon_{rec}\rho_{liq}c_{p,liq}T_{rec}+(1-\varepsilon_{rec})\rho_{crys}c_{p,crys}T_{rec}]-...\\ &\quad \dot{V}_{out}[\varepsilon_{out}\rho_{liq}c_{p,liq}T_{out}+(1-\varepsilon_{out})\rho_{crys}c_{p,crys}T_{out}]-...\\ &\quad \dot{V}_{vap}\rho_{vap}h_{evap}+P_{imp}-Q_{loss}+Q_{crys} \qquad \text{(B-12)}\end{aligned}$$

The same assumptions as before are applied here:

$$\begin{aligned}\frac{d}{dt}\left[\varepsilon V_C \rho_{liq} c_{p,liq} T + (1-\varepsilon) V_C \rho_{crys} c_{p,crys} T\right] &= \dot{V}_{feed}\rho_{liq} c_{p,liq} T_{feed} + ... \\ &\quad \dot{V}_{rec}[\varepsilon \rho_{liq} c_{p,liq} T_{rec} + (1-\varepsilon)\rho_{crys} c_{p,crys} T_{rec}] - ... \\ &\quad \dot{V}_{out}[\varepsilon \rho_{liq} c_{p,liq} T + (1-\varepsilon)\rho_{crys} c_{p,crys} T] - ... \\ &\quad \dot{V}_{vap}\rho_{vap} h_{evap}. \end{aligned} \tag{B-13}$$

The left hand side of equation (B-13) can be rewritten by the use of integration by parts.

$$\begin{aligned}\frac{d\varepsilon}{dt}\left[V_C \rho_{liq} c_{p,liq} T - V_C \rho_{crys} c_{p,crys} T\right] &= \dot{V}_{feed}\rho_{liq} c_{p,liq} T_{feed} + ... \\ &\quad \dot{V}_{rec}[\varepsilon \rho_{liq} c_{p,liq} T_{rec} + (1-\varepsilon)\rho_{crys} c_{p,crys} T_{rec}] - ... \\ &\quad \dot{V}_{out}[\varepsilon \rho_{liq} c_{p,liq} T + (1-\varepsilon)\rho_{crys} c_{p,crys} T] - ... \\ &\quad \dot{V}_{vap}\rho_{vap} h_{evap}. \end{aligned} \tag{B-14}$$

Equations (B-5), (B-8), (B-11) and (B-14) form a system of equations which can be solved for the feed volume flow, vapor volume flow and the concentration.

Appendix C

Matlab code

C-1 Crystallizer main model

```
function output = Ali_Main(p)
tic
%-------------------------------------------------------------------------
%Operational inputs
%-------------------------------------------------------------------------

%Volume flows
V_out=76/3600;                  %[m3/s], Outlet flow crystallizer
V_rec=60/3600;                  %[m3/s], Recirculation stream crystallizer

%Temperatures
T_feed=80;                      %[C], Feed stream temperature
T_rec=65;                       %[C], Recirculation stream temperature
T=60;                           %[C], Crystallizer temperature
Vc=34.1;                        %[m3], Crystallizer volume
Crys_frac=0.025;                %[-], Initial crystal fraction in the ...
    crystallizer
epsilon0=1-Crys_frac;           %[-], Initial liquid fraction in the crystallizer
%-------------------------------------------------------------------------
%Physical parameters (densities, concentrations, viscosities, specific heats, ...
    heat of evaporation)
%-------------------------------------------------------------------------

%Densities
rho_vap=0.1308;                 %[kg/m3], Vapor density @ 200mbar and ...
    quality=1 from FluidProp
rho_liq=1011;                   %[kg/m3], Liquid density (saturated and ...
    crystal free) from Westhoff
rho_crys=1344;                  %[kg/m3], Crystal density

%Specific heats and enthalpy of evaporation
h_evap=2358.11e3;               %[J/kg], Enthalpy of evaporation @ 60C from ...
    Marsh 1987
```

```
29 cp_liq=1590;                      %[J/(kg*K)], Specific heat of the saturated ...
       solution from Westhoff
30 cp_crys=4022;                     %[J/(kg*K)], Specific heat of the crystals ...
       from Westhoff
31
32 kv=0.55;                          %[-], Volumetric shape factor from BASF
33
34 %Concentrations
35 c_sat=0.7087*exp(0.0509*T)/100; %[-], Saturated concentration
36 c0=0.1697;%0.18;                        %[-], Initial concentration in the ...
       crystallizer
37 c_feed=0.4;                       %[-], Feed concentration
38
39 %Viscosities
40 vis=0.0004665;                   %[Pa.sec], Visosity of water at 60C
41 kin_vis=vis/rho_liq;             %[m2/s], Kinematic viscosity of the crystal ...
       free solution
42
43 %-------------------------------------------------------------------------
44 %Impeller
45 %-------------------------------------------------------------------------
46 Ne=0.72;                         %[-], Newton number from BASF
47 N_imp_crys=35;                   %[rpm], Impeller rotational speed
48 N_imp_crys=N_imp_crys/60;        %[1/s], Impeller rotational frequency
49 D_imp=2.1;                       %[m], Impeller diameter
50 epsilon_imp=(Ne*N_imp_crys^3*D_imp^5)/Vc;   %[m2/s3], Mean specific power ...
       input from Bermingham 2003
51 epsilon_imp2=(Ne*(40/60)^3*D_imp^5)/Vc;
52 %-------------------------------------------------------------------------
53 %Fitting factors
54 %-------------------------------------------------------------------------
55 % a1=p(1);
56 % a2=p(2);
57 % a3=p(3);
58 % a4=p(4);
59 % a5=p(5);
60 % a6=p(6);
61
62 a1=5e6;                            %[-], Nucleation parameter
63 a2=370e-7;%370e-7;                 %[-], Nucleation parameter
64 a3=1e-7;%;1e-7;                    %[-], Growth parameter
65 a4=0.7;                            %[-], Growth parameter
66 a5=1.05e5;%1.05e3                  %[-], K_eff
67 a6=p;
68 %a6=1.8e6;%4e6;%2e6;%3.35e-3;      %[-], K_agglo
69 %-------------------------------------------------------------------------
70 %Defining the grid
71 %-------------------------------------------------------------------------
72
73 %Grid parameters
74 N=100;                            %[-], Number of grid cells
75 Lmin=10e-6;                       %[m], Lower boundary grid
76 Lmax=1e-3;                        %[m], Upper boundary grid
77 q=12;                              %[-], Geometric grid factor
78 eps=1e-10;                        %[-], To avoid division by zero in the flux ...
       limiter
79
```

```
Lh(1) = Lmin;

for i=2:N+1
    Lh(i) = Lmin+2^((i-N-1)/q)*(Lmax-Lmin);    % L_(i-1/2)
end


for i=1:N
    L(i) = (Lh(i)+Lh(i+1))/2;                    % L_(i)
    dL(i) = (Lh(i+1)-Lh(i));
end

%For the agglomeration flux convert Lh, L and dL to volume
xh=kv.*Lh.^3;
x=kv.*L.^3;
dx=diff(xh);

%Converting the a2 parameter to a grid cell
for i=1:N
    if L(i)>a2
        LL=a2-L(i-1);
        LR=L(i)-a2;
        if LL<LR
            a2_int=i-1;
            break
        else
            a2_int=i;
            break
        end
    end
end
a2=a2_int;
%-------------------------------------------------------------------------
%Initial distribution
%-------------------------------------------------------------------------
mu=log(100e-6);                     %[m], Mean of the distribution (crystal size)
sigma=log(1.5);                     %[m], Standard deviation of the distribution
Y = lognpdf(L,mu,sigma);            %[-], Lognormal probability density function

%load('nlast.mat')
%ntilde0=nlast;
%Testing steady state

n0=Crys_frac*(Y./(kv.*L.^3));       %[#/m*m3], Initial number distribution
ntilde0=Crys_frac*Y;                %[#/m], Initial volume number density


t0=0;                               %[s], Starting time simulation
tmax=200000;                          %[s], Running time simulation

%-------------------------------------------------------------------------
%Agglomeration
%-------------------------------------------------------------------------
kernel=zeros(length(L),length(L));
for i=1:length(L)
    for j=1:length(L)
        kernel(i,j)=collision2(L(i),L(j),D_imp,epsilon_imp,kv,rho_crys,rho_liq,kin_vis,a5,a6,Vc)
```

```
    end
end
% figure(11)
% surf(kernel)
%tic

collisionrate1=zeros(N-1,N-1,N);
collisionrate2=zeros(N-1,N-1,N);

collisionrate11=zeros(N-1,N-1,N);
collisionrate22=zeros(N-1,N-1,N);


for i=1:N-1
    for k = 1:i
        xdif = xh(i+1)-x(k);
        if xdif < xh(2)
            xdif = xh(2);
        end

        for j=2:length(xh)
            if xdif ≤ xh(j) && xdif > xh(j-1)
                alpha=j;
            end
        end

        for j = alpha:N
            L1=L(i);%(x(i)/kv)^(1/3);
            L2=L(k);%(x(k)/kv)^(1/3);
            collisionrate1(i,k,j)=collision(L1,L2,D_imp,epsilon_imp,kv,rho_crys,rho_liq,kin_vis,
            collisionrate11(i,k,j)=collision(L1,L2,D_imp,epsilon_imp2,kv,rho_crys,rho_liq,kin_vi


            L1=(((xh(alpha) + xh(i+1) - x(k))/(kv))/2)^(1/3);
            L2=(x(k)/kv)^(1/3);
            collisionrate2(i,k,j)=collision(L1,L2,D_imp,epsilon_imp,kv,rho_crys,rho_liq,kin_vis,
            collisionrate22(i,k,j)=collision(L1,L2,D_imp,epsilon_imp2,kv,rho_crys,rho_liq,kin_vi
        end
    end
end
%toc

%-------------------------------------------------------------------------
%Solving the PBE
%-------------------------------------------------------------------------

col1=1;
col2=2;

options=odeset('Events',@eventsDTB,'RelTol',1e-3,'AbsTol',1e-6);%, 'Refine',15);
%tic
[t,X]=ode15s(@Ali_ode_model,[t0 tmax],[c0 ntilde0],options, a1, a2, a3, ...
    a4,c_feed, collisionrate1, collisionrate2, collisionrate11, ...
    collisionrate22,  cp_crys, cp_liq, c_sat, dL, h_evap, kv, L, Lmax, Lmin, ...
    N, q, rho_crys, rho_liq, rho_vap, T, T_feed, T_rec, V_out, V_rec, Vc, Lh, ...
    xh, x);
%toc
```

```
190
191 output=[t,X];
192
193 % %------------------------------------------------------------------------
194 % %Plotting the figures
195 % %------------------------------------------------------------------------
196 % %Splitting the output vector
197 %
198 % %Concentration vector
199 % conc=X(:,1);
200 %
201 % t=t/3600;
202 %
203 % %Number density
204 ntilde=X(:,2:size(X,2));
205 %
206
207 for i=1:length(t)
208     n(i,:)=ntilde(i,:)./(kv.*L.^3);
209 end
210
211 % C_sat=ones(length(conc))*c_sat;
212
213 % figure(1)
214 % plot(t,conc,t,C_sat,'red')
215 % title('Concentration versus time')
216 % xlabel('Time [hr]')
217 % ylabel('Concentration [-]')
218 % %
219 % for i=1:length(t)
220 %     m0(i)=sum(n(i,:).*dL);
221 %     m1(i)=sum(n(i,:).*L.*dL);
222 %     m2(i)=sum(n(i,:).*L.^2.*dL);
223 %     m3(i)=sum(n(i,:).*L.^3.*dL);
224 %     m4(i)=sum(n(i,:).*L.^4.*dL);
225 %     epsilon(i)=1-kv*m3(i);
226 % end
227 %
228 % figure(2)
229 % plot(t,epsilon)
230 % title('Liquid fraction versus time')
231 % xlabel('Time [hr]')
232 % ylabel('Liquid fraction [-]')
233
234 % figure(3)
235 % subplot(2,3,1)
236 % plot(t,m0)
237 % title('Zeroth moment of distribution versus time')
238 % xlabel('Time [hr]')
239 % ylabel('Zeroth moment [-]')
240 % subplot(2,3,2)
241 % plot(t,m1)
242 % title('First moment of distribution versus time')
243 % xlabel('Time [hr]')
244 % ylabel('First moment [-]')
245 % subplot(2,3,3)
246 % plot(t,m2)
```

```
% title('Second moment of distribution versus time')
% xlabel('Time [hr]')
% ylabel('Second moment [-]')
% subplot(2,3,4)
% plot(t,m3)
% title('Third moment of distribution versus time')
% xlabel('Time [hr]')
% ylabel('Third moment [-]')
% subplot(2,3,5)
% plot(t,m4)
% title('Fourth moment of distribution versus time')
% xlabel('Time [hr]')
% ylabel('Fourth moment [-]')

% %Initial distribution and distribution at tmax
% figure(4)
% plot(L,n(1,:),L,n(length(t),:),'red');

%Mean crystal size
% mu2=m4./m3;

% figure(5)
% plot(t,mu2)
% title('Mean crystal size versus time')
% xlabel('Time [hr]')
% ylabel('Mean size [-]')
%

%Calculating the L10, L50, L90
nopart=zeros(length(t),N);
for i=1:length(t)
    nopart(i,:)=cumsum(n(i,:).*dL);
    percentiles(i,1)=nopart(i,N)/100*10;
    percentiles(i,2)=nopart(i,N)/100*50;
    percentiles(i,3)=nopart(i,N)/100*90;
    L10(i)=interp1(nopart(i,:),L,percentiles(i,1));
    L50(i)=interp1(nopart(i,:),L,percentiles(i,2));
    L90(i)=interp1(nopart(i,:),L,percentiles(i,3));

end

% cum_sum=cumsum(n,2);
% for i=1:length(t)
%     percentiles(i,1)=cum_sum(i,N)/100*10;
%     percentiles(i,2)=cum_sum(i,N)/100*50;
%     percentiles(i,3)=cum_sum(i,N)/100*90;
%     L10(i)=interp1(cum_sum(i,:),L,percentiles(i,1));
%     L50(i)=interp1(cum_sum(i,:),L,percentiles(i,2));
%     L90(i)=interp1(cum_sum(i,:),L,percentiles(i,3));
% % end

% load('X10X50X90_fast20090408.mat')
%
% figure(20)
% plot(t,L10,t,L50,t,L90,time2,L10_exp/1e6,time2,L50_exp/1e6,time2,L90_exp/1e6)
% legend('L10','L50','L90', 'L10 exp','L50 exp', 'L90 exp')
% xlabel('Time [hr]')
```

```
% ylabel('Crystal size [m]')

%
% figure(20)
% plot(t,L10,t,L50,t,L90)
% legend('L10','L50','L90')
% xlabel('Time [hr]')
% ylabel('Crystal size [m]')

%
% global V_feed_glob V_vap_glob t_plot
% figure(6)
% subplot(1,2,1)
% plot(t_plot,V_feed_glob*3600)
% title('Feed volume flow versus time')
% xlabel('Time [s]')
% ylabel('Volume flow [m3/s]')
% subplot(1,2,2)
% plot(t_plot,V_vap_glob*3600)
% title('Vapor volume flow versus time')
% xlabel('Time [s]')
% ylabel('Volume flow [m3/s]')
%
% %
%  global B0_plot G_plot
% figure(7)
% subplot(1,2,1)
% plot(t_plot,B0_plot)
% title('Nucleation rate versus time')
% xlabel('Time [hr]')
% ylabel('Nucleation rate [#/s]')
% subplot(1,2,2)
% plot(t_plot,G_plot)
% title('Growth rate versus time')
% xlabel('Time [hr]')
% ylabel('Growth rate [m/s]')
% %
% %-------------------------------------------------------------------------
% %Plots for the steady state solution testing
% %-------------------------------------------------------------------------
%

% for i=2:length(mu2)
%     mu2_diff(i)=((mu2(i)-mu2(i-1))/mu2(i-1))*100;
% end
%
% figure(8)
% plot(t,mu2_diff)
% xlabel('Time [hr]')
% ylabel('Difference between two subsequent calculated values [%]')
%
%
%
%
%
% %Analytical solution of the MSMPR
% global G_plot
```

```
% %Calculation of residence time
% tau=Vc/(V_out-V_rec);
% for i=1:N
%     n_ana(i)=n(size(n,1),1)*(1)*exp(-L(i)/(G_plot(length(G_plot))*tau));
% end
%
% figure(9)
% semilogy(L,n_ana,L,n(size(n,1),:),'x')
%
% global Q_agg_plot
% figure(10)
% surf(Q_agg_plot)

%Calculating the sum of squares
SS(1)=L10(length(L10))*1e6-32;
SS(2)=L50(length(L50))*1e6-150;
SS(3)=L90(length(L90))*1e6-367;

output=sum(SS.^2)
toc
```

C-2 Crystallizer differential equations

```
%Differential equations for the DTB model

function dXdt = Ali_ode_model(t, X0, a1, a2, a3, a4, c_feed, collisionrate1, ...
    collisionrate2, collisionrate11, collisionrate22, cp_crys, cp_liq, c_sat, ...
    dL, h_evap, kv, L, Lmax, Lmin, N, q, rho_crys, rho_liq, rho_vap, T, ...
    T_feed, T_rec, V_out, V_rec, Vc, Lh, xh, x)
t;

% if t>2200 && t<18000
% V_rec=30/3600;
% end

%Splitting the input vector in the PBE and the concentration
c=X0(1);                    %[-], Concentration
ntilde=X0(2:length(X0))';    %[-], Volumer number density
n=ntilde./(kv.*L.^3);       %[-], Number density

%Calculating the liquid fraction
m3=n.*L.^3.*dL;
epsilon=1-kv*sum(m3);        %[-], Liquid fraction

%-------------------------------------------------------------------------
%Secondary nucleation
%-------------------------------------------------------------------------
global B0_plot
B0=a1*sum(m3(a2:length(m3)));   %[-], Nucleation rate
B0=B0*kv*Lh(1)^3;
B0_plot(length(B0_plot)+1)=B0;

%-------------------------------------------------------------------------
%Growth
%-------------------------------------------------------------------------
```

```
global G_plot
G=a3*((c-c_sat)/c_sat)^a4;        %[-], Growth rate
G_plot(length(G_plot)+1)=G;

%-------------------------------------------------------------------------
%Agglomeration
%-------------------------------------------------------------------------
Fhalfmin=0;
Fhalfmax=0;
for i=1:N-1
    sumk = zeros(N,1);
    for k = 1:i
        xdif = xh(i+1)-x(k);
        if xdif < xh(2)
            xdif = xh(2);
        end

        for j=2:length(xh)
            if xdif <= xh(j) && xdif > xh(j-1)
                alpha=j;
            end
        end

        for j = alpha:N
            int1(j)=(xh(j+1)-xh(j))*collisionrate1(i,k,j)*ntilde(j);
        end
        int2=(xh(alpha)-(xh(i+1)-x(k)))*collisionrate2(i,k,j)*ntilde(alpha-1);
        sumk(k)=(sum(int1)+int2)*(xh(k+1)-xh(k))*ntilde(k);
    end
    Fphalf(i)=sum(sumk);
end

Q_agg(1)=(Fphalf(1)-Fhalfmin)/(xh(2)-xh(1));    %First grid cell
for i=2:N-1
   Q_agg(i)=(Fphalf(i)-Fphalf(i-1))/(xh(i+1)-xh(i));    %Grid cells in between
end
Q_agg(N)=(Fhalfmax-Fphalf(N-1))/(xh(N+1)-xh(N));    %First grid cell

global Q_agg_plot

Q_agg_plot(length(Q_agg_plot)+1,:)=(Q_agg);

%-------------------------------------------------------------------------
%Balance equations (mass, energy and concentration)
%-------------------------------------------------------------------------

%Liquid fraction over time
de_dt=-3*kv*sum(G.*n.*L.^2.*dL)+((V_out/Vc)*(1-epsilon))-((V_rec/Vc)*(1-epsilon));

%System of equations for the calculation of V_feed and V_vap (based on
%energy and mass balance)


V_vap=((1/(rho_vap*h_evap))*((((V_out*((epsilon*rho_liq)+((1-epsilon)*rho_crys))-V_rec*((epsilon
      (V_out*((epsilon*rho_liq*cp_liq)+((1-epsilon)*rho_crys*cp_crys))*T)-(de_dt*((Vc*rho_liq*cp

V_feed=(V_out*((epsilon*rho_liq)+((1-epsilon)*rho_crys))-V_rec*((epsilon*rho_liq)+((1-epsilon)*r
```

```
    ;
87
88
89  % %Left side matrix
90  % P=[-rho_liq*cp_liq*T_feed rho_vap*h_evap;...
91  %    rho_liq -rho_vap];
92  %
93  % %right side matrix
94  % ...
        Q=[V_rec*((epsilon*rho_liq*cp_liq*T_rec)+((1-epsilon)*rho_crys*cp_crys*T_rec))-...
95  %    V_out*((epsilon*rho_liq*cp_liq*T)+((1-epsilon)*rho_crys*cp_crys*T))-...
96  %    de_dt*((Vc*rho_liq*cp_liq*T)-(Vc*rho_crys*cp_crys*T));...
97  %    V_out*((epsilon*rho_liq)+((1-epsilon)*rho_crys))-...
98  %    V_rec*((epsilon*rho_liq)+((1-epsilon)*rho_crys))+...
99  %    de_dt*(rho_liq-rho_crys)*Vc];
100 %
101 % global P2 Q2
102 % P2=[-rho_liq*cp_liq*T_feed; rho_vap*h_evap;...
103 %    rho_liq; -rho_vap];
104 %
105 % ...
        Q2=[V_rec*((epsilon*rho_liq*cp_liq*T_rec)+((1-epsilon)*rho_crys*cp_crys*T_rec));...
106 %     -V_out*((epsilon*rho_liq*cp_liq*T)+((1-epsilon)*rho_crys*cp_crys*T));...
107 %     -de_dt*((Vc*rho_liq*cp_liq*T)-(Vc*rho_crys*cp_crys*T));...
108 %    V_out*((epsilon*rho_liq)+((1-epsilon)*rho_crys));...
109 %    -V_rec*((epsilon*rho_liq)+((1-epsilon)*rho_crys));...
110 %    de_dt*(rho_liq-rho_crys)*Vc];
111 %
112 % %Solving
113 % U=(P\Q)';
114 %
115 global V_feed_glob V_vap_glob t_plot
116 % V_feed=U(1);        %[m3/s], Feed volume flow rate
117 % V_vap=U(2);        %[m3/s], Vapor volume flow rate
118 V_feed_glob(length(V_feed_glob)+1)=V_feed;
119 V_vap_glob(length(V_vap_glob)+1)=V_vap;
120 t_plot(length(t_plot)+1)=t;
121
122
123
124 %Concentration balance
125 dc_dt=(1/(Vc*epsilon*rho_liq))*((V_feed*rho_liq*c_feed)-...
126       (V_out*((epsilon*rho_liq*c)+((1-epsilon)*rho_crys)))+...
127       (V_rec*((epsilon*rho_liq*c)+((1-epsilon)*rho_crys)))-...
128       (de_dt*((rho_liq*c)-rho_crys)*Vc));
129
130 %-------------------------------------------------------------------------
131 %Population balance equation
132 %-------------------------------------------------------------------------
133
134 %First grid cell
135 Gnim(1)=B0;                 %[-], Left boundary flux (stiff nucleation)
136 Gnip(1)=G*ntilde(1);
137
138 %In between cells
139 for i=2:N-1
140     Gnim(i)=Gnip(i-1);      %[-] Left boundary flux is equal to the right ...
```

```
        boundary flux of the neighbouring cell
141
142     r=(ntilde(i)-ntilde(i-1)+1e-10)/(ntilde(i+1)-ntilde(i)+1e-10);
143     FluxL=(abs(r)+r)/(1+abs(r));
144     Gnip(i) = ...
            G*(ntilde(i)+dL(i)/(2*(L(i)-L(i-1)))*FluxL*(ntilde(i+1)-ntilde(i)));
145
146 end
147
148 %Last cell
149 Gnim(N)=Gnip(N-1);            %[-] Left boundary flux is equal to the right ...
        boundary flux of the neighbouring cell
150  Gnip(N) = G*(ntilde(N)+dL(N)/(2*(L(N)-L(N-1)))*(ntilde(N)-ntilde(N-1)));
151
152 %-------------------------------------------------------------------------
153 %Solving the population balance equation
154 %-------------------------------------------------------------------------
155 for i=1:N
156     dntilde_dt(i)=-1/dL(i)*(Gnip(i)-Gnim(i))+(3*G*ntilde(i)/L(i))+(V_rec*ntilde(i)/Vc)-(V_out*nt
157 end
158
159
160 %-------------------------------------------------------------------------
161 %Defining the output
162 %-------------------------------------------------------------------------
163 dXdt=[dc_dt; dntilde_dt'];
```

C-3 Data matching program

```
1  %Data filter for xls file to matlab
2
3  clear all
4  clc
5  close all
6
7  %-------------------------------------------------------------------------
8  %Loading and combining data sets from CSD, Sensor and Process
9  %-------------------------------------------------------------------------
10
11 %Loading data set measuring probe
12 [Filename1, Pathname1, Filterindex1]=uigetfile('*.xls','Select the CSD ...
       measurements file','MultiSelect','on');
13 for i=1:length(Filename1)
14     numi=strcat('num1_',int2str(i));
15     texti=strcat('text1_',int2str(i));
16     Filename=char(Filename1(i));
17   eval(['[' numi ' ' texti ']=xlsread(Filename);']);
18 end
19
20 %Combining the measuring probe data sets
21 num1=num1_1;
22 for i=2:length(Filename1)
23     num1=eval(['[num1' ';' 'zeros(1,size(num1_1,2))' ';' 'num1_' int2str(i) ...
           ']']);
24 end
```

```
25
26 text1=text1_1;
27 for i=2:length(Filename1)
28     text1=eval(['[text1' ';' 'text1_' int2str(i) ']']);
29 end
30
31 %Loading data set process conditions
32 [Filename2, Pathname2, Filterindex2]=uigetfile('*.xls','Select the ...
       measurement probe data file','MultiSelect','on');
33
34 for i=1:length(Filename2)
35     numi=strcat('num2_',int2str(i));
36     texti=strcat('text2_',int2str(i));
37     Filename=char(Filename2(i));
38   eval(['[' numi ' ' texti ']=xlsread(Filename);']);
39 end
40
41 %Combining the measuring probe data sets
42 num2=num2_1;
43 for i=2:length(Filename2)
44     num2=eval(['[num2' ';' 'num2_' int2str(i) ']']);
45 end
46
47 text2=text2_1;
48 for i=2:length(Filename2)
49     text2=eval(['[text2' ';' 'text2_' int2str(i) ']']);
50 end
51
52 %Importing the data (temperature, pressure etc.) from excel
53 [Filename3, Pathname3, Filterindex3]=uigetfile('*.xls','Select the DP3 ...
       process control system data file');
54 [num3 text3]=xlsread(Filename3);
55
56
57
58 %-------------------------------------------------------------------------
59 %Calculating time/date matrices
60 %-------------------------------------------------------------------------
61 j=1;
62 for i=1:length(text1)
63     if isempty(text1{i})==0
64        text1_final(j)=text1(i);
65        j=j+1;
66     end
67 end
68 text1_final=text1_final';
69
70
71
72 %Calculating date/time vector
73 i=1:size(text1_final,1);
74 timedate1=datevec(text1_final(i),'dd.mm.yyyy HH:MM:SS');
75
76
77 %Calculating time vector 2
78 timedate2=text2(1:length(text2),15);
79 timedate2=datevec(timedate2,'dd/mm/yyyy HH:MM:SS');
```

```
80
81 %Calculating time vector 3
82
83 timedate3=text3(6:length(text3),2);
84 %Correcting the import bug for 00:00:00
85 for i=1:length(timedate3)
86     if length(char(timedate3(i)))<19
87         timedate3(i)=strcat(timedate3(i),' 12:00:00 AM');
88     end
89 end
90
91
92 timedate3=datevec(timedate3);
93
94 %Start vector date and time (timevector 1)
95 start=datevec(text1_final(1),'dd.mm.yyyy HH:MM:SS');
96 stop=datevec(text1_final(length(text1_final)),'dd.mm.yyyy HH:MM:SS');
97
98 start2=timedate2(1,1:6);
99 stop2=timedate2(length(timedate2),1:6);
100
101 %Comparing the two start and stop date/time vectors to see which is the
102 %smallest/largest
103 % if datenum(start) > datenum(start2)
104 %     start=start2;
105 % end
106 %
107 % if datenum(stop)>datenum(stop2)
108 % else stop=stop2;
109 % end
110
111 %Checking the ADS data for starting and stopping point
112 start3=datenum(start);
113 stop3=datenum(stop);
114 timedate32=datenum(timedate3);
115 save_vector= timedate32>start3 & timedate32<stop3;
116
117 num3=[save_vector.*num3(:,1) save_vector.*num3(:,3) save_vector.*num3(:,5)...
118     save_vector.*num3(:,7) save_vector.*num3(:,9) save_vector.*num3(:,11)...
119     save_vector.*num3(:,13) save_vector.*num3(:,15) save_vector.*num3(:,17)...
120     save_vector.*num3(:,19) save_vector.*num3(:,21) save_vector.*num3(:,23)...
121     ]%save_vector.*num3(:,25) save_vector.*num3(:,27)];
122
123 %Removing the zero rows from the num3 matrix
124 num3(¬any(num3,2),:)=[];
125
126 %Multiplying the time vector with the save vector
127 timedate3=[save_vector.*timedate3(:,1) save_vector.*timedate3(:,2)...
128     save_vector.*timedate3(:,3) save_vector.*timedate3(:,4) ...
129     save_vector.*timedate3(:,5) save_vector.*timedate3(:,6)];
130
131 %Removing the zero rows from the time vector
132 timedate3(¬any(timedate3,2),:)=[];
133
134 %Converting time and date to elapsed seconds (the mathematical model uses
135 %elapsed seconds instead of time and date
136
```

```
137 %The elapsed seconds of the starting date/time
138 time_elapsed_initial=(start(1,4)*3600)+(start(1,5)*60)+start(1,6);
139
140 %Individual time vectors
141 for i=2:size(timedate1);
142     time_elapsed1(i)=(timedate1(i,4)*3600)+(timedate1(i,5)*60)+timedate1(i,6)-time_elapsed_initi
143 end
144
145 for i=2:size(timedate2);
146     time_elapsed2(i)=(timedate2(i,4)*3600)+(timedate2(i,5)*60)+timedate2(i,6)-time_elapsed_initi
147 end
148
149 for i=2:size(timedate3);
150     time_elapsed3(i)=(timedate3(i,4)*3600)+(timedate3(i,5)*60)+timedate3(i,6)-time_elapsed_initi
151 end
152
153 %-------------------------------------------------------------------------
154 %Cleaning up workspace, clearing all unneccesary variables, vectors and
155 %matrices
156 %-------------------------------------------------------------------------
157
158 clear Filename Filename1 Filename2 Filename3 Filterindex1 Filterindex2 ...
159     Filterindex3 Pathname1 Pathname2 Pathname3 i j num1_1 num1_2 ...
160     num2_1 num2_2 numi save_vector start start2 start3 stop stop2 ...
161     stop3 text1 text1_1 text1_2 text1_final text2 text2_1 text2_2 ...
162     text3 texti time_elapsed_initial timedate1 timedate2 timedate3 timedate32
163
164
165 %-------------------------------------------------------------------------
166 %Creating the x graphs from the csd data
167 %-------------------------------------------------------------------------
168
169 %Separating different data from data structure
170 j=1;
171 for i=2:17:17*ceil((size(num1,1)-2)/17)
172     ferret_max(j,:)=num1(i,:);
173     j=j+1;
174 end
175
176 j=1;
177 for i=4:17:17*ceil((size(num1,1)-2)/17)
178     ferret_min(j,:)=num1(i,:);
179     j=j+1;
180 end
181
182 j=1;
183 for i=6:17:17*ceil((size(num1,1)-2)/17)
184     twod_equi(j,:)=num1(i,:);
185     j=j+1;
186 end
187
188 j=1;
189 for i=8:17:17*ceil((size(num1,1)-2)/17)
190     elongation(j,:)=num1(i,:);
191     j=j+1;
192 end
193
```

```
194 j=1;
195 for i=10:17:17*ceil((size(num1,1)-2)/17)
196     heywood(j,:)=num1(i,:);
197     j=j+1;
198 end
199
200 j=1;
201 for i=12:17:17*ceil((size(num1,1)-2)/17)
202     volume(j,:)=num1(i,:);
203     j=j+1;
204 end
205
206 j=1;
207 for i=14:17:17*ceil((size(num1,1)-2)/17)
208     threed_qui(j,:)=num1(i,:);
209     j=j+1;
210 end
211
212 j=1;
213 for i=16:17:17*ceil((size(num1,1)-2)/17)
214     unknown(j,:)=num1(i,:);
215     j=j+1;
216 end
217
218
219 %For making arbitrary Xxx graphs
220 lwrb=10;
221 lwrbs=strcat('X',int2str(lwrb));
222 mean=50;
223 means=strcat('X',int2str(mean));
224 uprb=90;
225 uprbs=strcat('X',int2str(uprb));
226
227
228 %Actual making of the x graphs from the defined diameter name
229 diam(1,:)=num1(1,:);
230
231 for i=1:size(twod_equi,1)
232     [B,I,J]=unique(twod_equi(i,:));
233     A=diam(I);
234     x_lwrb(i)=interp1(B,A,(lwrb/100));
235 end
236
237 for i=1:size(twod_equi,1)
238     [B,I,J]=unique(twod_equi(i,:));
239     A=diam(I);
240     x_mean(i)=interp1(B,A,(mean/100));
241 end
242
243 for i=1:size(twod_equi,1)
244     [B,I,J]=unique(twod_equi(i,:));
245     A=diam(I);
246     x_uprb(i)=interp1(B,A,(uprb/100));
247 end
248
249
250 %Plotting the Xxx graphs
```

```
subplot(2,1,1)
plot(time_elapsed1,x_lwrb,time_elapsed1,x_mean,'red',time_elapsed1,x_uprb,'green')
xlabel('Time [s]')
ylabel('Crystal size, [\mum]')
legend(lwrbs,means,uprbs)
subplot(2,1,2)
plot(time_elapsed3,num3(:,4),time_elapsed3,num3(:,3),'--')
```

```
%
%
%
%
%
%
%
% %Plotting the Xxx graphs
% subplot(2,1,1)
% plot(time_elapsed,x_lwrb,time_elapsed,x_mean,'red',time_elapsed,x_uprb,'green')
% xlabel('Time [s]')
% ylabel('Crystal size, [\mum]')
% legend(lwrbs,means,uprbs)
% subplot(2,3,4)
% plot(time_elapsed,x_lwrb)
% title(lwrbs)
% subplot(2,3,5)
% plot(time_elapsed,x_mean,'red')
% title(means)
% subplot(2,3,6)
% plot(time_elapsed,x_uprb,'green')
% title(uprbs)
%
%
%
```

Bibliography

J. Abrahamson. Collision rates of small particles in a vigorously turbulent fluid. *Chemical Engineering Science*, 30(11):1371–1379, 1975.

J. Baldyga, M. Hasinka, and W. Orciuch. Barium sulphate agglomeration in a pipe - An experimental study and CFD modeling. *Chemical Engineering Technology*, 26(3):334–340, 2003.

R.D. Braatz. Advanced control of crystallization processes. *Annual Reviews in Control*, (26): 87–99, 2002.

R.D. Braatz and S. Hasebe. Particle size and shape control in crystallization processes. *AICheE Symposium Series: Proceedings of the 6th International Conference on Chemical Process Control*, pages 307–327, 2002.

B. Carnahan and H.A. Luther. *Applied Numerical methods*. Krieger Pub Co, 1990.

A.K. Chester. The modeling of coalescence processes in fluid liquid dispersions - A review of current understanding. *Chem. Eng. Res. Des.*, 69(4):259–270, 1991.

C.B.B. Costa, M.R.W. Maciel, and R.M. Filho. Considerations on crystallization modeling: Population balance solution. *Computers and Chemical Engineering*, 31(3):206–218, 2007.

J. Costes and J.P. Courderc. Study by laser doppler anemometry of turbulent flow - II. *Chemical Engineering Science*, 43:2765–2772, 1988.

R. David, P. Marchal, J-P Klein, and J. Villermaux. Crystallization and precipitation engineering–III. a discrete formulation of the agglomeration rate of crystals in a crystallization process. *Chemical Engineering Science*, 46(1):205–213, 1991a.

R. David, J. Villermaux, P. Marchal, and J-P Klein. Crystallization and precipitation engineering–IV. kinetic model of adipic acid crystallization. *Chemical Engineering Science*, 46(4):1129–1136, 1991b.

R. David, P. Marchal, and B. Marcant. Modeling of agglomeration in industrial crystallization from solution. *Chemical Engineering and Technology*, 18(5):302–309, 1995.

R. David, F. Espitalier, and A. Cameiro. Developments in the understanding and modeling of the agglomeration of suspended crystals in crystallization from solutions. *KONA*, 21: 40–53, 2003.

R.A. Eek. *Control and dynamic modeling of industrial suspension crystallizers*. PhD thesis, 1995.

G. Falkovich. *Fluid Mechanics: A Short Course for Physicists*. Cambridge University Press, 2011.

F. Filbet and P. Laurencot. Numerical simulation of the Smoluchowski coagulation equation. *SIAM Journal on Scientific Computing*, 25:2004–2048, 2004.

R. Fitzpatrick. Introduction to computational physics (lecture notes) - The University of Texas at Austin, 2011.

C. Gahn and A. Mersmann. Theoretical prediction and experimental determination of attrition rates. *Chemical Engineering Research and Design*, 75(2):125–131, 1997.

J. Garside, A. Mersman, and J. Nyvelt. *Measurement of crystal growth and nucleation rates*. Inst. of Chemical Engineers UK, 2002.

R. Gunawan, I. Fusman, and R.D. Braatz. High resolution algorithms for multidimensional population balance equations. *AIChE Journal*, 50(11):2738–2749, 2004.

M.J. Hounslow, H.S. Mumtaz, A.P. Collier, J.P. Barrick, and A.S. Bramley. A micromechanical model for the rate of aggregation during precipitation from solution. *Chemical Engineering Science*, 56(7):2543 – 2552, 2001.

H.M. Hulburt and S. Katz. Some problems in particle technology: A statistical mechanical formulation. *Chemical Engineering Science*, 19(8):555–574, 1964.

D. Ilievski and I. Livk. An agglomeration efficiency model for gibbsite precipitation in a turbulently stirred vessel. *Chemical Engineering Science*, 56(7):2010–2022, 2006.

A. Imran. Contribution of crystal-impeller and crystal-crystal collisions to secondary nucleation. *Proceedings of European Congress of Chemical Engineering*, 2007.

S.J. Jancic and P.A.M. Grootscholten. *Industrial Crystallization*. Delft University Press, Dordrecht, 1984.

A.G. Jones. *Chrystallization Process Systems*. Elsevier Science, Oxford, 2002.

F.E. Kruis and K.A. Kusters. The collision rate of particles in turbulent flow. *Chemical Engineering Communications*, 158(1):201–230, 1996.

S. Kumar and D. Ramkrishna. On the solution of population balance equations by discretization–III. Nucleation, growth and aggregation of particles. *Chemical Engineering Science*, 52(24):4659–4679, 1997.

H.D. Laufhütte and A. Mersmann. Laser-Doppler velocimetry as a suitable measuring technique for the determination of the flow behavior in stirred fluids. *German Chemical Engineering*, 8:371–379, 1985.

G. Lee, X.M. Meyer, B. Biscans, J.M. Le Lann, and E.S. Yoon. Adaptive finite difference method for the simulation of batch crystallization. *Computers and Chemical Engineering*, 23(Supplement 1):S363 – S366, 1999. European Symposium on Computer Aided Process Engineering, Proceedings of the European Symposium.

B.P. Leonard and H.S. Niknafs. Sharp monotonic resolution of discontinuities without clipping of narrow extrema. *Computers and Fluids*, 19(1):141–154, 1991.

R.J. LeVeque. *Numerical methods for conservation laws*. Birkhäuser, CH-4010 Basel Switzerland, 2004.

Y.I. Lim, J-M Le Lann, X.M. Meyer, X. Joulia, G. Lee, and E.S. Yoon. On the solution of population balance equations (PBE) with accurate front tracking methods in practical crystallization processes. *Chemical Engineering Science*, 57(17):3715–3732, 2002.

Y. Lin, K. Lee, and T. Matsoukas. Solution of the population balance equation using constant-number Monte Carlo. *Chemical Engineering Science*, 57(12):2241–2252, 2002.

C. Lindenberg, J. Schöll, L. Vicum, M. Mazzotti, and J. Brozio. L-glutamic acid precipitation: Agglomeration effects. *Crystal Growth and Design*, 8(1):224–237, 2007.

J.D. Lister, D.J. Smit, and M.J. Hounslow. Adjustable discretized population balance for growth and aggregation. *AIChE Journal*, 41(3):591–603, 1995.

A. Mersmann. *Crystallization Technology Handbook*. Marcel Dekker, 2nd edition, 2001.

A. Mersmann, R. Sangl, M. Kind, and J. Pohlisch. Attrition and secondary nucleation in crystallizers. *Chemical Engineering and Technology*, 11(1):80–88, 1988.

A. Mesbah. *Optimal operation of industrial batch crystallizers; A nonlinear model-based control approach*. PhD thesis, 2010.

N. Moldovanyi and B.G. Lakatos. Model predictive control of continuous crystallizers. *Hungarian journal of industrial chemistry*, 33:97–104, 2005.

J.W. Mullin. *Crystallization*. Reed Educational and Professional Publishing, 3rd edition, 1993.

M.T. Musser. *Adipic Acid - Ullman's Encyclopedia of industrial chemistry*. John Wiley and Sons, 2008.

A.S. Myerson. *Handbook of industrial crystallization*. Elsevier Science, 2nd edition, 2002.

A. Neumann. *Characterizing industrial crystallizers of different scale and type*. PhD thesis, 2001.

R. Ó Meadhra. *Modeling of the kinetics of suspension crystallizers; a new model for secundary nucleation*. PhD thesis, 1995.

E.P.K. Ottens and E.J. de Jong. A model for secondary nucleation in a stirred vessel cooling crystallizer. *Industrial and Engineering Chemistry Fundamentals*, 12(2):179–184, 1973.

PAON. Paon course material - Industrial crystallization and precipitation, 2003.

S. Patankar. *Numerical Heat Transfer and Fluid Flow.* Taylor and Francis, 1980.

S. Qamar. *Modeling and simulation of population balances for particulate processes.* PhD thesis, 2008.

S. Qamar and G. Warnecke. Numerical solution of population balance equations for nucleation, growth and aggregation processes. *Computers and Chemical Engineering*, 31(12): 1576–1589, 2007.

D. Ramkrishna. *Population balances, theory and applications to particulate systems in engineering.* Academic Press, San Diego, CA, 2000.

A.D. Randolph and M.A. Larson. *Theory of particulate processes.* Academic Press, San Diego, CA, 2nd edition, 1988.

C.D. Rielly and A.J. Marquis. A particle's eye view of crystallizer fluid mechanics. *Chemical Engineering Science*, 56(7):2475 – 2493, 2001.

Riemann and Gerstlauer. Modeling and simulation of adipic acid crystallization accounting for crystal growth, attrition and agglomeration. Technical Report 103.0313.0Q, BASF Ludwigshafen, 2003.

S. Rigopoulos and A.G. Jones. Finite-element scheme for solution of the dynamic population balance equation. *AIChE Journal*, 49(5):1127–1139, 2003.

C. Ruiter. Dynamic modeling and validation of an industrial adipic acid plant - MSc. Thesis, 2009.

P.G. Saffman and J.S. Turner. On the collision of drops in turbulent clouds. *Journal of Fluid Mechanics*, 1:16–30, 1956.

W.T. Scott. Analytic studies of cloud droplet coalescence. *Journal of the atmospheric sciences*, 25:54–65, 1968.

B. H. Shah, D. Ramkrishna, and J. D. Borwanker. Simulation of particulate systems using the concept of the interval of quiescence. *AIChE Journal*, 23(6):897–904, 1977.

L.F. Shampine. *Solving ODEs with MATLAB.* Cambridge, 1st edition, 2003.

M. Smith and T. Matsoukas. Constant-number Monte Carlo simulation of population balances. *Chemical Engineering Science*, 53(9):1777–1786, 1998.

M. Smoluchowski. Versuch einer mathematischen theorie der koagulationkinetik kolloider lösungen. *Zeitschrift fur Physilische Chemie*, pages 92–129, 1917.

L. A. Spielman and O. Levenspiel. A monte carlo treatment for reacting and coalescing dispersed phase systems. *Chemical Engineering Science*, 20(3):247 – 254, 1965.

M.N. Spijker. Numerical stability (lecture notes) - Leiden University, 1998.

J.W. Su, Z.L. Gu, and X. Xu. Advances in numerical methods for the solution of population balance equations for disperse phase systems. *Science in China Series B: Chemistry*, 52: 1063–1079, 2009.

J.R. van Peborgh Gooch and M.J. Hounslow. Monte carlo simulation of size-enlargement mechanisms in crystallization. *AIChE Journal*, 42(7):1864–1874, 1996.

C. Virone. *A fundamental approach to crystal growth and sonocrystallization*. PhD thesis, 2006.

M. Volmer. *Kinetik der Phasenbildung*. Steinkopf, Leipzig, 1939.

E. Wolf. Modeling the behavior of solution crystallization processes for different scales and configurations MSc. Thesis, 2007.

S. Yuu. Collision rate of small particles in a homogeneous and isotropic turbulence. *AIChE Journal*, 30(5):802–807, 1984.

S. Yuu. *Micromixing and parallel reactions*. PhD thesis, 1993.

Glossary

List of Acronyms

PBE	Population Balance Equation
ODE	Ordinary Differential Equation
PDE	Partial Differential Equation
CSD	Crystal Size Distribution
MC	Monte Carlo
DTB	Draft Tube Baffle
MSMPR	Mixed Suspension Mixed Product Removal
CSTR	Continuous Stirred Tank Reactor
HR-FVM	High Resolution Finite Volume Methods